1-1-2013

Plasma Proteins and Their interaction With Synthetic Polymers at the Air-Water interface

Zhengzheng Liao
University of Pennsylvania, liaoz2013@gmail.com

Plasma Proteins and Their interaction With Synthetic Polymers at the Air-Water interface

Abstract
The adsorption of proteins and synthetic polymers at the air-water interface (AWI) has broad significance in biomedicine and biotechnology. Protein behavior at the AWI can be guided to control the structure of the two-dimensional biopolymer film. In addition, synthetic polymers affect how plasma proteins act on implant or drug carrier surfaces, and can also decrease the potential for gas embolism. In this thesis, fluorescence microscopy was applied in combination with tensiometry and atomic force microscopy to study plasma proteins at the AWI alone and under the effect of synthetic polymers. First, the morphology of serum albumin layer controlled by the solution conditions was explored by fluorescence microscopy. Heterogeneity at the micron scale was observed for the protein film during adsorption and at reduced concentrations. Moreover, the competition for interfacial area between Pluronic surfactant F-127 and fibrinogen or serum albumin was studied by semi-quantitative confocal fluorescence methods. A transition stage where F-127 and protein underwent lateral phase separation was found. Two competing processes were revealed--the disintegration of protein-rich phase by F-127 and the coalescence of protein phase. Lastly, the interaction of immunoglobulin and the thin film of a widely used polydimethylsiloxane synthetic polymer was studied at the AWI. The compression state of the polymer film was shown to significantly affect protein adsorption and guide proteins into circular domain structures. Overall, this work has demonstrated the wide utility of fluorescence microscopy to study protein-protein and protein-synthetic polymer interactions at the AWI.

Degree Type
Dissertation

Degree Name
Doctor of Philosophy (PhD)

Graduate Group
Chemistry

First Advisor
Ivan J. Dmochowski

Keywords
Air-water interface, Confocal microscopy, Plasma protein, Polymer, Self-assembly

Subject Categories
Chemistry | Physical Chemistry

PLASMA PROTEINS AND THEIR INTERACTION WITH SYNTHETIC POLYMERS AT THE AIR-WATER INTERFACE

Zhengzheng Liao

A DISSERTATION

in

Chemistry

Presented to the Faculties of the University of Pennsylvania

in

Partial Fulfillment of the Requirements for the

Degree of Doctor of Philosophy

2013

Supervisor of Dissertation

_____

Dr. Ivan J. Dmochowski, Associate Professor of Chemistry

Graduate Group Chairperson

_____

Dr. Gary A. Molander, Professor of Chemistry

Dissertation Committee

Dr. Feng Gai, Professor of Chemistry

Dr. Tobias Baumgart, Associate Professor of Chemistry

Dr. Barry Cooperman, Professor of Chemistry

Dedicated to

my Grandpa

Mr. Junchang Liao

1931-2010

who will always be an inspiration in my life

ACKNOWLEDGEMENT

First of all, I would like to thank my advisor Prof. Ivan Dmochowski for his guidance and support throughout my grad career. I joined Prof. Dmochowski's group as a fresh college graduate with limited experience in research, and Prof. Dmochowski was always encouraging whenever I showed him data or presented him a paper that I found interesting. His encouragement has been a motivation for me to continue the exploration in the ups and downs in my research. Under his influence, I had the opportunity to be exposed to different scientific fields and had collaborations with many people from diverse backgrounds, which greatly expanded my horizon and sharpened my skills.

Furthermore, I want to express my appreciation to my thesis committee members--Prof. Feng Gai, Prof. Tobias Baumgart and Prof. Barry Cooperman. They generously provided advice and criticism of my work, which prompted me to be a better researcher. I'm especially thankful to Prof. Baumgart, with whom I collaborated for the PDMS/protein and the SH3/PRM project. His great prudence and dedication to science have taught me much through the collaboration.

Moreover, I would like to express my gratitude to Prof. David Eckmann, Prof. Portonovo Ayyaswamy, Prof. Roderic Eckenhoff and Prof. Daniel Hammer for the guidance on my other collaborative projects. I'm also grateful to Prof. Zahra Fakhraai, who was generous with her time in discussing ellipsometry. It has been an honor to work with so many great scholars and to absorb the knowledge from them.

I have worked with many graduate students and postdocs at Penn, and I thank them all sincerely. I am sorry if I miss any names in the following list. Dr. Joshua Lampe from Prof. Eckmann's lab was my first lab mentor and passed the torch of the air-water interface project to me. Dr. Xinjing Tang taught me many important experimental techniques including confocal microscopy, which became perhaps the most important part of my skill sets. Dr. Neha Kamat was a talented researcher from whom I learned a lot and with whom I absolutely enjoyed working. Dr. Ashley Fiamengo, Daniel Emerson, John Psonis, Breanna Caltagarone and James Hui collaborated with me on the interesting and challenging fluorescent anesthetic project. Thanks to their intellectual contributions, I have learned much more about the mechanism of anesthetics than I knew five years ago. Dr. Wan-Ting Hsieh is one of my best friends and worked closely with me on both the PDMS/protein project and SH3/PRM project. I learned from her the hardworking attitude and precious patience in doing research. Dr. Brittani Ruble and Sean Yeldell brought me into the TIVA-folate project in my last few months, which further enriched my research experience. Besides, a lot of people have helped me in research through many ways; I want to thank Yu-Hsiu Wang, Dr. Xi-Jun Chen, Helen Cativo, Zhaoxia Qian, Ethan Glor for their assistance in my experiments, and the staff of the Chemistry dDepartment for their support. Also, I would like to thank all the past and present members of the Dmochowski group. It has been a pleasure to be labmates with them.

I am grateful to all my friends at Penn, without whom I would have never made it this far. During grad school, I was extremely lucky to get to know a lot of friends. I know that by mentioning some names I will likely miss some. Nevertheless, I want to particularly

thank Jasmina Cheung-Lau, Chih-Jung Hsu, Xiaojing Liu, Wan-Ting Hsieh, Yu-Hsiu Wang, Keymo Chen, Claire Hsieh, Tingting Wu, Zheng Shi, Chun-Wei Lin, Jin Park, Min Pan, Yi-Ru Chen and Yi-Chi Lin. These people are not only my friends who I grow and learn with, but also essentially my family here in Philadelphia who generously have provided me company and support throughout the years. I also want to thank Zi Liang and Na Liu, who are always willing to lend an ear or travel hundreds of miles for me. We have been as close as sisters for about ten years and they are also part of my family in the U.S.

Finally, I would like to thank my family. My grandma's optimism and resilience after the passing of my grandpa has inspired me to be persistent in my pursuit. My parents, Zhonghong Liao and Huagui Zhang, are my ultimate support both financially and emotionally. They have given me unconditional love and trust, so that I can always find strength in adversity when I think of them. With that strength, I will continue on the journey following my heart and dreams.

ABSTRACT

PLASMA PROTEINS AND THEIR INTERACTION WITH SYNTHETIC POLYMERS AT THE AIR-WATER INTERFACE

Zhengzheng Liao

Dr. Ivan J. Dmochowski

The adsorption of proteins and synthetic polymers at the air-water interface (AWI) has broad significance in biomedicine and biotechnology. Protein behavior at the AWI can be guided to control the structure of the two-dimensional biopolymer film. In addition, synthetic polymers affect how plasma proteins act on implant or drug carrier surfaces, and can also decrease the potential for gas embolism. In this thesis, fluorescence microscopy was applied in combination with tensiometry and atomic force microscopy to study plasma proteins at the AWI alone and under the effect of synthetic polymers. First, the morphology of serum albumin layer controlled by the solution conditions was explored by fluorescence microscopy. Heterogeneity at the micron scale was observed for the protein film during adsorption and at reduced concentrations. Moreover, the competition for interfacial area between Pluronic surfactant F-127 and fibrinogen or serum albumin was studied by semi-quantitative confocal fluorescence methods. A transition stage where F-127 and protein underwent lateral phase separation was found. Two competing processes were revealed—the disintegration of protein-rich phase by F-127 and the coalescence of protein phase. Lastly, the interaction of immunoglobulin and the thin film of a widely used polydimethylsiloxane synthetic polymer was studied at the AWI. The compression state of the polymer film was shown to significantly affect

protein adsorption and guide proteins into circular domain structures. Overall, this work has demonstrated the wide utility of fluorescence microscopy to study protein-protein and protein-synthetic polymer interactions at the AWI.

TABLE OF CONTENTS

LIST OF TABLES

LIST OF FIGURES

Chapter 1 Introduction to proteins at the air-water interface

Proteins are macromolecules composed of polypeptide chains. Because different amino acid side chains have different hydrophobicity (e.g., tryptophan and phenylalanine are more hydrophobic than threonine and serine),[1] after proper folding of the protein, the hydrophobic and hydrophilic regions are formed, giving the protein its amphiphilic nature. Post-translational modifications such as lipidation or phosphorylation further change the amphiphilicity of proteins. Like other amphiphiles, proteins can adsorb at many interfaces and self-assemble into higher-order structures to reduce the surface energy. In the case of protein adsorption at the air-water interface (AWI), protein assembly serves to exclude water molecules from the hydrophobic regions. Exploring how protein behaves at this fundamental and widely presented interface is the focus of this thesis. In this chapter, the motivation for studying proteins at the AWI will be explained in section I. Then a brief description of the experimental techniques used in this thesis and described in the scientific publications will be presented in section II, which provides a foundation for reviewing protein behavior at the AWI as reported in the literature in section III. Finally, the research scope of this thesis will be defined in section IV.

I. Proteins at the air-water interface play crucial roles in many scenarios

a. Biological and technological relevance of proteins at the AWI

The surface properties of proteins are of general interest in material science, food science and medical science. Much attention has been focused on the proteins partitioning at the lipid-water interface in order to understand the mechanism of signal transduction and material transportation in and out of cells.[2,3] Meanwhile, protein adsorption at the solid-liquid interface has also been a popular research topic due to the desire of developing more biocompatible materials for implants and drug delivery.[4,5] In addition to all the foregoing, proteins at the AWI is an important system that not only serves as the basis to understand more complicated lipid-water or solid-liquid interface, but also has direct applications to various areas.

In material science, for example, ranaspumin identified from frog nest foams has been found to adsorb at the AWI and play a crucial role in forming foams composed of 90% air and 10% liquid, with excellent mechanical stability.[6] This bio-foam system has potential application as a biochemical reactor in the micro- and nano- scale.[7] The spider silk proteins and their self-assembled structure at the AWI have been studied in order to understand how these proteins assemble into filaments of exceptional elasticity and extensibility.[8] Block copolymers sharing characteristics of the silk proteins have been designed and synthesized, which are shown to form viscoelastic thin films at the AWI.[8,9] Hydrophobin, which is a protein secreted by filamentous fungi, is one of the best studied proteins at the AWI due to the potential application in changing the wettability and

biocompatibility of implant materials by surface modification.[10] In food science, the milk proteins β-casein, β-lactoglobulin and their interaction with surfactants have been investigated because they are essential in the stability of the foam in dairy products, by adsorbing at the air-water or oil-water interface.[11,12] In medical science, lung surfactant (also called pulmonary surfactant), which is a mixture of phospholipoprotein and lipids, lines the AWI of the alveoli to reduce surface tension. Deficiency of lung surfactant leads to the collapse of the alveoli which could further cause respiratory failure.[13]

b. Plasma proteins

Besides the above mentioned proteins, plasma proteins and their interaction with other molecules at the AWI have also drawn attention. There are at least 289 plasma proteins detected in blood plasma or serum.[14] In terms of concentration, serum albumin, fibrinogen and immunoglobulin G are among the most abundant species in human plasma.[14] Plasma proteins' surface properties are of particular interest to researchers due to the following reasons: 1) the behavior of plasma proteins at the AWI provides the fundamentals, to help elucidate the activities of plasma proteins at solid surfaces without the complication of surface charge and morphology of solid surfaces;[15] 2) during air embolism, the plasma proteins lining the air bubble surface were tied to air embolism pathogenesis, thus intervention or manipulation of such processes requires a greater understanding of the composition and structure of the film formed by plasma proteins at the AWI;[16,17] 3) with the increasing interest of fabricating antibody based sensors in biotechnology, understanding the surface properties of immunoglobulin could aid the design and improve the sensitivity.[18] Because of the above reasons, this thesis focused on

the study of the plasma proteins serum albumin, fibrinogen and immunoglobulin G at the AWI.

II. Experimental methods to study proteins at the air-water interface

a. Tensiometry and Langmuir trough

Tensiometry is one of the most commonly used methods to study surface properties of amphiphiles. It measures the surface tension (γ) of air-liquid interface. Surface tension is a force parallel to the interface caused by the intermolecular forces between solvent molecules (Figure 1.1). Surface tension has the unit of Newton per meter (N/m), and tends to shrink the surface area of liquid in order to decrease the surface energy. The AWI has the highest surface tension in nature because of strong hydrogen bonding. When amphiphiles adsorb at the interface, the hydrogen bonds between water molecules are disrupted, therefore causing a decrease of γ. The dependency of γ on the concentration of surfactants is described by the Gibbs isotherm:

$$\Gamma = -\frac{1}{RT}\left(\frac{\partial \gamma}{\partial \ln C}\right)_{T,P} \qquad \text{(Eq 1.1)}$$

R is the gas constant, T is the temperature, Γ is the surface excess (or surface concentration), and has the unit as mol/m^2 or mg/m^2, while C is the bulk concentration, and has the unit as mol/m^3 or mg/m^3. The idea of surface excess was explained explicitly in Figure 1.2. Clearly, the surface concentration and bulk concentration are different due to the enrichment of amphiphiles at the interface. Through tensiometry, one could obtain

the surface excess when surface tension γ and bulk concentration C of amphiphile is known using Eq 1.1. However, in the case of proteins, the surface excess and surface tension usually do not follow the Gibbs isotherm. The reasons are discussed in section IIIa.

Another term frequently used in tensiometry is surface pressure (π), which is the difference between the surface tension of solvent (γ_0, clean surface) and the surface tension of the solution (γ, the surface that has solute molecules adsorbed). The relationship between γ and π is defined by Eq 1.2. In the context of aqueous solution, γ_0 is usually used as the surface tension of pure water at 20 ^{o}C (72.8 mN/m).[19] Thus, the adsorption of amphiphiles leads to the increase in π.

$$\pi = \gamma_0 - \gamma \qquad \text{(Eq 1.2)}$$

There are several types of tensiometers including Du Noüy-Padday probe,[20] Wilhelmy plate,[21] bubble pressure tensiometer,[22] goniometer[23] and Du Noüy ring,[24] each measures surface tension/pressure using slightly different principals. Methods used in this thesis are described in Chapters 2-4 under the "Material and experimental methods" section.

Moreover, Du Noüy-Padday probe, Du Noüy ring and Wilhelmy plate methods are often coupled with Langmuir-Blodgett (LB) trough to measure the surface pressure at different surface concentrations of amphiphiles. In LB trough, the solute molecules adsorb at the flat AWI and form a thin layer. Under adsorption equilibrium, the surface concentration of solute molecules could be controlled by changing the surface area of the 2D layer between a pair of barriers through compressing or relaxing as the surface

concentration (Γ) is inversely proportional to surface area (*A*). By moving the barriers steadily and measuring the surface pressure by tensiometry at the same time, a surface pressure-surface area (π-*A*) or surface pressure-surface concentration (π-Γ) isotherm could be measured. The kinks in the isotherm often indicate lateral phase transitions in lipid monolayers as shown in Figure 1.3 (A),[25,26] but the shape changes in the isotherm are absent in protein systems due to the flexibility of protein chains as indicated in Figure 1.3 (B).[27]

A prominent advantage of the Langmuir trough is that the interfacial film could be easily transferred to solid substrate for further characterization by Langmuir-Blodgett (LB) transfer (solid substrate perpendicular to the interface) or Langmuir-Schaefer (LS) transfer (solid substrate parallel to the interface), which has greatly expanded the application of LB trough.[28] However, LB trough does have the drawback of being compound consuming due to the large sample volume required, therefore is not very cost effective to study some proteins which could be expensive or labor-intensive to obtain.

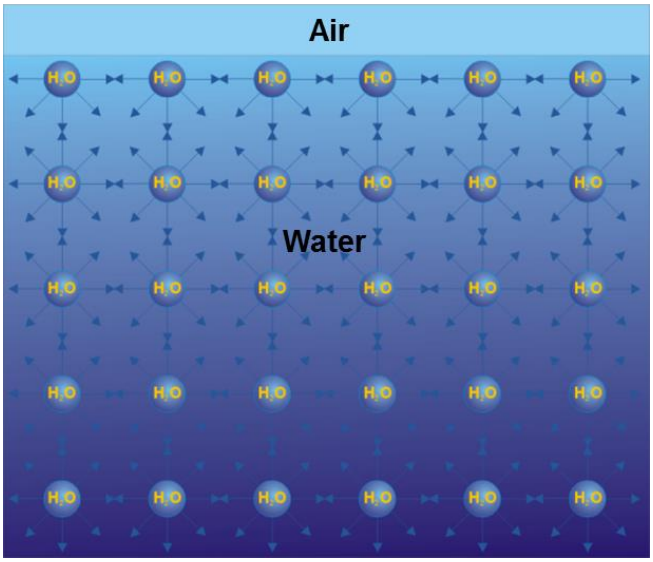

Figure 1.1 Interaction between water molecules at the air-water interface causes surface tension.

On the surface, the interaction between the neighboring water molecules is limited compared to the bulk, which leads to the increase in free energy and decrease in hydrogen bonding between water molecules.

Figure adapted from Kibron Inc (http://www.kibron.com/surface-tension)

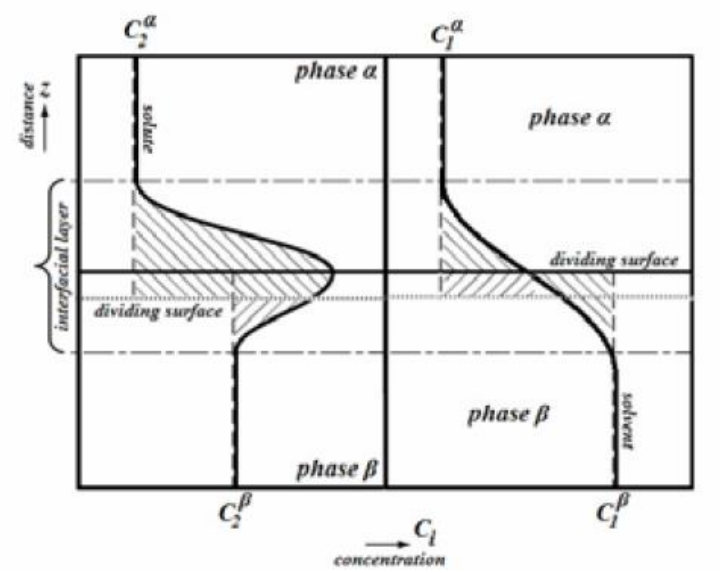

Figure 1.2 Definition of surface excess.

X-axis is the concentration, and Y-axis is the distance normal to the phase boundary. Bold curved lines are the concentration profiles of the solute (left) and the solvent (right), vertical broken lines are the concentrations in the reference system. Chain dotted lines indicate the boundaries of the interfacial layer. Bold horizontal line is the dividing surface and dotted horizontal line is another choice for the location of the dividing surface. The surface excess is the sum of the shaded areas above and under the dividing surface. By choosing the upper dividing surface (a suitable one) the resulting surface excess is zero, whereas by choosing the lower one, surface excess is not zero.

Figure adapted from: Mitropoulos, A. C.: J. Eng. Sci. Technol. Rev. 2008, 1, 1-3.

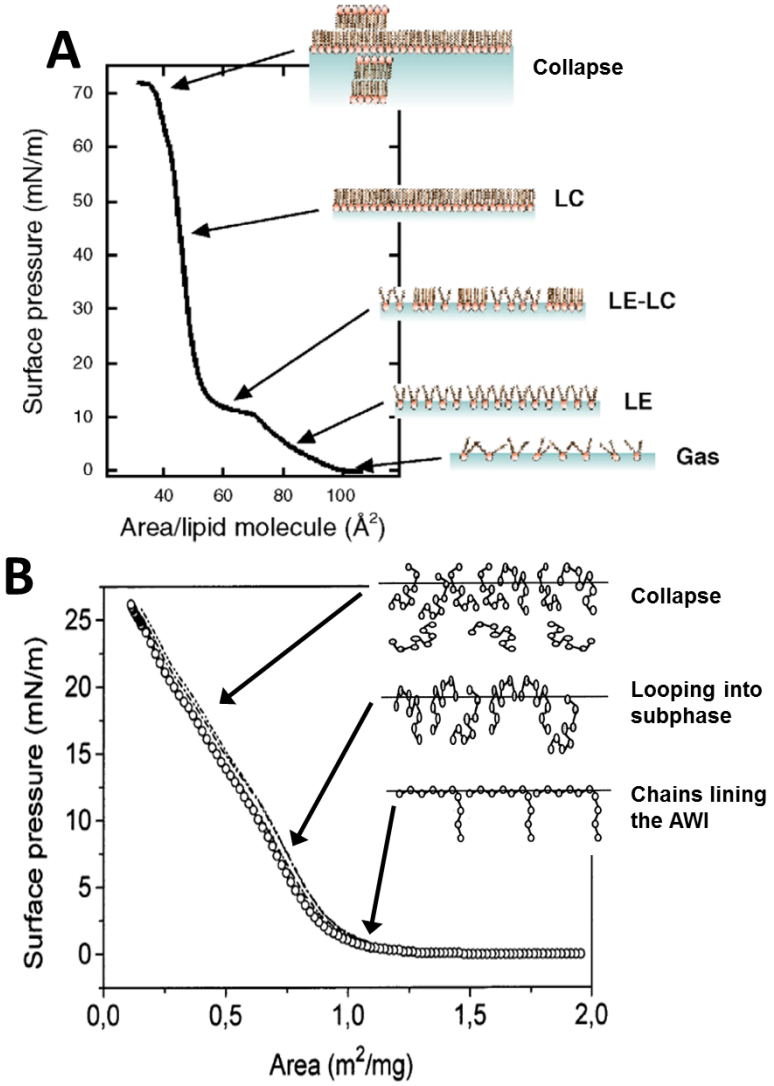

Figure 1.3 Comparison of π-*A* isotherms of lipid and protein at the AWI.

(A) The isotherm of dipalmitoylphosphatidylcholine (DPPC) monolayer and schematic diagrams showing the lateral phase transitions in the DPPC film at different surface pressures. Gas: gaseous phase, LE: liquid-expanded phase, LC: liquid-condensed phase, LE–LC: liquid-condensed–liquid-expanded coexistence. Collapse: collapse of interfacial film. (B) The isotherm of β-casein and schematic diagrams showing the structural changes in the protein film.

Figure 1.3 (A) is adapted from: Wüstneck, R. et al.; Adv. Colloid Interface Sci. 2005, 117, 33-58.

Figure 1.3 (B) is adapted from: Nino, M. R. R. et al.; Colloid Surf. B-Biointerfaces 1999, 12, 161-173.

b. Fluorescence microscopy

Fluorescence microscopy was first applied to study molecules at the AWI in lipid monolayer systems in the 1980s,[29,30] and was soon applied to study the interaction between protein and lipids.[31,32] Thus, the application of fluorescence microscopy in studying protein films at the AWI is a natural extension of these works.[33,34] Fluorescence microscopy has sub-micron spatial resolution and high signal-to-noise ratio, hence is ideal for imaging the film morphology. Besides, the millisecond to a few seconds temporal resolution of fluorescence microscopy could be utilized to study dynamic processes occurring at the interface. Fluorescence microscopy could be used independently or coupled with other methods such as Langmuir trough for *in situ* measurement.

With the development of fluorescence microscopy itself, its application in studying interfacial phenomenon is further expanded. Confocal laser scanning microscopy (CLSM) greatly enhanced the spatial resolution of widefield fluorescence microscopy with the added optical sectioning capability. The optical aperture in CLSM eliminates out of focus light, hence reducing image degradation. Besides, the sectioning ability allows researchers to image the plane perpendicular to the AWI as shown in Figure 1.4. From the change of fluorescence intensity, one can obtain semi-quantitative information about the amount of dye-labeled amphiphiles at the AWI.[35]

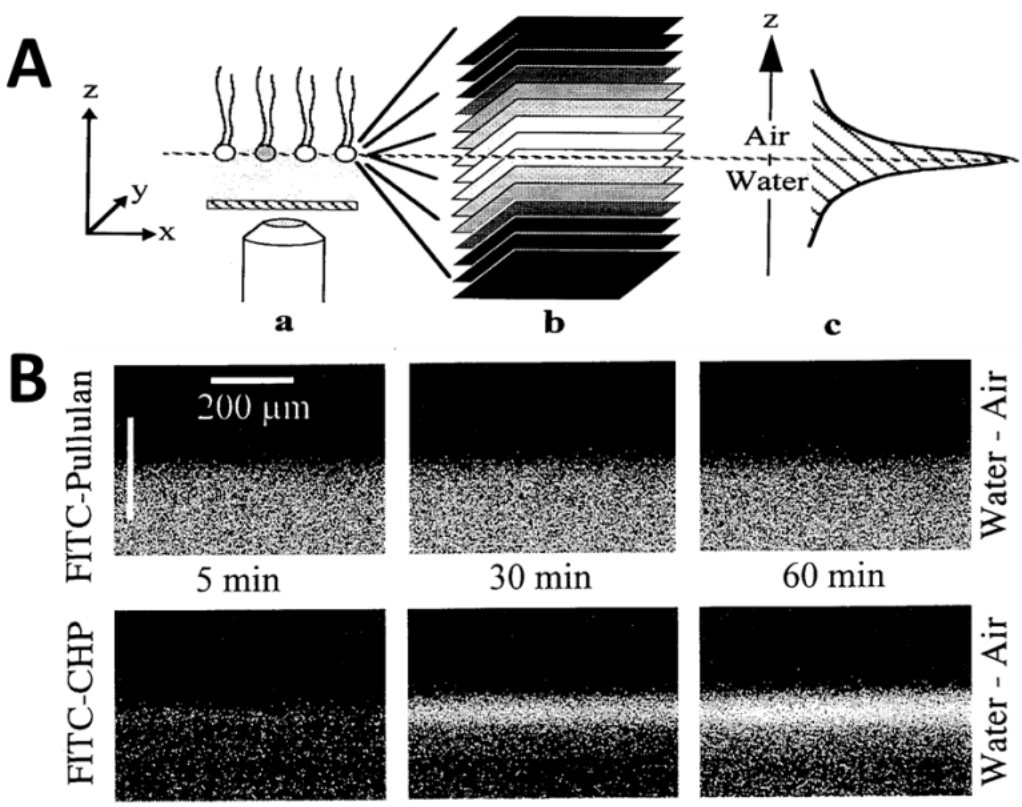

Figure 1.4 Vertical imaging of molecules at the AWI by CLSM.

(A) Procedures for obtaining vertical fluorescence intensity profile. a) scanning the xy plan with CLSM; b) stacking 2D images c) processing the image stack to get a fluorescence intensity profile along z-axis. (B) Fluorescence image stacks of FITC-labeled pullulan (not surface-active) and FITC-labeled cholesterol-bearing-pullulan (surface-active) at the AWI.

Figure adapted from: Gluck, G. et al.; Chem. Lett. 1996, 209-210.

c. Atomic force microscopy

Atomic force microscopy (AFM) is a powerful tool to directly image the topography of thin films with nanometer resolution. It has been adapted to study protein layers formed at the AWI first by Gunning et. al.[12,36,37] They imaged the layer of β-casein at the AWI and bovine serum albumin (BSA) at the hexadecane/water interface and demonstrated that the AFM could resolve the detailed structure as small as a few protein molecules.[36] However, AFM also has obvious drawbacks: to measure the thickness or image the morphology, an extra step is required to transfer the film onto a solid substrate from the AWI. The type of solid substrate and change of hydration state may alter the film structure after transfer.[38] As a result, the transfer quality is crucial for the correct interpretation of the film structure by AFM measurements. Complementary methods, which could confirm the transfer quality and compare the film before and after the transferring step, are desired.[33]

d. Other methods

Besides the above mentioned methods, several other techniques have been developed and applied to study molecules at the AWI. Although these approaches were not directly used in the research projects covered in this thesis, results here are often compared to those reported in the literature using different techniques. A brief introduction of the other methods is hence included in this section to facilitate data interpretation.

Interfacial sheer rheology (ISR) is a technique to study the flow properties of interfacial layers. It measures the storage moduli (G') and the loss moduli (G'') of the 2D layer during shear deformation, and extracts information on elasticity and viscosity.[39] Because

elasticity measures the strength of intermolecular forces, while viscosity measures the diffusion of molecules in the layer, this technique could provide useful information about the organization of molecules at the AWI.[40] Depending on the size of the probe, ISR could be divided into macroscopic and microscopic. Macroscopic rheology measures the average elasticity and viscosity,[39] while the microscopic rheology could resolve the heterogeneity in the 2D layer in the micrometer scale, which was demonstrated to be especially useful in the case of protein films.[41]

Reflectometry and ellipsometry are useful techniques in measuring the thickness and density of thin films. Reflectometry encompasses neutron reflectivity and X-ray reflectivity, which differ in the type of incident beams used but share similar principles. In reflectometry and ellipsometry, the signal is generated by the reflection and/or refraction of the electromagnetic wave by the substances in the interfacial film,[42,43] and these methods do not require any exogenous probes such as the dyes used in fluorescence microscopy or the rheometer sensor used in ISR. However, the thickness and the surface concentration have to be obtained by regression analysis using hypothesized models, thus, prior knowledge of the interfacial film is required in order to make precise measurements.[43]

Brewster angle microscopy (BAM) is a technique to image 2D layers at the AWI. When the p-polarized light beam is directed at the air-liquid interface at the Brewster angle, all light is refracted. If there are any additional materials at the AWI, a small amount of light will be reflected, creating contrast for BAM imaging.[44] BAM is also a non-invasive method, and is capable of resolving micrometer-scale structure.[45,46]

Sum Frequency Generation (SFG) is a non-linear spectroscopic technique suited to study the conformation of molecules at interfaces. Because the second-order nonlinear process is forbidden in centrosymmetric media, signals only come from the molecules at the interface, where the symmetry is broken.[47] SFG could scan wavelengths across the vibrational spectrum, giving information on specific chemical bonds such as the C-H bond, to deduce how the proteins are oriented at the interface.[48]

III. Protein behaviors at the air-water interface

a. Adsorption, conformation and structure of protein assembly at the AWI

Different from small-molecule surfactants, during protein adsorption, the increase in surface pressure and surface excess is often not simultaneous and their correlation does not follow the Gibbs isotherm.[49] This is caused by two distinct characteristics of protein: 1) The proteins in the surface layer could slowly change conformation at the AWI, leading to continuous change in surface pressure.[49] 2) Protein could form multilayers at the interface at high bulk concentrations;[50] because surface pressure is dominated by the surface layer, the surface excess could increase without an obvious change in surface pressure.[51] As a result, the surface pressure and surface excess are not correlated, and the two parameters need to be measured independently. Due to the large structural and compositional variance in proteins, the adsorption kinetics for different proteins needs to be studied on a case-by-case basis.

It is still controversial whether protein adsorption at the AWI is reversible.[52,53] But a slow desorption rate of protein from the interface has been commonly observed, which is primarily due to the change of conformation in the surface layer.[54] In solution or the sub-

layers where the proteins are surrounded by water molecules, the folded structure of the protein will tend to bury hydrophobic regions within the interior of the molecule and expose hydrophilic regions at the protein surface, which reduces the solvation energy.[55] When protein adsorbs at the interface, it will partially unfold and expose its hydrophobic regions in order to reduce surface energy, therefore may undergo some structural distortion. This process could last for hours or even days, demonstrated by the continuous increase of surface pressure after surface excess reached equilibrium due to the change of conformation.[49] Conformational change may lead to denaturation depending on the stability of the protein.[56]

Intermolecular forces, which include the chemical, electrostatic and hydrodynamic interactions between protein molecules, could further drive the proteins into assemblies and networks. Rheological studies showed that the shear viscosity of 8 different protein films kept increasing over 30 hours aging time, which indicates a continuous increase in intermolecular cohesion or covalent bonding.[40] Structural differences of the films formed by different proteins were reported as a result of the different conformation and stability: Previous AFM studies showed that the globular shape of BSA was kept in the interfacial film while a more disordered network was observed in β-casein film shown in Figure 1.5.[36] Heterogeneity in the protein film formed by a single component was also reported by imaging studies. Powers et al. reported microdomains with various geometry in a synthetic amphiphilic peptide at the AWI using fluorescent imaging.[57] BAM imaging also showed domains were formed when globulin 11S adsorbed to the AWI.[58] Mechanical

heterogeneity in the micrometer scale was also observed in β-lactoglobulin film at the AWI by microrheology indicating domain formation.[41]

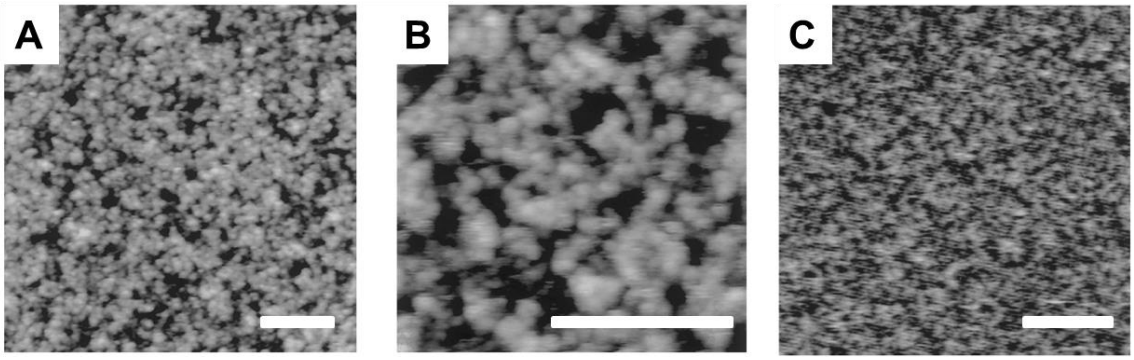

Figure 1.5 AFM images of interfacial film of BSA or β-casein transferred onto mica.

(A, B) BSA prepared at the hexadecane/water interface, (C) β-casein prepared at the AWI. Height in gray scale (black to white) (A) 0-7.6 nm, (B) 0-7.0 nm, (C) 0-2.7 nm. Scale bar: 100 nm

Figure adapted from: Gunning, A. P. et al.; J. Colloid Interface Sci. 1996, 183, 600-602.

A representative plasma protein, serum albumin has a heart-shaped structure resolved by crystallography (Table 1.1), but an ellipsoid shape has been historically used in hydrodynamic studies.[59] It was thought to undergo structural elongation after absorption at the AWI,[60] but is not fully denatured due to the stability of the intramolecular scaffold.[56] The degree of conformational change is dependent on serum albumin bulk concentrations. It was found by SFG that the higher the surface coverage of BSA, the less change in structure that was observed.[61] Recent microrheology study showed that in albumin films, surface elasticity did not increase accordingly with viscosity, indicating an annealing mechanism instead of covalent bonding between albumin molecules.[62]

The shape of fibrinogen could be simplified as three balls connected linearly by two sticks (Table 1.1), so the packing density of fibrinogen at the interface is limited geometrically.[63] Fibrinogen aqueous solution was shown to have moderate surface activity.[63] In accordance with the geometric estimation, ellipsometry of fibrinogen layers at the AWI indicate high water content.[64] Studies using BAM and SEM showed fibrils are formed during organization at the AWI.[65]

IgG is a Y-shaped antibody (Table 1.1). It was found to form a monolayer at the AWI even at high bulk concentration, and the orientation of the molecule changed from side-on to end-on when the surface area was reduced or the bulk concentration was increased.[66] Study using fluorescent antigen binding showed that after adsorption at the interface, IgG underwent partial unfolding.[67]

Table 1.1 Crystal structures and geometric dimensions of serum albumin, fibrinogen and IgG.

	Serum albumin	Fibrinogen	Immunoglobulin G
Crystal structure		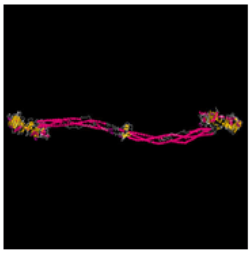	
PDB ID	1E7I	1M1J	1IGT
Geometric dimensions	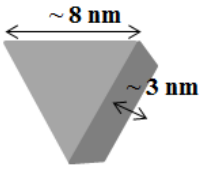 [*]	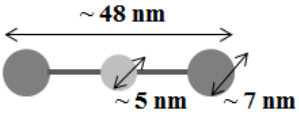 [**]	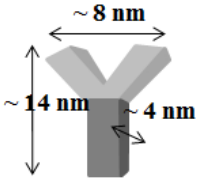 [***]

[*] Ferrer, M. L. et al.; Biophys. J. 2001, 80, 2422-2430. [**] Hall, C. E. et al.; J. Biophys. Biochem. Cytol. 1959, 5, 11-16. [***] Zhao, X. et al.; J. R. Soc., Interface 2009, 6, S659-S670.

b. Interactions between proteins

In biological systems, there is usually more than one type of protein present in solution, and the same is also true at biological interfaces. Signaling proteins interact with each other through specific recognition at the water-lipid interface.[68] For plasma proteins, the competition for the available interfacial area is the dominant interaction. The competition process could be separated into two steps: the diffusion rate, which decides how fast the protein reaches the interface from the bulk, and the affinity of the protein to the interface, which decides the most stable protein interfacial assembly.[15,69] Because the size of molecules decides the diffusion rate to the interface, smaller proteins arrive first at the interface but can be later replaced by larger proteins with higher affinity to the interface. This is the so-called Vroman effect, which was first discovered by Vroman et al. in blood protein adsorption on solid surfaces.[70] Among the few reported studies on protein-protein competition at the AWI, Krishnan et al. measured the surface tensions of blood plasma and serum proteins, and found that different samples exhibited nearly identical concentration dependence.[15] Therefore just from tensiometry, it is hard to resolve the composition of different protein species at the AWI. Moreover, when different proteins adsorb at the interface, the mechanical properties of the interfacial film are strongly affected by the interaction between different species. Rheological study found that mixing serum albumin into IgG greatly reduced the elasticity of the interfacial film, indicating that serum albumin intercalated into IgG and weakened the intermolecular interactions in the film.[39] Overall, the competition between proteins at the AWI is challenging to study.

c. Interaction with polymers

Due to the wide application of synthetic polymers in biomaterials, biosensors, and drug delivery,[71] understanding and controlling the interaction between synthetic polymers and proteins at interfaces has become an important topic. New methods have been reported for incorporating antibody into polymeric thin films for immunosensing,[72-74] demanding deeper understanding of protein-polymer interactions at biological interfaces.

Many polymers—particularly copolymers—are surfactants,[75] and tend to adsorb at interfaces, thus able to compete with protein adsorption. Surfactants are known to interact with proteins at the AWI to reduce significantly the surface tension and change the rheological behavior of the surface layer.[76] It is proposed that surfactants displace proteins heterogeneously from the AWI, as described by an "orogenic" model from previous AFM studies by Morris et al.[12] However, direct proof from in situ measurements has only been provided by BAM studies,[77] and aspects of dynamic transitions remain under-explored.

On the other hand, if polymer layers were pre-spread at the AWI, the polymer film could modulate the interfacial energy and encourage protein adsorption to the interface. Enhanced protein adsorption on polymer films has been accomplished by making superhydrophobic polymer surfaces or incorporating specific protein ligands into the polymer.[4] More recently, tunable adsorption of proteins on polymer films has been achieved by preferential adsorption on spatially separated chemical components that differ in hydrophobicity,[78,79] or by changing the surface charge of polymer thin films.[80,81] Understanding how a polymer thin film at the AWI can act as a template for protein

assembly could further expand the chemical toolbox for controlling protein adsorption and assembly.

IV. Research scope

Work in this thesis utilized fluorescence microscopy alone or in combination with tensiometry and AFM to study plasma proteins and their interaction with polymers at the AWI, contributing to methodological development as well as understanding interfacial behavior of these plasma proteins. The morphological study of human serum albumin (HSA) self-assembly controlled by solution conditions will be presented in Chapter 2. Semi-quantitative study of the adsorption and competition between plasma proteins and a block copolymer Pluronic F-127 at the AWI will be presented in Chapter 3. The interaction between Polydimethylsiloxane film and serum proteins will be investigated in Chapter 4. Finally, conclusions and future directions are summarized in Chapter 5.

V. References

(1) Nozaki, Y.; Tanford, C.: Solubility of amino acids and 2 glycine peptides in aqueous ethanol and dioxane solutions-establishment of a hydrophobicity scale. *J. Biol. Chem.* **1971**, *246*, 2211-2217.

(2) Hessa, T.; Kim, H.; Bihlmaier, K.; Lundin, C.; Boekel, J.; Andersson, H.; Nilsson, I.; White, S. H.; von Heijne, G.: Recognition of transmembrane helices by the endoplasmic reticulum translocon. *Nature* **2005**, *433*, 377-381.

(3) Conner, S. D.; Schmid, S. L.: Regulated portals of entry into the cell. *Nature* **2003**, *422*, 37-44.

(4) Elbert, D. L.; Hubbell, J. A.: Surface treatments of polymers for biocompatibility. *Annu. Rev. Mater. Sci.* **1996**, *26*, 365-394.

(5) Roach, P.; Farrar, D.; Perry, C. C.: Interpretation of protein adsorption: Surface-induced conformational changes. *J. Am. Chem. Soc.* **2005**, *127*, 8168-8173.

(6) Cooper, A.; Kennedy, M. W.: Biofoams and natural protein surfactants. *Biophys. Chem.* **2010**, *151*, 96-104.

(7) Choi, H. J.; Ebersbacher, C. F.; Quan, F. S.; Montemagno, C. D.: pH stability and comparative evaluation of ranaspumin-2 foam for application in biochemical reactors. *Nanotechnology* **2013**, *24*, 055603.

(8) Yang, Y.; Dicko, C.; Bain, C. D.; Gong, Z.; Jacobs, R. M. J.; Shao, Z.; Terry, A. E.; Vollrath, F.: Behavior of silk protein at the air–water interface. *Soft Matter* **2012**, *8*, 9705-9712.

(9) Krishnaji, S. T.; Huang, W.; Rabotyagova, O.; Kharlampieva, E.; Choi, I.; Tsukruk, V. V.; Naik, R.; Cebe, P.; Kaplan, D. L.: Thin film assembly of spider silk-like block copolymers. *Langmuir* **2011**, *27*, 1000-1008.

(10) Zampieri, F.; Wösten, H. A. B.; Scholtmeijer, K.: Creating surface properties using a palette of hydrophobins. *Materials* **2010**, *3*, 4607-4625.

(11) Russev, S. C.; Arguirov, T. V.; Gurkov, T. D.: Beta-casein adsorption kinetics on air-water and oil-water interfaces studied by ellipsometry. *Colloid Surf. B-Biointerfaces* **2000**, *19*, 89-100.

(12) Mackie, A. R.; Gunning, A. P.; Ridout, M. J.; Wilde, P. J.; Morris, V. J.: Orogenic displacement in mixed beta-lactoglobulin/beta-casein films at the air/water interface. *Langmuir* **2001**, *17*, 6593-6598.

(13) Zuo, Y. Y.; Veldhuizen, R. A. W.; Neumann, A. W.; Petersen, N. O.; Possmayer, F.: Current perspectives in pulmonary surfactant - Inhibition, enhancement and evaluation. *Biochimica et Biophysica Acta - Biomembranes* **2008**, *1778*, 1947-1977.

(14) Anderson, N. L.: The human pplasma proteome: history, character, and diagnostic prospects. *Molecular & Cellular Proteomics* **2002**, *1*, 845-867.

(15) Krishnan, A.; Wilson, A.; Sturgeon, J.; Siedlecki, C. A.; Vogler, E. A.: Liquid-vapor interfacial tension of blood plasma, serum and purified protein constituents thereof. *Biomaterials* **2005**, *26*, 3445-3453.

(16) Mukundakrishnan, K.; Ayyaswamy, P. S.; Eckmann, D. M.: Bubble motion in a blood vessel: shear stress induced endothelial cell injury. *J. Biomech. Eng.* **2009**, *131*, 074516.

(17) Sobolewski, P.; Kandel, J.; Eckmann, D. M.: Air bubble contact with endothelial cells causes a calcium-independent loss in mitochondrial membrane potential. *PLoS One* **2012**, *7*, e47254.

(18) Deng, Y.; Zhu, X. Y.; Kienlen, T.; Guo, A.: Transport at the air/water interface is the reason for rings in protein microarrays. *J. Am. Chem. Soc.* **2006**, *128*, 2768-2769.

(19) Vargaftik, N. B.; Volkov, B. N.; Voljak, L. D.: International tables of the surface-tension of water. *J. Phys. Chem. Ref. Data* **1983**, *12*, 817-820.

(20) Padday, J. F.; Pitt, A. R.; Pashley, R. M.: Menisci at a free liquid surface: surface tension from the maximum pull on a rod. *J. Chem. Soc., Faraday Trans. I* **1975**, *71*, 1919-1931.

(21) Holmberg, K.: Handbook of Applied Surface and Colloid Chemistry, Volumes 1-2. John Wiley & Sons; pp 219.

(22) Holmberg, K.: Handbook of Applied Surface and Colloid Chemistry, Volumes 1-2. John Wiley & Sons; pp 227.

(23) Kwok, D. Y.; Gietzelt, T.; Grundke, K.; Jacobasch, H. J.; Neumann, A. W.: Contact angle measurements and contact angle interpretation .1. Contact angle measurements by axisymmetric drop shape analysis and a goniometer sessile drop technique. *Langmuir* **1997**, *13*, 2880-2894.

(24) du Nouy, P. L.: An interfacial tensiometer for universal use. *J. Gen. Physiol.* **1925**, *7*, 625-631.

(25) Kaganer, V. M.; Mohwald, H.; Dutta, P.: Structure and phase transitions in Langmuir monolayers. *Rev. Mod. Phys.* **1999**, *71*, 779-819.

(26) Wüstneck, R.; Perez-Gil, J.; Wüstneck, N.; Cruz, A.; Fainerman, V. B.; Pison, U.: Interfacial properties of pulmonary surfactant layers. *Adv. Colloid Interface Sci.* **2005**, *117*, 33-58.

(27) Nino, M. R. R.; Sanchez, C. C.; Patino, J. M. R.: Interfacial characteristics of beta-casein spread films at the air-water interface. *Colloid Surf. B-Biointerfaces* **1999**, *12*, 161-173.

(28) Petty, M. C.: Langmuir-Blodgett Films - An Introduction. Cambridge University Press; pp 39-63.

(29) McConnell, H. M.; Tamm, L. K.; Weis, R. M.: Periodic structures in lipid monolayer phase-transitions. *Proc. Natl. Acad. Sci. U. S. A.* **1984**, *81*, 3249-3253.

(30) Lösche, H.; Möhwald, H.: Fluorescence microscopy on monomolecular films at an air/water interface. *Colloids and Surfaces* **1984**, *10*, 217-224.

(31) Heckl, W. M.; Zaba, B. N.; Mohwald, H.: Interactions of cytochromes b5 and c with phospholipid monolayers. *Biochim. Biophys. Acta* **1987**, *903*, 166-176.

(32) Möhwald, H.: Phospholipid and phospholipid-protein monolayers at the air/water interface. *Annu. Rev. Phys. Chem.* **1990**, *41*, 441-476.

(33) Morris, V. J.; Gunning, A. P.: Microscopy, microstructure and displacement of proteins from interfaces: implications for food quality and digestion. *Soft Matter* **2008**, *4*, 943-951.

(34) Liu, W.; Johnson, S.; Micic, M.; Orbulescu, J.; Whyte, J.; Garcia, A. R.; Leblanc, R. M.: Study of the aggregation of human insulin Langmuir monolayer. *Langmuir* **2012**, *28*, 3369-3377.

(35) Gluck, G.; Ringsdorf, H.; Okumura, Y.; Sunamoto, J.: Vertical sectioning of molecular assemblies at air water interface using laser scanning confocal fluorescence microscopy. *Chem. Lett.* **1996**, 209-210.

(36) Gunning, A. P.; Wilde, P. J.; Clark, D. C.; Morris, V. J.; Parker, M. L.; Gunning, P. A.: Atomic force microscopy of interfacial protein films. *J. Colloid Interface Sci.* **1996**, *183*, 600-602.

(37) Mackie, A. R.; Gunning, A. P.; Pugnaloni, L. A.; Dickinson, E.; Wilde, P. J.; Morris, V. J.: Growth of surfactant domains in protein films. *Langmuir* **2003**, *19*, 6032-6038.

(38) Viswanathan, R.; Schwartz, D. K.; Garnaes, J.; Zasadzinski, J. A. N.: Atomic force microscopy imaging of substrate and pH effects on Langmuir-Blodgett monolayers. *Langmuir* **1992**, *8*, 1603-1607.

(39) Ariola, F. S.; Krishnan, A.; Vogler, E. A.: Interfacial rheology of blood proteins adsorbed to the aqueous-buffer/air interface. *Biomaterials* **2006**, *27*, 3404-3412.

(40) Bos, M. A.; van Vliet, T.: Interfacial rheological properties of adsorbed protein layers and surfactants: a review. *Adv. Colloid Interface Sci.* **2001**, *91*, 437-471.

(41) Lee, M. H.; Reich, D. H.; Stebe, K. J.; Leheny, R. L.: Combined passive and active microrheology study of protein-layer formation at an air-water interface. *Langmuir* **2010**, *26*, 2650-2658.

(42) De Feijter, J. A.; Benjamins, J.; Veer, F. A.: Ellipsometry as a tool to study the adsorption behavior of synthetic and biopolymers at the air-water interface. *Biopolymers* **1978**, *17*, 1759-1772.

(43) Zhou, X. L.; Chen, S. H.: Theoretical foundation of X-ray and neutron reflectometry. *Phys. Rep.-Rev. Sec. Phys. Lett.* **1995**, *257*, 223-348.

(44) Honig, D.; Mobius, D.: Direct visualization of monolayers at the air-water-interface by brewster angle microscopy. *J. Phys. Chem.* **1991**, *95*, 4590-4592.

(45) Ruiz-Garcia, J.; Moreno, A.; Brezesinski, G.; Mohwald, H.; Mas-Oliva, J.; Castillo, R.: Phase transitions and conformational changes in monolayers of human apolipoproteins CI and AII. *J. Phys. Chem. B* **2003**, *107*, 11117-11124.

(46) Murray, B. S.; Xu, R.; Dickinson, E.: Brewster angle microscopy of adsorbed protein films at air-water and oil-water interfaces after compression, expansion and heat processing. *Food Hydrocolloids* **2009**, *23*, 1190-1197.

(47) Shen, Y. R.: Surface properties probed by 2nd harmonic and sum frequency generation. *Nature* **1989**, *337*, 519-525.

(48) Wang, J.; Buck, S. M.; Chen, Z.: Sum frequency generation vibrational spectroscopy studies on protein adsorption. *J. Phys. Chem. B* **2002**, *106*, 11666-11672.

(49) Graham, D. E.; Phillips, M. C.: Proteins at liquid interfaces .1. kinetics of adsorption and surface denaturation. *J. Colloid Interface Sci.* **1979**, *70*, 403-414.

(50) Lu, J. R.; Su, T. J.; Penfold, J.: Adsorption of serum albumins at the air/water interface. *Langmuir* **1999**, *15*, 6975-6983.

(51) Graham, D. E.; Phillips, M. C.: Proteins at liquid interfaces .2.adsorption-isotherms. *J. Colloid Interface Sci.* **1979**, *70*, 415-426.

(52) VanTassel, P. R.; Viot, P.; Tarjus, G.: A kinetic model of partially reversible protein adsorption. *J. Chem. Phys.* **1997**, *106*, 761-770.

(53) Fainerman, V. B.; Miller, R.; Ferri, J. K.; Watzke, H.; Leser, M. E.; Michel, M.: Reversibility and irreversibility of adsorption of surfactants and proteins at liquid interfaces. *Adv. Colloid Interface Sci.* **2006**, *123-126*, 163-171.

(54) Mosesson, M. W.: Fibrinogen and fibrin structure and functions. *J. Thromb. Haemost.* **2005**, *3*, 1894-1904.

(55) Chandler, D.: Interfaces and the driving force of hydrophobic assembly. *Nature* **2005**, *437*, 640-647.

(56) Lad, M. D.; Birembaut, F.; Matthew, J. M.; Frazier, R. A.; Green, R. J.: The adsorbed conformation of globular proteins at the air/water interface. *Phys. Chem. Chem. Phys.* **2006**, *8*, 2179-2186.

(57) Powers, E. T.; Kelly, J. W.: Medium-dependent self-assembly of an amphiphilic peptide: Direct observation of peptide phase domains at the air-water interface. *J. Am. Chem. Soc.* **2001**, *123*, 775-776.

(58) Garcia-Gonzalez, A.; Flores-Vazquez, A. L.; Maldonado, E.; de la Rosa, A. P. B.; Ruiz-Garcia, J.: Globulin 11S and its mixture with L-dipalmitoylphosphatidylcholine at the air/liquid interface. *J. Phys. Chem. B* **2009**, *113*, 16547-16556.

(59) Ferrer, M. L.; Duchowicz, R.; Carrasco, B.; de la Torre, J. G.; Acuna, A. U.: The conformation of serum albumin in solution: A combined phosphorescence depolarization-hydrodynamic modeling study. *Biophys. J.* **2001**, *80*, 2422-2430.

(60) Lu, J. R.; Su, T. J.; Thomas, R. K.: Structural conformation of bovine serum albumin layers at the air-water interface studied by neutron reflection. *J. Colloid Interface Sci.* **1999**, *213*, 426-437.

(61) Wang, J.; Buck, S. M.; Chen, Z.: The effect of surface coverage on conformation changes of bovine serum albumin molecules at the air-solution interface detected by sum frequency generation vibrational spectroscopy. *Analyst* **2003**, *128*, 773-778.

(62) Dhar, P.; Cao, Y. Y.; Fischer, T. M.; Zasadzinski, J. A.: Active interfacial shear microrheology of aging protein films. *Phys. Rev. Lett.* **2010**, *104*, 016001.

(63) Hernandez, E. M.; Phang, T. L.; Wen, X. Y.; Franses, E. I.: Adsorption and direct probing of fibrinogen and sodium myristate at the air/water interface. *J. Colloid Interface Sci.* **2002**, *250*, 271-280.

(64) Hernandez, E. M.; Franses, E. I.: Adsorption and surface tension of fibrinogen at the air/water interface. *Colloid Surf. A-Physicochem. Eng. Asp.* **2003**, *214*, 249-262.

(65) Sankaranarayanan, K.; Dhathathreyan, A.; Miller, R.: Assembling fibrinogen at air/water and solid/liquid interfaces using Langmuir and Langmuir-Blodgett films. *J. Phys. Chem. B* **2010**, *114*, 8067-8075.

(66) Tronin, A.; Dubrovsky, T.; Nicolini, C.: Comparative study of Langmuir monolayers of immunoglobulins-G formed at the air-water interface and covalently immobillized on solid supports. *Langmuir* **1995**, *11*, 385-389.

(67) Tronin, A.; Dubrovsky, T.; Dubrovskaya, S.; Radicchi, G.; Nicolini, C.: Role of protein unfolding in monolayer formation on air-water interface. *Langmuir* **1996**, *12*, 3272-3275.

(68) Li, P.; Banjade, S.; Cheng, H. C.; Kim, S.; Chen, B.; Guo, L.; Llaguno, M.; Hollingsworth, J. V.; King, D. S.; Banani, S. F.; Russo, P. S.; Jiang, Q. X.; Nixon, B. T.; Rosen, M. K.: Phase transitions in the assembly of multivalent signalling proteins. *Nature* **2012**, *483*, 336-340.

(69) Krishnan, A.; Siedlecki, C. A.; Vogler, E. A.: Mixology of protein solutions and the Vroman effect. *Langmuir* **2004**, *20*, 5071-5078.

(70) Vroman, L.; Adams, A. L.; Fischer, G. C.; Munoz, P. C.: Interaction of high molecular-weight kininogen, factor-XII, and fibrinogen in plasma at interfaces. *Blood* **1980**, *55*, 156-159.

(71) Stuart, M. A. C.; Huck, W. T. S.; Genzer, J.; Muller, M.; Ober, C.; Stamm, M.; Sukhorukov, G. B.; Szleifer, I.; Tsukruk, V. V.; Urban, M.; Winnik, F.; Zauscher, S.; Luzinov, I.; Minko, S.: Emerging applications of stimuli-responsive polymer materials. *Nat. Mater.* **2010**, *9*, 101-113.

(72) Caruso, F.; Niikura, K.; Furlong, D. N.; Okahata, Y.: Assembly of alternating polyelectrolyte and protein multilayer films for immunosensing .2. *Langmuir* **1997**, *13*, 3427-3433.

(73) Janmanee, R.; Baba, A.; Phanichphant, S.; Sriwichai, S.; Shinbo, K.; Kato, K.; Kaneko, F.: Detection of human IgG on poly(pyrrole-3-carboxylic acid) thin film by electrochemical-surface plasmon resonance spectroscopy. *Jpn. J. Appl. Phys.* **2011**, *50*, 01BK02.

(74) Valsesia, A.; Mannelli, I.; Colpo, P.; Bretagnol, F.; Rossi, F.: Protein nanopatterns for improved immunodetection sensitivity. *Anal. Chem.* **2008**, *80*, 7336-7340.

(75) Torchilin, V. P.: Structure and design of polymeric surfactant-based drug delivery systems. *J. Controlled Release* **2001**, *73*, 137-172.

(76) Kotsmar, C.; Pradines, V.; Alahverdjieva, V. S.; Aksenenko, E. V.; Fainerman, V. B.; Kovalchuk, V. I.; Krägel, J.; Leser, M. E.; Noskov, B. A.; Miller, R.: Thermodynamics, adsorption kinetics and rheology of mixed protein-surfactant interfacial layers. *Adv. Colloid Interface Sci.* **2009**, *150*, 41-54.

(77) Mackie, A. R.; Gunning, A. P.; Ridout, M. J.; Wilde, P. J.; Patino, J. R.: In situ measurement of the displacement of protein films from the air/water interface by surfactant. *Biomacromolecules* **2001**, *2*, 1001-1006.

(78) Lau, K. H. A.; Bang, J.; Kim, D. H.; Knoll, W.: Self-assembly of protein nanoarrays on block copolymer templates. *Adv. Funct. Mater.* **2008**, *18*, 3148-3157.

(79) Kidambi, S.; Chan, C.; Lee, I.: Tunable resistive m-dPEG acid patterns on polyelectrolyte, multilayers at physiological conditions: Template for directed deposition of biomacromolecules. *Langmuir* **2008**, *24*, 224-230.

(80) Eloi, J.-C.; Jones, S. E. W.; Poór, V.; Okuda, M.; Gwyther, J.; Schwarzacher, W.: Electrochemically triggered selective adsorption of biotemplated nanoparticles on self-assembled organometallic diblock copolymer thin films. *Adv. Funct. Mater.* **2012**, *22*, 3273-3278.

(81) Pernites, R. B.; Santos, C. M.; Maldonado, M.; Ponnapati, R. R.; Rodrigues, D. F.; Advincula, R. C.: Tunable protein and bacterial cell adsorption on colloidally templated superhydrophobic polythiophene films. *Chem. Mater.* **2012**, *24*, 870-880.

Chapter 2 Morphology of protein self-assembly at the air-water interface controlled by solution conditions—a study by confocal laser scanning microscopy*

I. Introduction

The AWI is a unique tool to guide proteins as small building units into larger, self-assembled structures. Proteins are naturally occurring biopolymers with unsymmetrical distribution of buried and solvent-exposed active sites, electrostatic charges and hydrophobic/hydrophilic residues. These features, combined with geometric constraints, dictate the structures of folded proteins and their larger assemblies. A strategy in assembling complex biological or synthetic systems is to promote interactions in just one or two dimensions. Liquid interfaces are particularly useful in this regard, based on the anisotropic forces residing therein and two-dimensional spatial confinement.[1-3] Besides the special characteristics of liquid interfaces, factors that commonly control self-assembly are the chemical and structural complementarity of the building blocks.[4] For macromolecules such as proteins, the active site, geometric structure, electrostatic and hydrophobic interactions are greatly affected by the surrounding solvent molecules and

*This chapter was adapted from Liao, Z.; Lampe, J. W.; Ayyaswamy, P. S.; Eckmann, D. M.; Dmochowski, I. J.: Protein Assembly at the Air-Water Interface Studied by Fluorescence Microscopy. *Langmuir* **2011**, *27*, 12775-12781.

other solutes.[5,6] Thus, solution conditions provide a convenient handle for controlling protein assembly at the AWI.

Previous tensiometry, reflectometry and ellipsometry studies explored the change in surface excess and structural conformation of proteins at the AWI in relation to solution conditions such as subphase concentration, pH and ionic strength.[7-10] These techniques provide ensemble-averaged properties of adsorbed proteins over a macroscopic scale. To study assembled structures at the AWI on the nanometer-to-micron scale, imaging techniques such as atomic force microscopy (AFM), Brewster angle microscopy (BAM) and fluorescence microscopy have been applied.[11-13] AFM affords nanometer spatial resolution, but involves transferring interfacial films onto a solid surface, which leads to potential loss of structural fidelity and temporal resolution.[11] BAM coupled with Langmuir trough is a widely used in situ method, but offers lower spatial resolution (2 μm) than many diffraction-limited optical imaging techniques, and offers little kinetic information.[12,14] Earlier studies by Gluck et al. on polysaccharide adsorption at the AWI showed the potential of fluorescence microscopy to serve as a facile in situ imaging tool for studying macromolecular self-assembly at the AWI.[15] By this technique, Powers et al. discovered medium-dependent micron-size phase domains of an amphiphilic peptide self-assembled at the AWI.[16] The observations made in this landmark study have not yet been generalized to protein systems. Here, we demonstrate for the first time the ability to control the microstructure of protein self-assembly at the AWI through systematic variation of solution conditions.

In this chapter, human serum albumin labeled with Texas Red (HSA-TR) was used as a model protein, and the microstructure of its self-assembly was studied by in situ fluorescence microscopy under various solution conditions. Human serum albumin (HSA) provides a useful model protein system as its biophysical properties have been very well studied.[17,18] Besides the background information on serum albumin reviewed in chapter 1 section III a, HSA is known to be composed of a single polypeptide chain with 585 amino acids, which include 35 cysteines and 59 lysines. Thirty-four cysteines form 17 intramolecular disulfide bridges while the single reactive Cys34 is extremely sensitive to redox state.[17,19] X-ray crystallography confirmed that HSA has alpha-helical secondary structure, and identified a heart-shaped or equilateral triangular tertiary structure under physiological conditions with 80 Å on a side and 30 Å in thickness,[17] as shown in Table 1.1. Reflectometry studies also found the thickness of a serum albumin layer at the interface to be 30–40 Å, but the proteins were approximated as an ellipsoid with long axis of 140 Å parallel to the interface, and a perpendicular short axis of 40 Å.[18]

The current study applied in situ fluorescence microscopy to study protein assembly at the AWI in a small imaging chamber with ~10 μL solution, while limiting competitive protein adsorption at the liquid-solid interface by covalently attaching a PEG layer to the glass surface. A stable AWI was formed, with negligible evaporation, which allowed both static and dynamic information of protein behavior at the AWI to be obtained with sub-micron spatial resolution and on time scales of milliseconds to hours. Our results revealed micro-scale protein assemblies formed at the AWI and highlighted the role of solution conditions, including ionic strength and reduction potential, in controlling the

assembled structures. Kinetic transitions of phase separation at the AWI were also observed.

II. Material and experimental methods

a. General reagents

For all steps, deionized water (DI water, Mar Cor Premium Grade Mixed Bed Service Deionization, 18.2 megohm-cm resistivity at 25 ℃) was used. The phosphate-buffered saline (PBS) solution used for fluorescence microscopy was made by dissolving NaH_2PO_4 and NaN_3 in DI water and then adjusting to pH 7.2 with 1 M HCl, the final concentration is 10 mM of phosphate and 30 mM of NaN_3 throughout the study. The ionic strength of PBS was adjusted by addition of NaCl. Dithiothreitol (DTT) was purchased from Fisher Scientific.

b. Protein labeling

Commercially available HSA (Sigma-Aldrich) was labeled with amine-reactive fluorophore Texas Red-X succinimidyl ester (Invitrogen). Texas Red-X was first dissolved in dimethylformamide (10 mg/mL), then a small volume of this concentrated dye solution was slowly added into the aqueous protein solution (2 mg/mL HSA in in 0.1 M $NaHCO_3$ buffer, pH 8.3) while stirring. The molar ratio of dye to protein was 10 to 1 upon mixing. The reaction solution was covered with aluminum foil and stirred continuously for 1 h at room temperature. Then the unreacted dyes were removed by running the reaction solution through a 10-DG column (Bio-Rad). The labeled proteins were eluted with PBS, and further concentrated and purified by 3 kDa cutoff molecular weight centrifugal filter units (Millipore) at 9 krpm for 30 min at 4 ℃ and dialyzed by 10

kDa dialysis cassettes (Thermo Scientific) against 1 L of 10 mM phosphate buffer for 1 week at 4 ℃ covered by alumni foil. The final concentration of labeled protein was determined by Lowry assay (Thermo Scientific) using bovine serum albumin (BSA, Thermo Scientific) as the standard. The product solution was aliquoted and stored under -20 ℃ for further use.

c. Dye-to-protein ratio (DPR) measurements

DPR was measured by both UV-Vis spectrometer and MALDI-TOF MS. For UV-Vis measurement, labeled proteins were diluted to appropriate concentration and the absorbance values at 280 nm and 595 nm were measured. DPR was calculated from the following equation:

$$DPR = \left(\frac{A_{595}}{\varepsilon_{595}^{TR}} \right) \Bigg/ \left(\frac{A_{280} - A_{595} \times 0.18}{\varepsilon_{280}^{HSA}} \right) \qquad \text{(Eq 2.1)}$$

where A_{595} and A_{280} are the absorbance at 595 nm and 280 nm measured using a diode-array Agilent 89090A spectrophotometer, ε is the extinction coefficient of TR or HSA provided by manufacturer (Invitrogen) and from literature,[20] and 0.18 is a correction factor to account for the contribution of the dye absorbance at A_{280}.[21]

d. MALDI-TOF MS of HSA and HSA-TR

MALDI-TOF MS measurements were performed with a Bruker Daltonic Ultraflex III MALDI-TOF-TOF mass spectrometer, in a mass range from m/z 10,000-160,000. Labeled proteins were diluted with HPLC grade water before loading onto sample plate. The protein solution (1 μL) was mixed with 1 μL of matrix solution (saturated sinapinic acid in 50% CH_3CN, 49.9% HPLC grade H_2O and 0.1% TFA, in volume percentage) by

repeated pipetting. After sample droplets were dried, on-plate washing was performed by spotting 0.1% TFA solution on dried sample spot for 10 s then removing excess liquid.

e. Circular dichroism (CD) measurement

CD measurements were carried out on a Chirascan CD spectrometer with a Peltier temperature controller. HSA and HSA-TR were diluted to 0.10 mg/mL with 10 mM NaCl in 10 mM phosphate buffer (pH = 7.2) then transferred to a 0.1 cm pathlength cuvette. Far-UV CD spectra of HSA and HSA-TR were collected at 25 ℃ over the wavelength range of 190-260 nm at scan rate of 0.5 nm/s with a slit bandwidth of 1.0 nm. CD signal was converted into mean residue ellipticity [θ] following Eq 2.2.[22]

[θ], in $deg \cdot cm^2 \cdot dmol^{-1}$ = (millidegrees × mean residue weight)/(pathlength in millimeters × concentration in $mg \cdot mL^{-1}$) (Eq 2.2)

Thermal denaturation curves were recorded between 25-95 ℃ with a 2 ℃ increase and 120 s equilibration time for each step. Melting temperature T_m was obtained by converting data points in thermal denaturation curves following Eq 2.3, 2.4 and fitting into Eq 2.5[23] using Matlab:

$$K = \frac{[\theta]_N - [\theta]}{[\theta] - [\theta]_D} \quad \text{(Eq 2.3)}$$

$$\Delta G(T) = -RT \ln K \quad \text{(Eq 2.4)}$$

$$\Delta G(T) = \Delta H_m (1 - T/T_m) + \Delta C_p [T - T_m - T \ln(T/T_m)] \quad \text{(Eq 2.5)}$$

where $[\theta]_N$ is ellipticity value of the protein under native conditions ($\theta_{25\,^\circ C}$ is used as $[\theta]_N$), $[\theta]_D$ is the ellipticity value of the protein under fully denatured conditions ($\theta_{95\,^\circ C}$ is used as $[\theta]_D$), and $[\theta]$ is the measured ellipticity value at temperature T. K is the equilibrium constant, $\Delta G(T)$ is the Gibbs free energy at temperature T, R is the gas constant, T_m (melting temperature) is the midpoint of the thermal denaturation, and ΔH_m is the enthalpy change at $T = T_m$.

f. Surface pressure measurement in LB trough and film transfer

Surface pressure was measured using a MicroTroughX Langmuir trough with a Du Noüy-Padday probe (Kibron, Inc.). HSA or HSA-TR (0.10 mg/mL) in 10 mM PBS was pipetted into the microtrough. Surface pressure was recorded over 1 h after immediate AWI formation. Then the layer at the AWI was transferred onto a freshly cleaved mica surface using the Langmuir-Schaefer technique via a Kibron Microtrough S controller.[24] A rinsing step was performed with DI water to wash away excess salt on the sample surface. The sample was left drying in air before being studied by AFM.

g. AFM characterization of transferred film

The transferred protein layers formed by the labeled or unlabeled proteins at the AWI were measured using tapping mode AFM (Digital Instruments) and processed by NanoScope IIIa software (v. 5.12; Digital Instruments). Ultrasharp cantilevers (NSC16, MikroMasch) were used. AFM images were analyzed using WSxM software (Nanotec) to determine film thickness.[25]

h. Sample chamber fabrication and surface modification

The sample chamber for fluorescence microscope imaging was assembled by placing a thin piece of polydimethylsiloxane (PDMS, 1 cm × 1 cm, ~0.5 mm thick) in between two pieces of cover glass. The cover glass was cleaned by sonication in acetone for 5 minutes followed by sonication in DI water 3 times. Then the surface –OH group of the cover glass was prepared by sonicate the cover glass in 200mM KOH for 20 minutes. The cover glass was subsequently rinsed by DI water 3 times, and sonicated in ethanol for 5min and left dry in air.

PDMS is fabricated using a commercially available PDMS kit (Sylgard 184, Dow Corning), the elastomer and curing reagent are mixed at weight ratio of 10:1. After thorough mixing and degassing, the liquid PDMS was poured into a Petri dish and cured at 80 ℃ for 2.5 h. The thin slab of PDMS after curing was peeled off the dish and cut into 1 cm × 1 cm pieces. A 0.7-cm diameter cylindrical hole was punched through the middle of the PDMS. The PDMS pieces were washed with di-water thoroughly, then blown dry with compressed air. It was put onto the center of a cleaned cover glass. Bonding between PDMS and cover glass could be seen immediately. This chamber serves as the sample holder of protein solutions, and leaking was prevented by conformal contact between the PDMS and the bottom cover glass.

The inner-chamber surface of the bottom cover glass was modified with mPEG-silane (Laysan Bio, Inc., MW 5000) in order to reduce protein adsorption.[26] And inner-chamber PDMS surfaces were oxidized and subsequently modified with the same mPEG-silane reagent, using solution phase surface modification method.[27] The surface modification

steps are as following: mPEG-silane was stored in -20℃ freezer and warmed to r.t. before use. It was dissolved in 5% acetic acid/ methanol solution at 250 mg/mL. A glass pipet was used to add mPEG-silane solution into the chamber. Another cover glass was put on top of it to prevent evaporation. The whole assembly was incubated at 40℃ for 30 min. The top cover glass was discarded and the chamber was rinsed with ample DI water and blown dry with argon and stored at –20 ℃ until used for imaging.

i. Confocal and epi-fluorescence imaging.

Confocal images were captured using an Olympus IX81 inverted microscope. Epi-fluorescence images were captured by a hyperspectral CCD (CRi Nuance FX) camera coupled to the Olympus IX81 system. The objective lens (40X, water immersion, 1.15 NA) imaged the sample solution from below by exciting the dyes with a 543 nm laser or by a mercury lamp with excitation filter of 530-550 nm bandpass. Emission was collected in the 575-655 nm range. Images were analyzed using ImageJ software.[28]

III. Results and discussion

a. Characterization of HSA-TR in comparison with HSA

Although fluorescent probes are widely used to study protein behaviors, concerns have been generated about the perturbation of exogenous fluorophores on the conformation of proteins.[29] It is especially important in surface related studies to carefully characterize the dye-labeled protein in comparison with the native protein, because the dye molecules could both alter the conformation and change the hydrophobicity of the protein.

In our study, we tried to achieve minimal labeling by adjusting the amount of dye and protein in the labeling reaction, and characterized the DPR by UV-Vis spectroscopy and MALDI-TOF MS. DPR was 1.3 measured by UV-Vis spectroscopy, and 1.5 measured by MALDI-TOF MS shown in Figure 2.1. Proteins were charged by receiving protons from the matrix. From left to right, the peaks are assigned to $A + 2H^+$, $A + H^+$, and $2A + H^+$ for HSA and HSA-TR, respectively, where "A" represents the protein molecule. Using $A + H^+$ peaks of HSA and HSA-TR the mass difference (Δm) = m(HSA-TR) - m(HSA) = 1119 g/mol. Because MW(TR) = 723 g/mol, thus DPR = Δm/MW(TR) = 1.5.

The secondary structures of HSA and HSA-TR were compared by circular dichroism (CD) spectroscopy shown in Figure 2.2. Far-UV CD spectra of HSA and HSA-TR overlap with each other well (Figure 2.2 A), indicating that TR does not cause detectable changes to the characteristic α-helical structure of HSA. In thermal denaturation curves (Figure 2.2 B), HSA-TR appears to be more thermally stable. The melting temperature of HSA-TR is 5 ℃ higher than that of HSA. We hypothesize that Texas Red dye can interact with ligand binding sites in HSA as reported in literature, and thus enhance the structural stability of the protein.[30]

The surface pressure curves of HSA-TR and HSA were also measured to compare their surface activities. In Figure 2.3, the surface pressure of HSA is slightly higher than that of HSA-TR. However, the difference is within 1 mN/m, which is in the range of experimental error. Thus the perturbation of Texas Red on HSA surface activity is quite small if there was any.

By AFM, we imaged the HSA-TR or HSA layer formed at the AWI at similar solution conditions (C = 0.1 mg/mL at neutral pH) reported in the literature for a study on BSA[31] to compare the interfacial layer structure at standard conditions. The morphology of both transferred films showed connected small spherical dots which resembled that of BSA shown in literature.[31] Section analysis of the AFM image showed that the thickness of the protein layer is around 3 nm, which is in accordance with the "height" of a HSA molecule when it is lying flat at the AWI by neutron reflectivity study[18]

Thus, by CD, tensiometry and AFM, we conclude that minimally labeled, near-native HSA provides a useful model protein sample for studying assembly at the AWI by fluorescence microscopy.

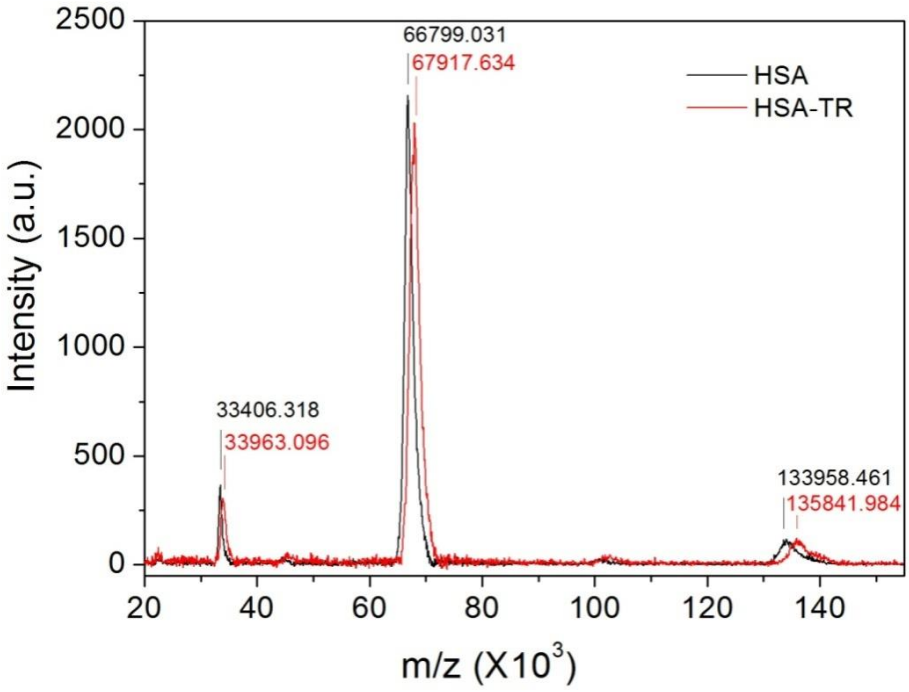

Figure 2.1 MALDI-MS spectra of HSA and HSA-TR

Black line is the spectra of HSA, and red line is the spectra of HSA-TR. From left to right, the peaks are assigned to $A + 2H^+$, $A + H^+$, and $2A + H^+$ for HSA and HSA-TR, respectively, where "A" represents the protein molecule.

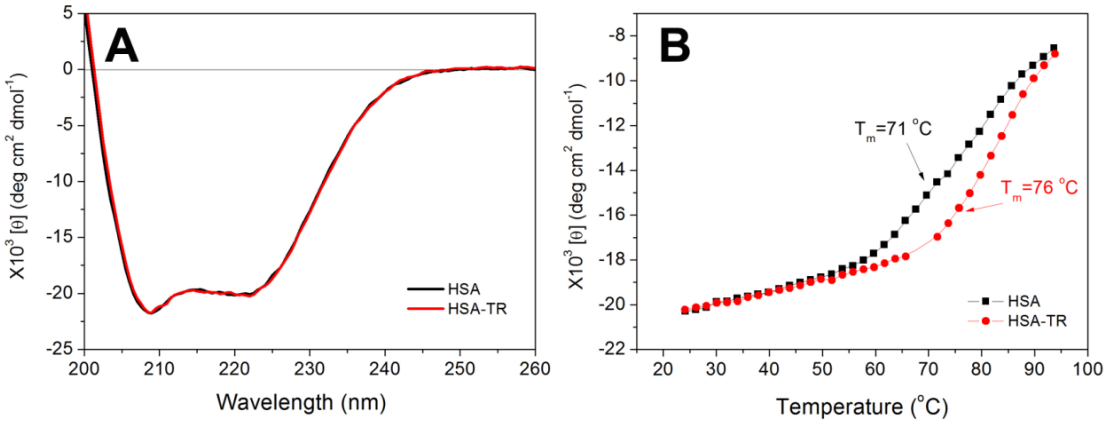

Figure 2.2 Characterization of HSA and HSA-TR by CD spectroscopy

(A) Far-UV CD spectra of HSA (black) and HSA-TR (red) at 25 ℃. (B) Thermal denaturation curves of HSA (black) and HSA-TR (red). The melting temperature T_m is 71 ℃ for HSA and 76 ℃ for HSA-TR. Thermal denaturation curves were recorded between 25-95 ℃ with a 2 ℃ increase and 120 s equilibration time for each step.

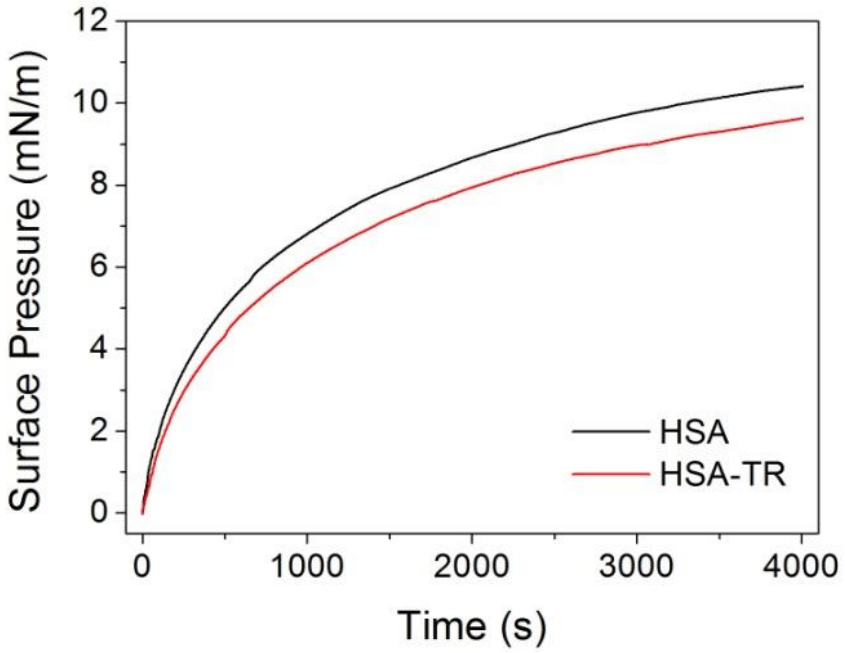

Figure 2.3 Surface pressure of HSA and HSA-TR

$C_{protein}$ = 0.10 mg/mL in 10 mM PBS buffer, pH = 7.2. Each curve is the average of two independent experiments.

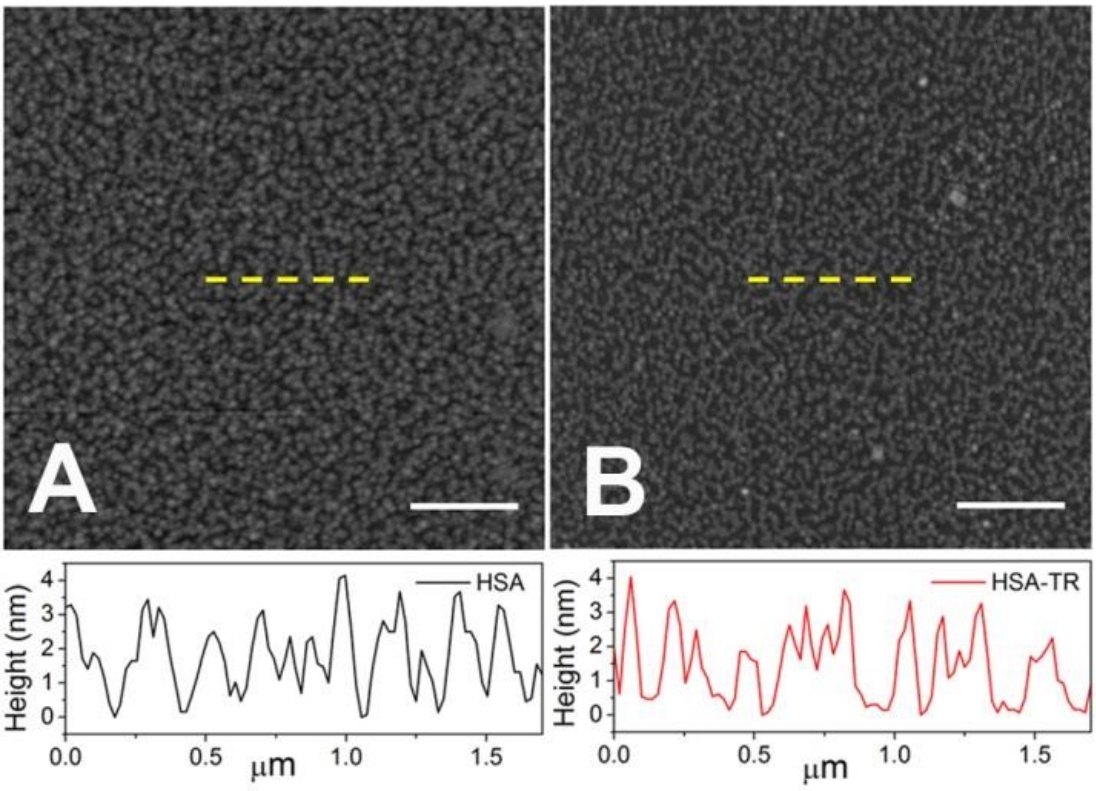

Figure 2.4 AFM images of HSA and HSA-TR films formed at the AWI and transferred onto mica surface

Initial subphase concentrations were 0.10 mg/mL, pH = 7.2. Top row: AFM images of (A) HSA, (B) HSA-TR. Scale bar: 1.0 μm. Bottom row: height of protein films plotted along yellow dashed line drawn in (A, black) and (B, red).

b. Effect of surface modification of imaging chamber with PEG

The imaging chamber is a microliter size reservoir of protein solution, in which the adsorption of proteins onto the solid surfaces will strongly compete with adsorption at the AWI. So we use mPEG-silane to covalently modify exposed hydroxyl groups on the inner chamber surfaces with a layer of PEG chains to reduce protein adsorption as shown in Figure 2.5.

The efficiency of reducing HSA-TR adsorption was subsequently monitored by confocal microscopy. In Figure 2.6, before surface modification with PEG, adsorption of HSA-TR on solid-liquid interface was observed as a small peak of fluorescence intensity from HSA-TR at solid-liquid interface (Figure 2.6 A2). After surface modification, no surface excess was observed at the solid-liquid interface by confocal imaging (Figure 2.6 B2). Same effects were observed on the PEG modified PDMS surface as shown in Figure 2.6 A3 and B3.

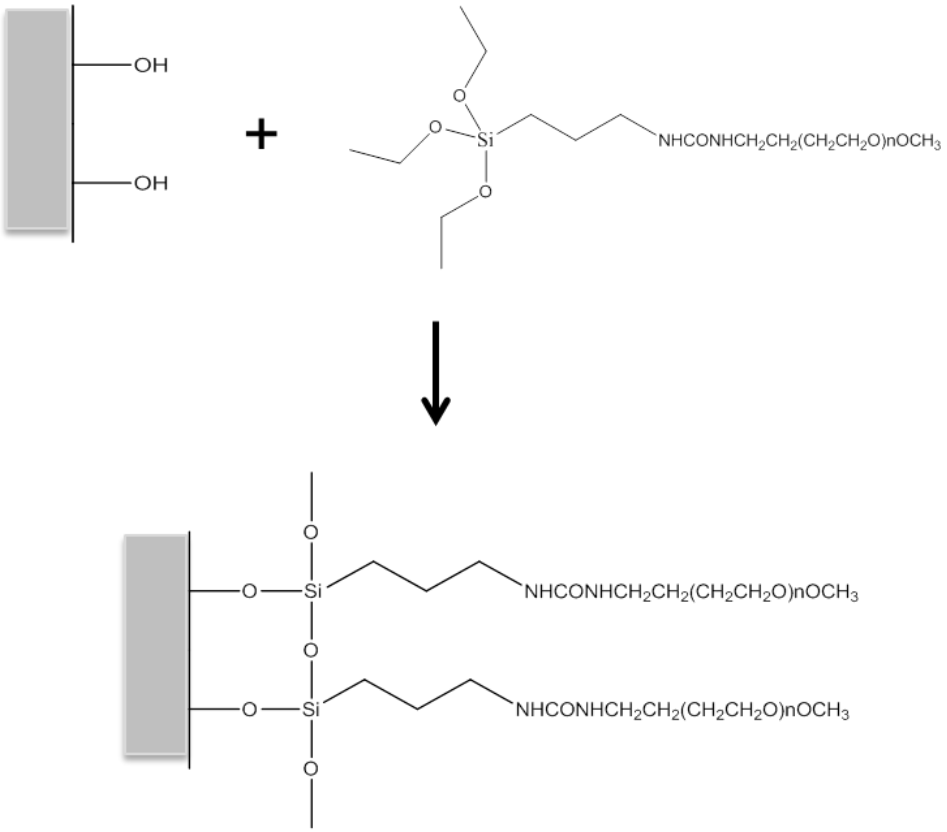

Figure 2.5 Covalent modification of surface hydroxyl groups by mPEG-silane.

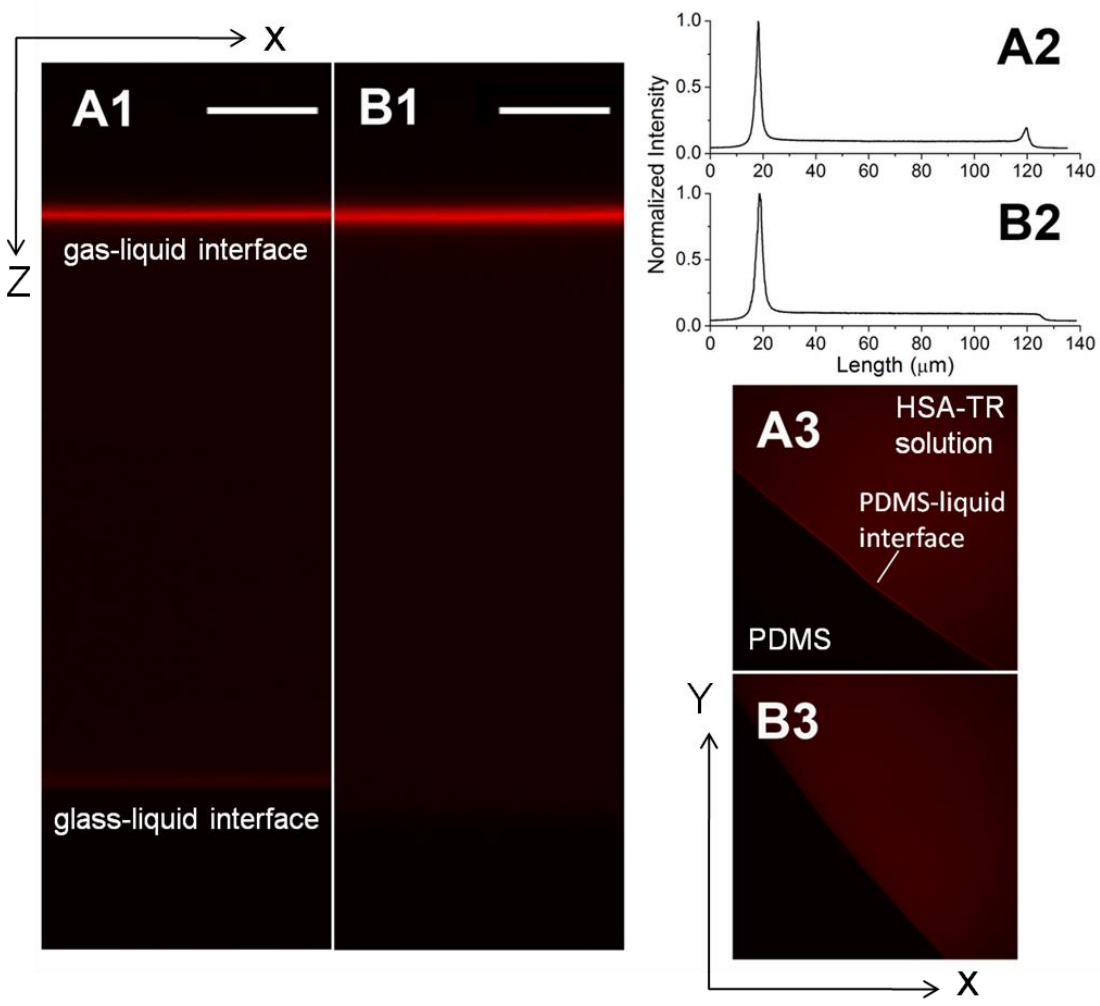

Figure 2.6 Confocal fluorescence images of HSA-TR in sample chamber before and after surface modification.

XZ-plane images of HSA-TR solution (C(HSA-TR) = 0.10 mg/mL in PBS buffer) in unmodified (A1) and modified (B1) sample chamber. (A2, B2) Intensity plot along z-axis of A1-B1. XY-plane images focused at the edge of unmodified (A3) and modified (B3) chamber (C(HSA-TR) = 0.50 mg/mL in PBS buffer).

c. Imaging protein assembly at the AWI by CLSM

As shown in Figure 2.7 A, HSA-TR was imaged in a specially designed, sealed chamber where the protein aqueous phase (10 μL in volume, 100-200 μm in thickness) coexisted with a layer of air, also 100-200 μm thick. The AWI formed in this chamber was parallel to the XY plane formed by the microscope stage. Images were collected by focusing either at the interface (called "XY plane images") or scanning perpendicular to the interface with a step size of 0.1 μm/step (called "XZ plane images"). HSA-TR was dissolved in PBS (ionic strength = 193 mM). When the concentration of HSA-TR ([HSA-TR]) was greater than or equal to 0.050 mg/mL, a uniform fluorescent layer was observed by confocal microscopy as shown in Figure 2.7 B. At optical resolution of ~0.2 μm, the 4X zoom image (Figure 2.7 C) showed no particular structure at the interfacial layer. However, when [HSA-TR] was less than or equal to 0.025 mg/mL, highly heterogeneous structure at the interface was observed as shown in Figure 2.7 D. The zoomed-in image (Figure 2.7 E) showed HSA-TR assembled into fractal structures of micrometer size. XZ-plane images further confirmed the different structures, where a fluorescent layer with uniform thickness was observed in Figure 2.7 F, while a discontinuous fluorescent layer was observed in Figure 2.7 G. Our results implied a surface-saturating bulk-solution concentration (C_B^{sat}) which fell between 0.025 mg/mL and 0.050 mg/mL under the condition of ionic strength at 193 mM in PBS. Below C_B^{sat}, the adsorbed proteins could not cover the AWI entirely, thus allowing the formation of protein domains at the interface. Previous reports using tensiometry and ellipsometry found that the critical concentration of BSA for covering the AWI is between 10^{-2} and 10^{-1} mg/mL,[7] which matches well with our results.

Although researchers in the field of protein adsorption generally accept the concept of C_B^{sat},[32,33] very few studies have revealed the microstructure of assembled proteins at concentrations below C_B^{sat}.[16] The study by Lee et al. using microrheology suggested that mechanical heterogeneity was present in a β-lactoglobulin layer at the AWI at a comparably low concentration.[34] It was predicted by early two-dimensional lattice-based simulations that fractal networks could be formed by diffusion-limited aggregation at low concentration.[35] The XY-plane images at the AWI (Figure 2.7 E), confirm the existence of fractal assembly at the AWI and a heterogeneous protein layer at the AWI at low subphase concentration.

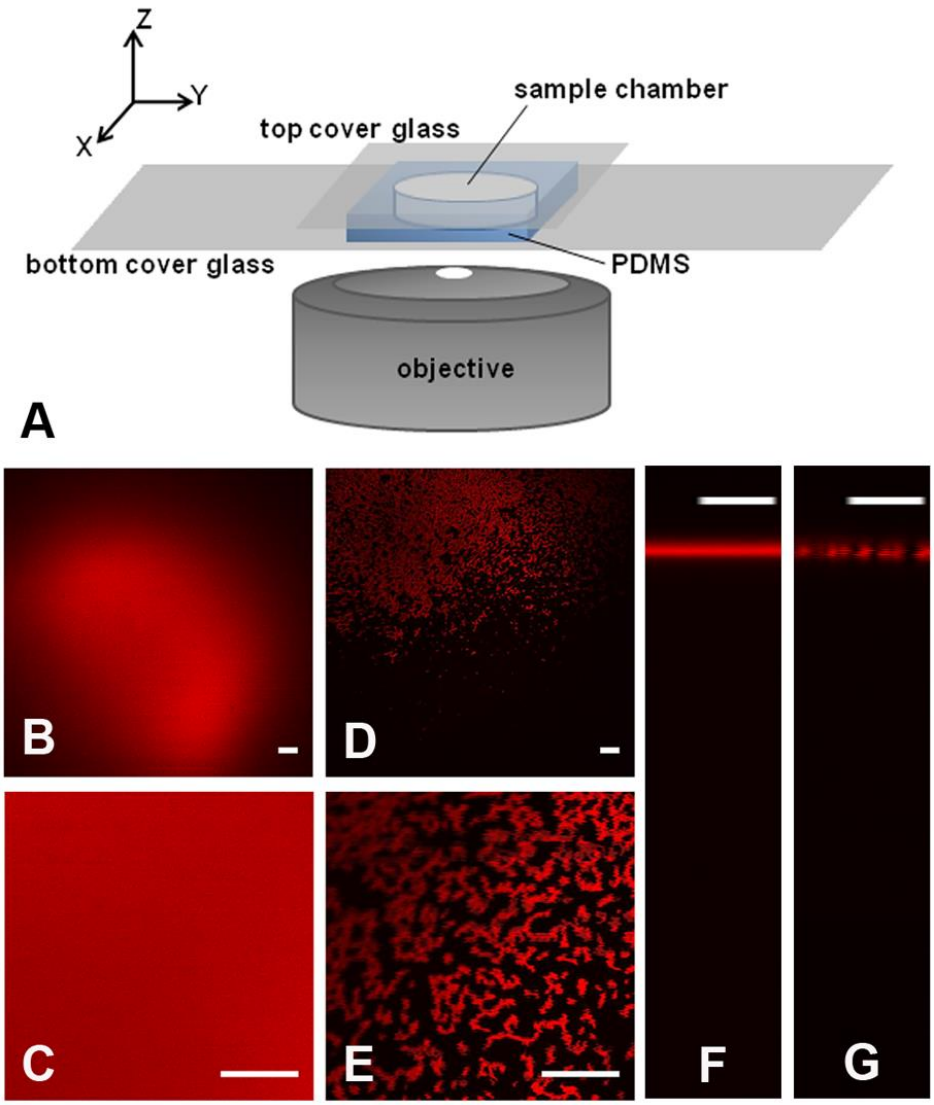

Figure 2.7 XY and XZ plane fluorescent images of protein assembly at the AWI

(A) Sample chamber and inverted microscope setup. (B-G) Confocal images of HSA-TR in PBS at pH = 7.2, ionic strength = 193 mM, at the AWI. (B, C) XY-plane images of HSA-TR (0.050 mg/mL) or (D, E) HSA-TR (0.025 mg/mL). Images (C) and (E) use 4X optical zoom. XZ-plane image across the AWI of (F) HSA-TR (0.050 mg/mL) or (G) HSA-TR (0.025 mg/mL). Scale bar: 20 μm.

d. Protein assembly controlled by ionic strength and reducing agent

We then varied the ionic strength and redox state of the solution and monitored the protein assemblies formed at the AWI. After pipetting solutions into the chamber, interfaces were left to age for 1 h before being imaged. A sample of 0.010 mg/mL HSA-TR in PBS (ionic strength = 53 mM) exhibited both fractal assembly (Figure 2.8 A) and interconnected "Swiss cheese" structures (Figure 2.8 B) at different locations at the interface. A Z-stack of XY plane images showed a high-resolution three-dimensional (3D) image of the interfacial protein layer (Figure 2.8 C) under the same conditions. The 3D image is an overlay of multiple XY plane images of size 45.0 μm × 45.0 μm, which were collected along the Z axis above and below the AWI, 10 μm in each direction (200 x 0.1 μm steps). This confirmed the "Swiss cheese" structure at the interface and showed almost no fluorescent signal from the subphase. Although the optical resolution along the Z-axis is ~2 μm for the confocal image, which is much larger than the estimated protein layer thickness (30-40 Å), the Z-stack image clearly indicated that protein domains only form at the AWI and assembly in the Z-direction was constrained compared to the hundreds-of-micron size domains formed in the XY plane.

Keeping the protein concentration constant, we increased the ionic strength of buffer to 530 mM. After 1 h aging time, we observed a homogeneous fluorescent layer (Figure 2.8 D), indicating an increased surface excess and shorter equilibration time. And in samples that had 30 mM DTT in the buffer, small fractal structures were observed (Figure 2.8 E), indicating a weaker interaction between adsorbed proteins.

We also studied the kinetics of interfacial layer formation when HSA-TR was dissolved in PBS, at high ionic strength (530 mM). A clear transition from crowded fractals (Figure 2.9 A) to "Swiss cheese" structure (Figure 2.9 B), and finally to a homogeneous fluorescent layer (Figure 2.9 C) was observed. In about 30 min, the AWI achieved equilibrium to form a homogeneous fluorescent layer. A recent study by Dhar et al. found a dramatic increase of surface viscosity over time in a BSA layer, and deduced a change in the organized structure.[36] Our study directly showed the morphological transition from fractals to a homogeneous, organized layer, which could serve to explain the observed increase in resistance to shear.

Our results indicated that solution conditions can modulate the structure of protein self-assembly. The isoelectric point of HSA is around 4.7.[17] Thus, at pH 7.2, HSA-TR is negatively charged. Electrostatic repulsion strongly affects the aggregation of HSA-TR at the AWI, leading to a low packing efficiency as shown in Figure 2.8 A, B. The co-existence of fractal and "Swiss cheese" structures indicates a non-equilibrium state, which is due to slow adsorption of proteins from the subphase hindered by the repulsive force from charged proteins already present at the interface. At higher ionic strength, where electrostatic repulsion between charged protein molecules is more effectively shielded, HSA-TR adsorbs faster to the interface and is able to pack more closely, thus forming a more uniform layer. As shown in Figure 2.9, full coverage of the AWI was achieved below C_B^{sat}. The value of C_B^{sat} between 0.025 mg/mL and 0.050 mg/mL was determined at a lower ionic strength (193 mM) after 1 h of adsorption time. At higher ionic strength (530 mM), the adsorption of bulk solution protein to the AWI was faster

due to less repulsion between adsorbed proteins and proteins from the bulk. In addition, the packing of protein molecules at the interface was more efficient, thus higher protein coverage was achieved.

It has been reported that proteins adsorbed at the AWI can form intermolecular disulfide bonds, which stabilize the protein network and enhance the elasticity of the adsorbed layer.[37] HSA has one reactive cysteine, Cys34, which could readily form a disulfide bond with adjacent proteins at the AWI. And post adsorption conformation change could result in the breaking of intramolecular disulfide bonds, providing more reactive sites for the formation of intermolecular disulfide bonds. Reducing agents such as DTT inhibit the formation of intermolecular disulfide bonds, thus only small aggregates remain, which are presumably held together by hydrophobic interactions. Vogler et al. have applied interfacial rheology to study HSA at the AWI, and found that adsorbed layers exhibit both viscous and elastic properties.[38] However, microrheology studies with BSA identified a primarily viscous protein film, without strong intermolecular-bond formation.[36] Our results support the hypothesis that elasticity arises from a network of intermolecular interactions.

It is worth mentioning that we also studied the effect of solution acidity on the protein assembly structure at the AWI. However, PDMS elastomer was not stable at acidic conditions, and leaching of PDMS oligomers was found to cause interesting features in the interfacial film. Detailed studies on PDMS and plasma proteins interactions were presented in Chapter 4.

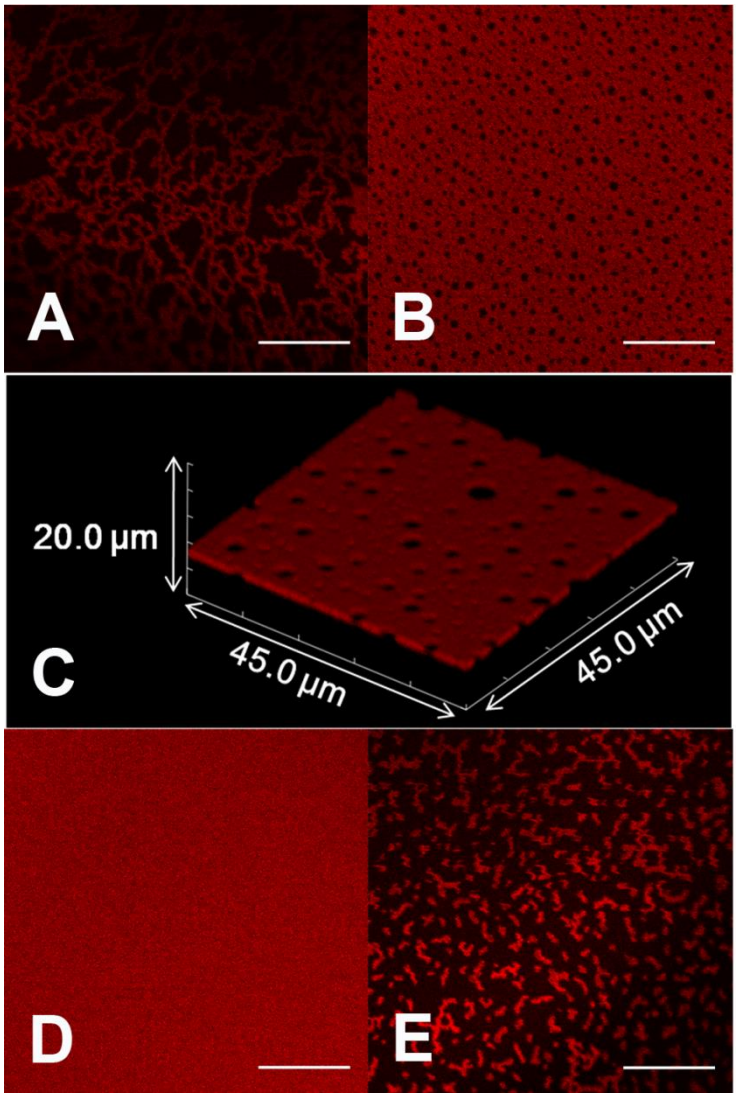

Figure 2.8 Morphology of protein assembly varied with ionic strength and addition of reducing agent

Self-assembly of HSA-TR (0.01 mg/mL) at the AWI in (A, B) PBS, pH = 7.2, ionic strength = 53 mM, (C) Rendered Z-stack of confocal images corresponds to (B) in the scanned volume of 45.0 µm × 45.0 µm × 20.0 µm. (D) PBS, pH = 7.2, ionic strength = 530 mM, (E) PBS with 30 mM DTT, pH =7.2, ionic strength = 53 mM. Scale bar: 20 µm.

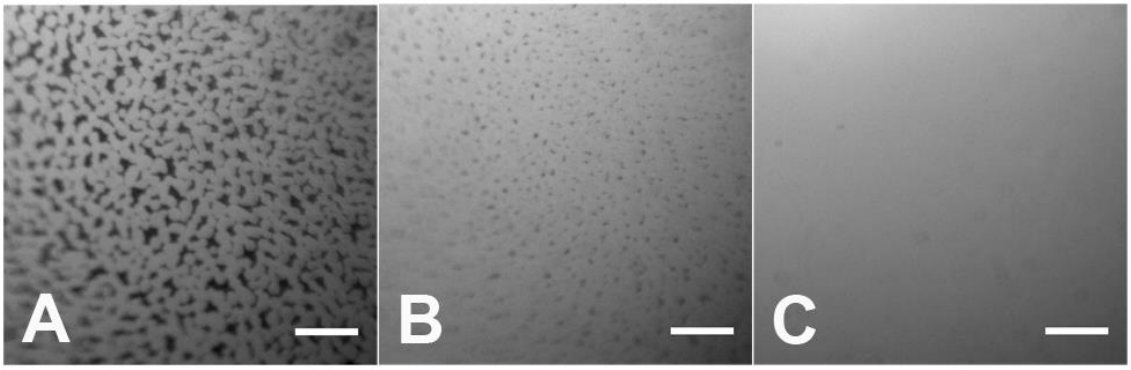

Figure 2.9 Epi-fluorescence images showing transition of heterogeneous domains into homogeneous layer.

C(HSA-TR) = 0.01 mg/mL, in PBS, pH = 7.2, ionic strength = 530 mM. (A) 3 min, (B) 8 min, (C) 36 min after protein solution introduced into chamber. Scale bar: 50 μm.

IV. Conclusions

In conclusion, we have applied fluorescence microscopy as an in situ method to study protein behavior at the AWI, on timescales of milliseconds to hours. We found that below surface-saturating bulk-solution concentration, self-assembly of a model protein HSA-TR shows varied morphologies at the AWI in response to changes of solution condition including protein concentration, ionic strength and redox state. The static and dynamic behavior of HSA-TR at the AWI is detected by our method. Our method should be easily accessible and applicable to study of other macromolecular self-assembly at the AWI. By the same approach, it is possible to study also the glass-water interface, and this could potentially be used to monitor competitive adsorption of surface-active species at both gas-liquid and solid-liquid interfaces. Our study shows the potential of controlling protein assembly at the AWI for biomaterials applications.

V. References

(1) Campbell, D. J.; Freidinger, E. R.; Hastings, J. M.; Querns, M. K.: Spontaneous assembly of soda straws. *J. Chem. Educ.* **2002**, *79*, 201-202.

(2) Bowden, N.; Terfort, A.; Carbeck, J.; Whitesides, G. M.: Self-assembly of mesoscale objects into ordered two-dimensional arrays. *Science* **1997**, *276*, 233-235.

(3) Huang, S. J.; Tsutsui, G.; Sakaue, H.; Shingubara, S.; Takahagi, T.: Experimental conditions for a highly ordered monolayer of gold nanoparticles fabricated by the Langmuir-Blodgett method. *J. Vac. Sci. Technol. B* **2001**, *19*, 2045-2049.

(4) Zhang, S. G.: Fabrication of novel biomaterials through molecular self-assembly. *Nat. Biotechnol.* **2003**, *21*, 1171-1178.

(5) Murr, M. M.; Morse, D. E.: Fractal intermediates in the self-assembly of silicatein filaments. *Proc. Natl. Acad. Sci. U. S. A.* **2005**, *102*, 11657-11662.

(6) Vlasova, I. M.; Mikrin, V. E.; Saletsky, A. M.: Investigation of CsCl-induced aggregation of serum albumin depending on pH by Raman spectroscopy method. *Laser Phys. Lett.* **2005**, *2*, 204-207.

(7) McClellan, S. J.; Franses, E. I.: Effect of concentration and denaturation on adsorption and surface tension of bovine serum albumin. *Colloids Surf. B. Biointerfaces* **2003**, *28*, 63-75.

(8) De Feijter, J. A.; Benjamins, J.; Veer, F. A.: Ellipsometry as a tool to study the adsorption behavior of synthetic and biopolymers at the air–water interface. *Biopolymers* **1978**, *17*, 1759-1772.

(9) Grigoriev, D. O.; Fainerman, V. B.; Makievski, A. V.; Kragel, J.; Wustneck, R.; Miller, R.: Beta-casein bilayer adsorption at the solution/air interface: experimental evidences and theoretical description. *J. Colloid Interface Sci.* **2002**, *253*, 257-264.

(10) Lu, J. R.; Su, T. J.; Thomas, R. K.: Structural conformation of bovine serum albumin layers at the air-water interface studied by neutron reflection. *J. Colloid Interface Sci.* **1999**, *213*, 426-437.

(11) Gunning, A. P.; Wilde, P. J.; Clark, D. C.; Morris, V. J.; Parker, M. L.; Gunning, P. A.: Atomic force microscopy of interfacial protein films. *J. Colloid Interface Sci.* **1996**, *183*, 600-602.

(12) Mackie, A. R.; Gunning, A. P.; Ridout, M. J.; Wilde, P. J.; Patino, J. R.: In situ measurement of the displacement of protein films from the air/water interface by surfactant. *Biomacromolecules* **2001**, *2*, 1001-1006.

(13) Mackie, A. R.; Gunning, A. P.; Ridout, M. J.; Wilde, P. J.; Morris, V. J.: Orogenic displacement in mixed beta-lactoglobulin/beta-casein films at the air/water interface. *Langmuir* **2001**, *17*, 6593-6598.

(14) Murray, B. S.; Xu, R.; Dickinson, E.: Brewster angle microscopy of adsorbed protein films at air-water and oil-water interfaces after compression, expansion and heat processing. *Food Hydrocolloids* **2009**, *23*, 1190-1197.

(15) Gluck, G.; Ringsdorf, H.; Okumura, Y.; Sunamoto, J.: Vertical sectioning of molecular assemblies at air water interface using laser scanning confocal fluorescence microscopy. *Chem. Lett.* **1996**, 209-210.

(16) Powers, E. T.; Kelly, J. W.: Medium-dependent self-assembly of an amphiphilic peptide: Direct observation of peptide phase domains at the air-water interface. *J. Am. Chem. Soc.* **2001**, *123*, 775-776.

(17) Theodore, P., Jr.: *All About Albumin*; Academic Press, Inc.: San Diego, 1995.

(18) Lu, J. R.; Su, T. J.; Penfold, J.: Adsorption of serum albumins at the air/water interface. *Langmuir* **1999**, *15*, 6975-6983.

(19) Narazaki, R.; Maruyama, T.; Otagiri, M.: Probing the cysteine 34 residue in human serum albumin using fluorescence techniques. *Biochim. Biophys. Acta, Protein Struct. Mol. Enzymol.* **1997**, *1338*, 275-281.

(20) Malonga, H.; Neault, J. F.; Tajmir-Riahi, H. A.: Transfer RNA binding to human serum albumin: A model for protein-RNA interaction. *DNA Cell Biol.* **2006**, *25*, 393-398.

(21) Amine-Reactive Probes. Invitrogen MP-00143, 2009.

(22) Greenfield, N. J.: Using circular dichroism spectra to estimate protein secondary structure. *Nature Protocols* **2006**, *1*, 2876-2890.

(23) Pace, C. N.; Grimsley, G. R.; Scholtz, J. M.: Denaturation of Proteins by Urea and Guanidine Hydrochloride. In *Protein Folding Handbook*; Buchner, J., Kiefhaber, T., Eds.; WILEY-VCH Verlag GmbH & Co. KGaA: Weinheim, 2005; pp 45-45-69.

(24) Bantchev, G. B.; Schwartz, D. K.: Structure of β-Casein layers at the air/solution interface: Atomic force microscopy studies of transferred layers. *Langmuir* **2004**, *20*, 11692-11697.

(25) Horcas, I.; Fernandez, R.; Gomez-Rodriguez, J. M.; Colchero, J.; Gomez-Herrero, J.; Baro, A. M.: WSXM: A software for scanning probe microscopy and a tool for nanotechnology. *Rev. Sci. Instrum.* **2007**, *78*, 013705.

(26) Jo, S.; Park, K.: Surface modification using silanated poly(ethylene glycol)s. *Biomaterials* **2000**, *21*, 605-616.

(27) Sui, G.; Wang, J.; Lee, C. C.; Lu, W.; Lee, S. P.; Leyton, J. V.; Wu, A. M.; Tseng, H. R.: Solution-phase surface modification in intact poly(dimethylsiloxane) microfluidic channels. *Anal. Chem.* **2006**, *78*, 5543-5551.

(28) Rasband, W. S.: ImageJ. ImageJ; U. S. National Institutes of Health, Bethesda, Maryland, USA, http://imagej.nih.gov/ij/, , 1997-2011.

(29) Goldberg, J. M.; Speight, L. C.; Fegley, M. W.; Petersson, E. J.: Minimalist probes for studying protein dynamics: thioamide quenching of selectively excitable fluorescent amino acids. *J. Am. Chem. Soc.* **2012**, *134*, 6088-6091.

(30) Messina, P.; Prieto, G.; Dodero, V.; Ruso, J. M.; Schulz, P.; Sarmiento, F.: Ultraviolet-circular dichroism spectroscopy and potentiometric study of the interaction between human serum albumin and sodium perfluorooctanoate. *Biopolymers* **2005**, *79*, 300-309.

(31) Gunning, A. P.; Wilde, P. J.; Clark, D. C.; Morris, V. J.; Parker, M. L.; Gunning, P. A.: Atomic force microscopy of interfacial protein films. *J. Colloid Interface Sci.* **1996**, *183*, 600-602.

(32) McClellan, S. J.; Franses, E. I.: Effect of concentration and denaturation on adsorption and surface tension of bovine serum albumin. *Colloid. Surface. B* **2003**, *28*, 63-75.

(33) Krishnan, A.; Siedlecki, C. A.; Vogler, E. A.: Traube-rule interpretation of protein adsorption at the liquid-vapor interface. *Langmuir* **2003**, *19*, 10342-10352.

(34) Lee, M. H.; Reich, D. H.; Stebe, K. J.; Leheny, R. L.: Combined passive and active microrheology study of protein-layer formation at an air-water interface. *Langmuir* **2010**, *26*, 2650-2658.

(35) Meakin, P.: Formation of fractal clusters and networks by irreversible diffusion-limited aggregation. *Phys. Rev. Lett.* **1983**, *51*, 1119-1122.

(36) Dhar, P.; Cao, Y. Y.; Fischer, T. M.; Zasadzinski, J. A.: Active interfacial shear microrheology of aging protein films. *Phys. Rev. Lett.* **2010**, *104*, 016001.

(37) Magdassi, S.: *Surface activity of proteins: chemical and physicochemical modifications*; Marcel Dekker, Inc.: New York, 1996.

(38) Ariola, F. S.; Krishnan, A.; Vogler, E. A.: Interfacial rheology of blood proteins adsorbed to the aqueous-buffer/air interface. *Biomaterials* **2006**, *27*, 3404-3412.

Chapter 3 Semi-quantitative confocal laser scanning microscopy method to study plasma protein adsorption in competition with Pluronic F-127 at the air-water interface[†]

I. Introduction

Pluronic® F-127 (F-127), also known as poloxamer 407, is an A-B-A-type tri-block copolymer, which has the chemical structure of PEO_m-PPO_n-PEO_m. The molecular weight of F-127 is ~12500 g/mol, in which the polyethylene oxide (PEO) constitutes ~70% and contributes to the hydrophilicity, while the polypropylene oxide (PPO) contributes to the hydrophobicity.[1] Clearly, F-127 is a non-ionic surfactant. A special property of F-127 is that its self-assembly is thermo-responsive—it undergoes phase transition from micellation to gelation as temperature increases.[2] This property has attracted many researchers' attention due to the application of F-127 as drug delivery vehicle to control the release of encapsulated small molecules, peptides and proteins inside of F-127 gels,[3] and it has also been approved for pharmaceutical use by the U.S. Food and Drug

[†] This chapter is adapted from (1) Lampe, J. W.; Liao, Z.; Dmochowski, I. J.; Ayyaswamy, P. S.; Eckmann, D. M.: Imaging macromolecular interactions at an interface. *Langmuir* **2010**, 26, 2452-2459. (2) Liao, Z. Z.; Lampe, J. W.; Ayyaswamy, P. S.; Eckmann, D. M.; Dmochowski, I. J.: Protein Assembly at the Air-Water Interface Studied by Fluorescence Microscopy. *Langmuir* **2011**, 27, 12775-12781.

Administration (FDA).[4] F-127 has a direct connection with plasma proteins because it has been shown to reduce air embolism after administration into rat vessels or human blood samples.[5-7] It is hypothesized that F-127 not only lowers the surface tension of the AWI but also reduces plasma protein adsorption at the bubble surface as a mechanism for reducing endothelial damage.[8] However, direct evidence of F-127 decreasing plasma protein adsorption at the AWI has not been reported to our knowledge and the interaction between the two moieties at the AWI is not well-understood.

Meanwhile, it is proposed that surfactants displace proteins from the AWI heterogeneously described by an "orogenic" model from previous studies of milk proteins and surfactants used in food additives.[9-11] The orogenic model describes a mechanism that surfactant localizes at the defects in the heterogeneous protein film, and then aggregates at these sites which leads to compression of the protein network. When the surfactant domains grow large enough, they push the proteins back into the bulk phase, effectively displacing proteins from the AWI.[11] The experimental evidence mostly comes from AFM and fluorescence images of transferred films of protein and surfactant mixtures.[10,12] In situ measurements have only been reported by Brewster Angle Microscopy,[13] and aspects of dynamic transitions remain unexplored.

In this chapter, we have applied semi-quantitative CLSM fluorescence methods to study plasma-protein adsorption at the AWI in competition with F-127. A ratiometric method enables semi-quantitative measurement of the amount of protein at the interface based on differences in the fluorescence intensity in the bulk and at the interface. Moreover, kinetic information and morphology of HSA and F-127 mixture at the AWI is

also revealed. Our study identifies pitfalls of this method, and limitations in the precise measurement of surface protein concentration.

II. Material and experimental setup

a. General reagents

Phosphate buffered saline (PBS) was used as the buffer throughout this chapter unless otherwise stated. The PBS buffer solution was made by dissolving 136 mM NaCl, 8.1 mM Na_2HPO_4, 2 mM KCl, 1.5 mM KH_2PO_4, and 31 mM NaN_3 in DI water. The PBS buffer was maintained at pH 7.4 and stored at room temperature. Human fibrinogen labeled with Oregon Green (HFib-OG, Cat# F7496) was purchased from Life Technologies. Human serum albumin (HSA, Cat# A3782) was purchased from Sigma and used without further purification. Proteins were dissolved in PBS by votexing, then filtered by sterilized Millex® Syringe Filter Units (Cat# SLGV004SL, Millipore) with 0.22 μm pore size. Pluronic F-127 10% solution in water (MW~12500, Cat# P-6866) was purchased from Life Technologies. HSA was covalently labeled by fluorophores following the same steps described in Chapter 2 IIb. Concentrations of protein or dye-labeled protein stock solution were measured by Lowry assay (Thermo Scientific).

b. CLSM setup

The CLSM setup is the same as described in Chapter 2. The Oregon Green dye was excited by the argon laser (488 nm, 30 mW), Texas Red was excited by HeNe laser (543 nm, 1 mW). Fluorescence recovery after photobleaching (FRAP) experiments were carried out on the same confocal microscope with an Olympus SIM scanner unit that allowed selectively bleach multiple regions in the same frame. A 351 nm laser at 100%

power was used to photobleach small regions of the protein layer at the AWI for 20 s. The confocal images of the regions were captured before, during, and after photobleaching using a 543 nm laser with a dwell time of 2 μs/pixel.

III. Results and discussion

a. Methodology

We initially developed the semi-quantitative method in a droplet system, shown in Figure 3.1 A. The droplet of interest, which was 10 μL in volume, was deposited on the coverslip of the MatTek Petri dish. The lid was kept closed after addition of droplet. The space surrounding the coverslip area was filled by a donut-shaped sponge wetted with DI water to control the humidity and reduce the evaporation of sample droplet. The Petri dish was cleaned with HPLC grade ethanol and water between each use. The focal plane was about 150 μm above the bottom coverglass to reduce light scattering from the glass surface. A representative fluorescence image of a HSA-TR droplet was shown in Figure 3.1 B. The bright rim between the dark gas phase and the weakly fluorescent liquid phase was the AWI where HSA-TR was concentrated due to adsorption. Then a rectangular region of interest (ROI) was chosen with length of 200 pixels along the radial axis of the droplet, and width of 50 pixels (noted as x-axis and y-axis respectively in Figure 3.1 B). Fluorescence intensity was first averaged by pixels along the y-axis and then plotted along the x-axis (Figure 3.1 C).

Using this method, we studied HFib-OG in competition with F-127 at the AWI by comparing the intensity profiles. In Figure 3.2, two concentrations of HFib-OG were chosen. Without F-127, the intensity peak of HFib-OG at both concentrations at the

interface was observed, showing that HFib-OG was prone to adsorb at the interface. With the addition of F-127 to 80 μM, the intensity peaks at around 7 μm from the origin of the ROI disappeared, indicating that HFib-OG was competed off the interface. This interesting finding encouraged us to develop further the CLSM method to investigate how F-127 competes with plasma proteins at the AWI. Applying the imaging setup described in Chapter 2, we studied both the adsorption competition of the protein/F-127 mixture and phase behavior of the interfacial layer.

The semi-quantitative method was further developed in the home-built imaging chamber system. The advantage of the imaging chamber was that the AWI could be studied by both XY scan (morphological information) and XZ scans (semi-quantitative intensity information). The fabrication of the imaging chamber was detailed in Chapter 2 and is omitted here. An XZ plane image taken in the imaging chamber is shown in Figure 3.3 A. The image is equivalent to the ROI in Figure 3.1 B rotated clockwise by 90 degrees. Images were analyzed with MATLAB to enable facile analysis of multiple frames (all original codes included in Appendix I), following the main algorithm shown in Figure 3.3 B. A single image or multiple images were first loaded into MATLAB using the program named “readtif”. Then the main calculations were done by the program named “PC”. In this program, TIFF format RGB images were converted into grayscale images and background intensity was subtracted from ROI for intensity analysis. Intensity was plotted along the z-axis (Figure 3.3 B).

The total intensity I_{total} in ROI is determined to be:

$$I_{total} = \sum_{j=1}^{n} I_j \qquad \text{(Eq 3.1)}$$

I_j is the averaged intensity of pixel j along x-axis, n is the total number of pixels along z-axis of ROI. Then average bulk intensity $I_{avgbulk}$ is:

$$I_{avgbulk} = \frac{\sum_{j=m}^{n} I_j}{n-m+1} \qquad \text{(Eq 3.2)}$$

m is a starting pixel chosen from the bulk region, which is at the right shoulder of the interface intensity peak. Then bulk intensity I_{bulk} and interface intensity I_{int} were calculated by:

$$I_{bulk} = I_{avgbulk} \times (n-z+1) \qquad \text{(Eq 3.3)}$$

$$I_{\text{int}} = I_{total} - I_{bulk} \qquad \text{(Eq 3.4)}$$

z is the first pixel at the left shoulder of the interface intensity peak where $I_z \geq I_{avgbulk}$.

Finally, partition coefficient (P) which represents the partitioning of dye-labeled protein between bulk phase and interface phase was determined:

$$P = \frac{I_{\text{int}}}{I_{avgbulk}} \qquad \text{(Eq 3.5)}$$

The definition of P is analogous to the definition of surface excess. Surface excess is a two-dimensional quantity, while P here is unitless. Assuming the bulk concentration change is minimal after protein adsorption at the interface, the surface concentration (a

three-dimensional quantity) could be roughly correlated to $P \times C_{bulk}$. The reasons that $P \times C_{bulk}$ cannot precisely quantify the surface concentration are discussed in the last section of this chapter.

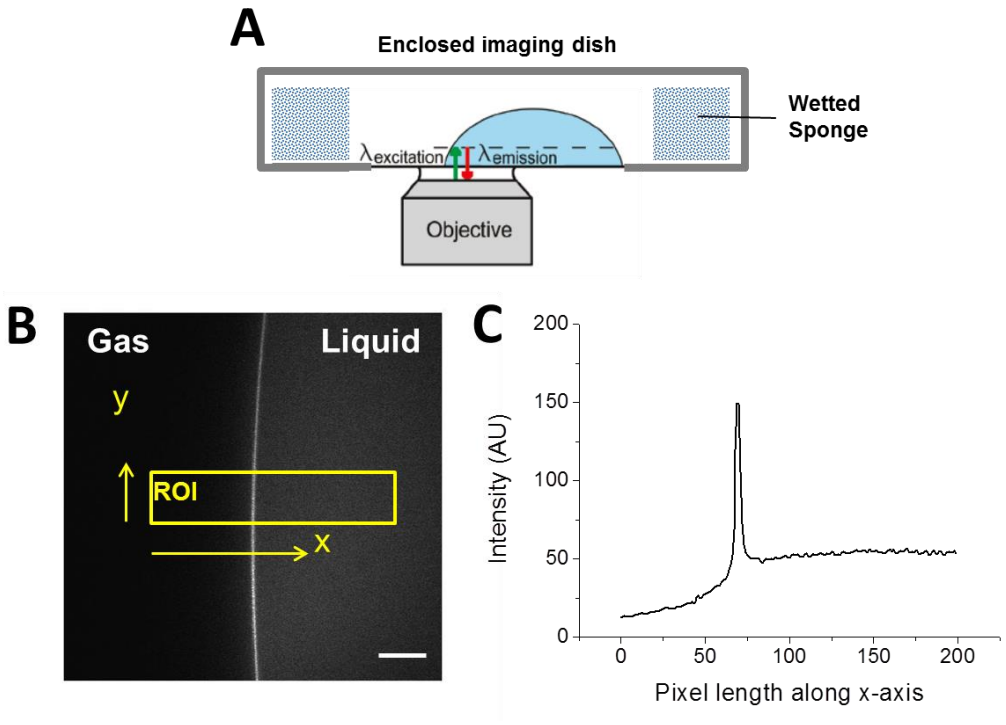

Figure 3.1 Experimental setup and data analysis of the droplet system to study protein adsorption at the AWI.

(A) Cartoon showing the imaging setup. The horizontal dashed line indicates where the image slice was taken. (B) A representative image of the AWI of a BSA-TR aqueous droplet. Yellow box indicates the region of interest (ROI) selected for intensity analysis. Scale bar: 20 μm. (C) Intensity profile of the ROI. The pixel intensity was averaged along the y-axis in ROI then the intensity profile was plotted along the x-axis.

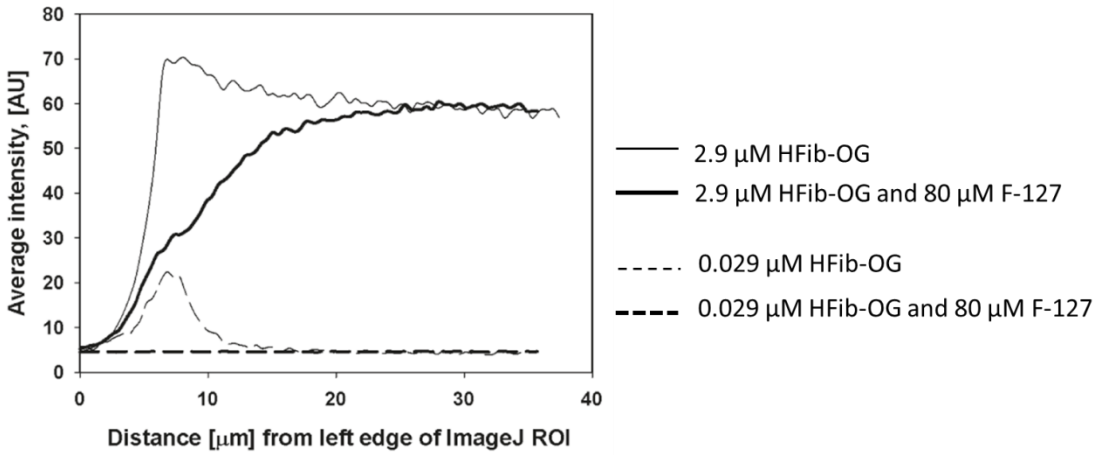

Figure 3.2 Intensity profiles of F-127 and HFib-OG mixtures show that F-127 blocks protein adsorption.

Plot shows four intensity profiles measured at 1 h near the droplet edge.

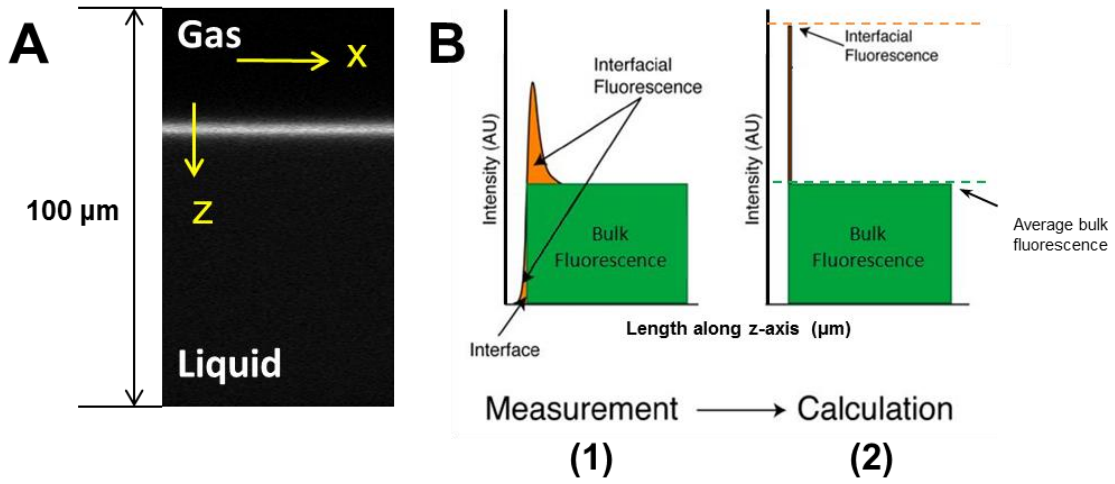

Figure 3.3 Analysis of an XZ plane image to obtain partition coefficient.

(A) An XZ plane image, 100µm in depth, scanning across the AWI of a HSA-TR sample in imaging chamber. (B) Calculating partition coefficient from the intensity profile. Interfacial fluorescence is the sum of the orange area re-assigned to a single pixel, while bulk fluorescence is the average pixel intensity of the green area. Partition coefficient is the ratio of interfacial fluorescence (orange dashed line) to average bulk fluorescence (green dashed line).

b. HSA-TR/F-127 adsorption competition at AWI

HSA-TR was used in our study because it is the most abundant protein in human serum,[14] and also because the surface activity and protein conformation before and after labeling were well characterized in our studies. We first measured the partition coefficient of HSA-TR at different bulk concentrations as the standard curve. *P* dropped dramatically from 0.05 mg/mL to 0.25 mg/mL, and slowly decreased above 0.5 mg/mL (Figure 3.4). This is in accordance with the assumption that the energy barrier for proteins to adsorb at the interface increases with increasing surface coverage. Once full coverage of the interface by protein is achieved, the proteins adsorb loosely in the sub-layer, reflected in a small change in *P*. From earlier microscopy studies mentioned in Chapter 2, we learned that at 0.05 mg/mL, a uniform layer was observed by CLSM at the AWI. However, from the partition coefficient trend, we could deduce that HSA-TR doesn't form a densely packed interfacial layer until the concentration reaches ~0.5 mg/mL.

Next, we measured the partition coefficient of the HSA-TR/F-127 mixture. In Figure 3.5, the concentration of HSA-TR was fixed at 0.1 mg/mL and 0.5 mg/mL, respectively, while the concentration of F-127 in solution changed. P was measured 1h after the introduction of solution into the chamber. Addition of F-127 from 0~0.01 mg/mL slightly decreased *P* compared to the value measured in HSA-TR-only samples indicated by the red dashed lines. As concentration of F-127 further increased, phase separation was observed in the XY-plane images, and *P* became an averaged value of multiple different areas. At concentrations above the range where lateral phase separation was observed,

fluorescence intensity at the interface was completely lost, which resulted in *P* dropping to 0 and showed that HSA-TR was completely competed off the interface. Higher concentration of HSA-TR required higher concentration of F-127 to cause the lateral phase separation and drive the proteins off the interface.

Furthermore, the morphology of the interfacial layer was observed to change with concentration of surfactant and time. Observed at 10 min after AWI formation (top row in Figure 3.6 from left to right), interfacial structures changed from an evenly fluorescent layer at low surfactant concentration (Figure 3.6 A) to a fluorescent layer with "cracks" (Figure 3.6 B); and with further increase in the amount of F-127, the dark area in the interfacial layer expanded while the fluorescent regions shrank into small "islands" (Figure 3.6 C and D). With even higher concentrations of F-127, the strong fluorescent signal from the interface was completely lost. The initial interfacial layers were heterogeneous, formed by the premixed solution with the protein/surfactant ratio *n(HSA-TR)/n(F-127)* between 4-1. After a longer aging time of the interface, the overall fluorescent signal was reduced in the bottom row compared to the top in Figure 3.6, and the boundary between the bright and dark regions became blurry. The disappearance of the sharp boundary indicates better mixing due to diffusion of protein and F-127 in the film. In HSA-TR at 0.50 mg/mL mixed with F-127 solution, the range of *n(HSA-TR)/n(F-127)* in which phase separation was observed at 10 min after interface formation was 6-2.

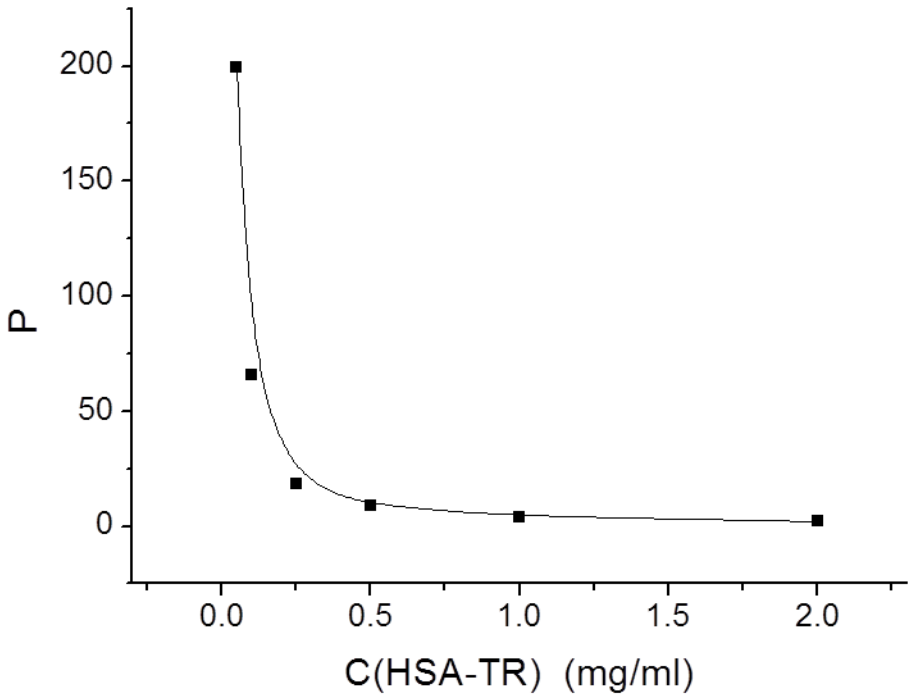

Figure 3.4 Partition coefficient of HSA-TR as a function of bulk concentration.

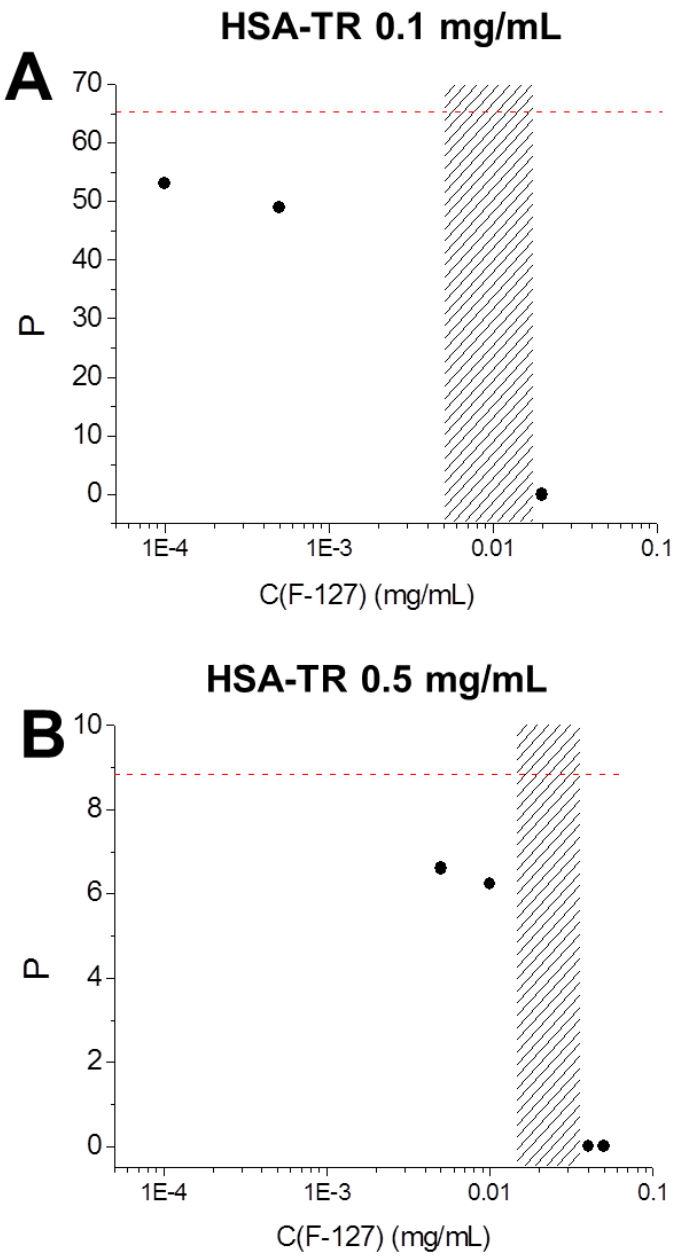

Figure 3.5 Change of partition coefficient *P* with increase in F-127 concentration.

Red dashed lines indicate *P* of HSA-TR at the same bulk concentration without F-127 present. Shadow areas indicate the concentration range where phase separations were observed at the AWI. P was measured 1h after the introduction of solution into the chamber.

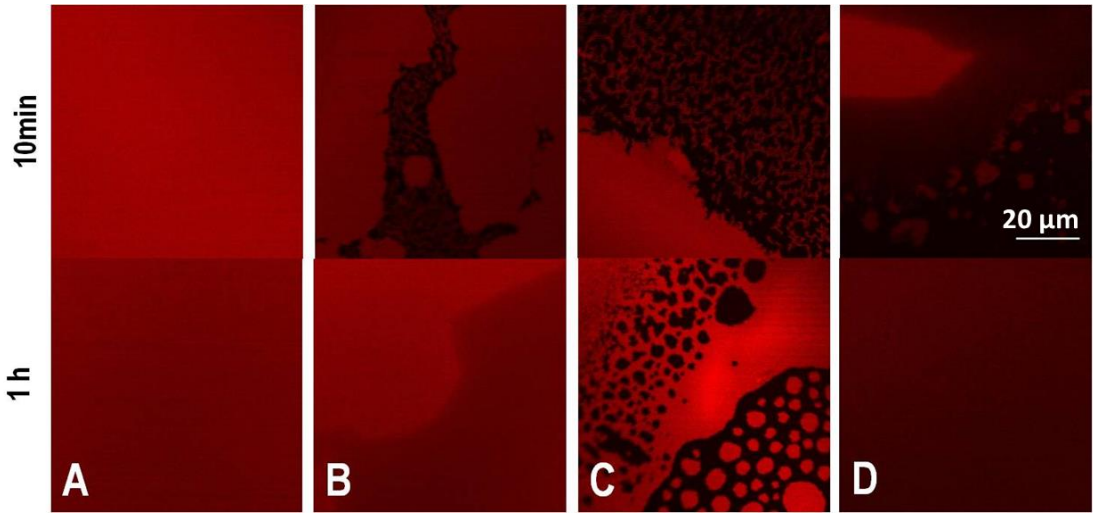

Figure 3.6 Phase separation in adsorbed HSA/F-127 layer at the AWI.

The bulk concentration of HSA-TR was constant at 0.10 mg/mL, while the bulk concentration of F-127 increased from 0.001-0.020 mg/mL. The corresponding molar ratio of HSA-TR/F-127 is listed in Error! eference source not found..

Table 3.1 concentration of F-127 and molar ratio of HSA-TR/F-127 corresponding to Figure 3.6

	A	B	C	D
c(F-127) (mg/mL)	0.0010	0.0050	0.010	0.020
$\frac{n(HSA-TR)}{n(F-127)}$	19	4	2	1

c. FRAP experiments of HSA-TR/F-127 mixtures

Proteins form viscoelastic networks at the AWI, causing the protein to have molecular mobility two orders of magnitude smaller than that of protein-surfactant mixtures.[15] Thus, we expect that the fluorescence recovery rate of protein-rich regions should be much slower than for surfactant-rich regions. To test this hypothesis, we conducted a fluorescence recovery after photobleaching (FRAP) experiment to assess the mobility of the interfacial layer with an HSA-TR/F-127 solution of HSA-TR at 0.10 mg/mL and F-127 at 0.0050 mg/mL. Two circular regions in strongly fluorescent and weakly fluorescent regions were bleached simultaneously with near-UV laser beam for 20 s shown in Figure 3.7. Images were taken both before and after bleaching using an attenuated 543 nm laser as excitation source. Ninety seconds after irradiation, the bleached region on the strongly fluorescent side became smaller, and after 25 min, the intensity almost fully recovered, while the bleached region on the weakly fluorescent did not change shape or intensity over time. A FRAP control experiment was performed at the interfacial layer of HSA-TR: after 520 s there was no change in the photobleached region (Figure 3.8). It could be deduced that the large difference in the intensity recovery rate indicated segregation of "protein-rich" and "surfactant-rich" regions at the interface. The regions with stronger fluorescence intensity were mostly composed of HSA-TR, while regions with weaker fluorescence intensity were composed of HSA-TR mixed with F-127. Proteins in the surfactant-rich region were separated by surfactant molecules and more free to diffuse, making the lateral mobility of HSA-TR much higher than in the protein-rich region. However, mass transport in the surfactant-rich domain was not homogeneous, indicated by the change of shape of the bleached region during

fluorescence recovery. This also prevented us from deriving the diffusion coefficient from the FRAP experiment.

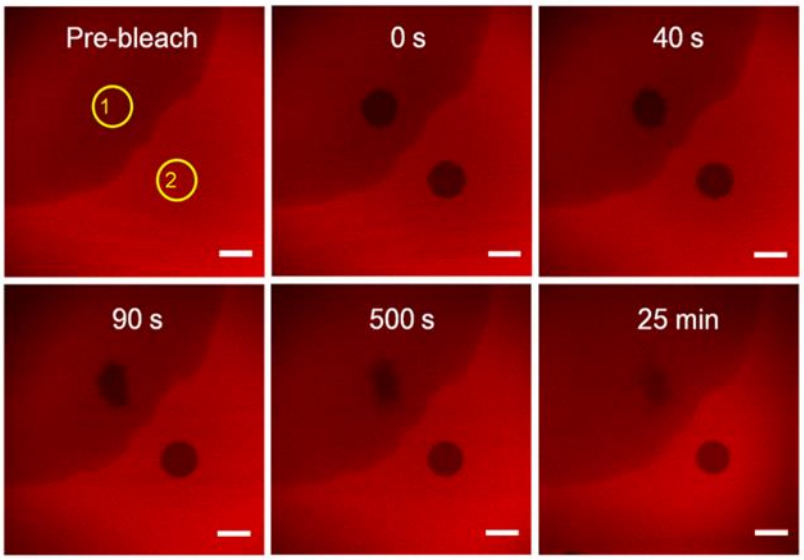

Figure 3.7 FRAP experiment of the mixed HSA-TR and F-127 interfacial layer.

ROIs (yellow circles) are the selected photobleached areas. ROI-1 is in surfactant-rich domain, ROI-2 is in HSA-TR-rich domain. The initial subphase concentration was C(HSA-TR) = 0.10 mg/mL, C(F-127) = 0.0050 mg/mL. Scale bar: 20 μm.

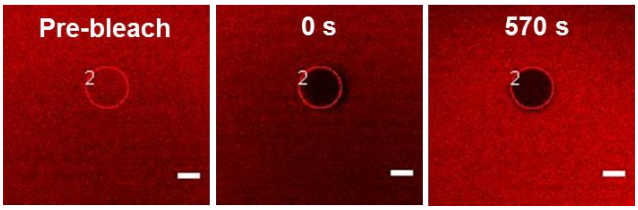

Figure 3.8 FRAP experiment of the HSA-TR interfacial layer.

ROI-2 (red circle) is the selected photobleached area. C(HSA-TR) = 0.10 mg/mL. Scale bar: 10 μm.

d. Dynamics of the phase behavior in HSA-TR/F-127 layer

We found that in the HSA-TR/F-127 mixtures, the protein-rich regions exhibited time-dependent morphological changes, which motivated us to study this dynamic phenomenon in greater detail. The results shown in Figure 3.9 are images taken by focusing at the AWI with HSA-TR (0.50 mg/mL) mixed with F-127 (0.015 mg/mL). Figure 3.9 A shows three images focused at the same region from 35 min to 60 min after pipetting solution into the chamber. Protein islands in small circular shapes with areas of 10-100 μm^2 were seen. The ROIs (yellow boxes in Figure 3.9) highlight some interesting observations: In ROI-1, small protein islands coalesced with surrounding protein islands to form a larger island at 50 min compared to the image at 35 min. In ROI-2 small black holes could be seen starting from 50 min, indicating F-127 replaced HSA-TR at these spots and formed cavities inside the protein-rich regions. In ROI-3, movement of the frontier of surfactant-rich region could be observed. It is evident that as time elapsed, the surfactant-rich regions continuously expanded. And in ROI-4, small protein islands merged into mesh-like networks. We analyzed the size distribution of protein islands using ImageJ (Figure 3.9 B).[16] Area fraction was defined as the sum of surface area of protein islands of the same size, divided by the total area of protein islands. A clear increasing trend in the island size distribution is shown in Figure 3.9 B. The average area of protein islands grew from 24 μm^2 (35 min) to 57 μm^2 (60 min). The movement of protein islands was also observed by using a faster scan rate of 30 frames/s, and the protein islands were observed to exhibit Brownian motion.

The observation of surfactant perforating the protein domains and the expansion of the surfactant-rich region is in accordance with the orogenic model.[11] This model states that

surfactants displace proteins from the interface by first perforating the protein layer, forming defects or holes. Then as the surfactants continue to accumulate in these regions, the surfactant regions expand and the protein layer is forced to buckle and extend into the subphase until the protein layer eventually collapses.[12] A different displacement mechanism has been shown in lung surfactant/polyethylene glycol/albumin mixtures, which suggests that the competitive adsorption process may be system-dependent.[17] Theoretical models have been developed to explain the adsorption kinetics and equilibrium states of mixed protein/surfactant solutions in surface tension and surface rheology studies.[18] Complementing these studies, our work provides more detailed information about the location of protein and surfactant at the interface and the structure of the assembly. The coalescence phenomenon observed in our study shows that neighboring protein domains have a tendency to reform a connected network whereas other protein is being displaced by surfactant, thus highlighting two competing processes of protein domain coalescence and protein displacement by surfactant in HSA-TR/F-127 mixtures.

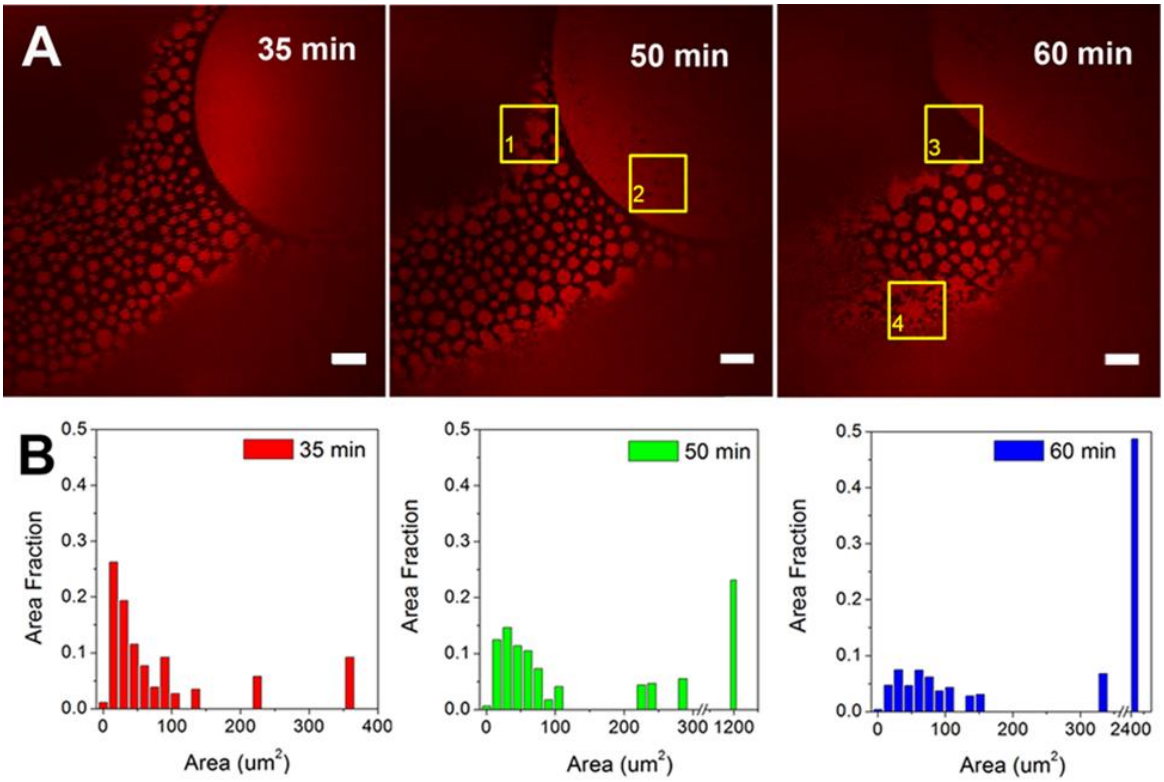

Figure 3.9 Coalescence of protein islands over time.

(A) Confocal fluorescence images taken at 35, 50 and 60 min after introduction. Scale bar: 20 μm. (B) Histograms of protein island size distribution. The initial subphase concentration was C(HSA-TR) = 0.50 mg/mL, C(F-127) = 0.015 mg/mL. ROI-1 indicates region (yellow box) where small protein islands coalesced with surrounding protein islands to form a larger island; ROI-2 demonstrates that small black holes formed in the region; ROI-3 indicates movement at the frontier of a surfactant-rich region; ROI-4 shows where small protein islands merged into mesh-like networks.

e. Validation and limitation of partition coefficient

First, to confirm that labeling protein with fluorophore did not change the surface activity, surface pressures of BSA vs. BSA-TR and HFib vs. HFib-OG at the same bulk concentration were measured (Figure 3.10). The surface pressure curves of BSA and BSA-TR at 0.01 mg/mL were nearly identical. The surface pressure of HFib-OG was slightly lower than that of HFib. Because the number of OG dyes covalently attached to HFib (DPR = 13) was much higher than the number of TR on BSA (DPR = 3), further reducing the DPR may diminish the change in surface pressure after labeling.

Next, to link the fluorescence intensity with protein concentration, the parameters in the following equation were examined:[19]

$$\frac{I_{\text{int}}}{I_{bulk}} = \frac{OD_{\text{int}}}{OD_{bulk}} \times \frac{n_{bulk}^2}{n_{\text{int}}^2} \times \frac{\phi_{\text{int}}}{\phi_{bulk}} \times \frac{c_{\text{int}}}{c_{bulk}} \qquad \text{(Eq 3.6)}$$

where *OD* is the optical density, *n* is the refractive index of the medium at the interfacial layer and the bulk. Φ is the quantum yield of the fluorophore.

The interface is crowded with labeled proteins due to adsorption, thus the inner filter effect could play a part in changing the fluorescence intensity at the interface.[19] To keep *n* and Φ the same and just test the effect of optical density, we measured the intensity of dye-labeled protein in solution over a hundred-fold range of concentrations. Eq 3.6 could be written as:

$$\frac{I_1}{I_2} = \frac{OD_1}{OD_2} \times \frac{c_1}{c_2} \qquad \text{(Eq 3.7)}$$

or, $$\frac{\left(I_1 / c_1\right)}{\left(I_2 / c_2\right)} = \frac{OD_1}{OD_2} \quad \text{(Eq 3.8)}$$

Images of the bulk were taken, and the intensity was quantified and plotted in Figure 3.11. A linear fit passing through the origin is found in both BSA-TR solution and HFib-OG solution at different laser power and photomultiplier sensitivity (Table 3.2). The different settings were chosen to ensure the intensity is above detection threshold and below saturation. At the same settings, I_n / c_n is the same, so the OD was constant within the range we tested (0.05-5 mg/mL).

The change of refractive index of protein solution as a function of concentration has been thoroughly studied by ellipsometry previously, and a linear correlation between *n* and *C* is reported:[20]

$$n = k \times c + n_{water} \quad \text{(Eq 3.9)}$$

n_{water} is the refractive index of water which equals 1.33. *k* is the refractive index increment, which is ~1.8 $\times 10^{-4}$ mL/mg for proteins.[20] Due to the small value of *k*, the change of refractive index is less than 7% even when the protein concentration reaches 500 mg/mL, thus could be treated as a constant.

Last but not the least, the quantum yield is highly dependent on the micro-environment where the fluorophore resides. Because of the potential for protein unfolding as well as the change in orientation at the interface greatly affect the quantum yield,[21,22] Φ is hard to

be defined precisely during the course of protein adsorption at the AWI. Thus Eq 3.6 could only be simplified as far as:

$$P = \frac{I_{\text{int}}}{I_{bulk}} = \frac{\phi_{\text{int}}}{\phi_{bulk}} \times \frac{c_{\text{int}}}{c_{bulk}} \qquad \text{(Eq 3.10)}$$

Therefore, partition coefficient contains both information on conformational change and surface concentration. If we define $P \times C_{bulk}$ as the apparent surface density with a unit of mg/mL, then we could compare our data to surface excess (mg/m^2) values reported in the literature, by dividing $P \times C_{bulk}$ by the pixel resolution in Z-direction (l_{pixel}). Using BSA-TR as an example, we measured P at different BSA-TR bulk concentrations and converted it to apparent surface excess (Γ') through Eq 3.11:

$$\Gamma' = \frac{P \times c_{bulk}}{l_{pixel}} \qquad \text{(Eq 3.11)}$$

Figure 3.12 indicates that although the apparent surface excess estimated by the CLSM method falls in the same range of the surface excess measured by neutron reflectivity and radioactivity, the trend of surface excess change is inconsistent at lower protein concentrations (0.05-0.2 mg/mL), which is likely due to the change of quantum yield of fluorophores induced by the change of conformation of BSA at the AWI. The lower the bulk concentration, the larger the conformational change of proteins at the interface, due to the small surface coverage of proteins.[23] Hence, it complicates the interpretation of P, and highlights the limitation of this method. The information on the either surface concentration or conformation is only reliable when the other parameter is known or the change is minimal.

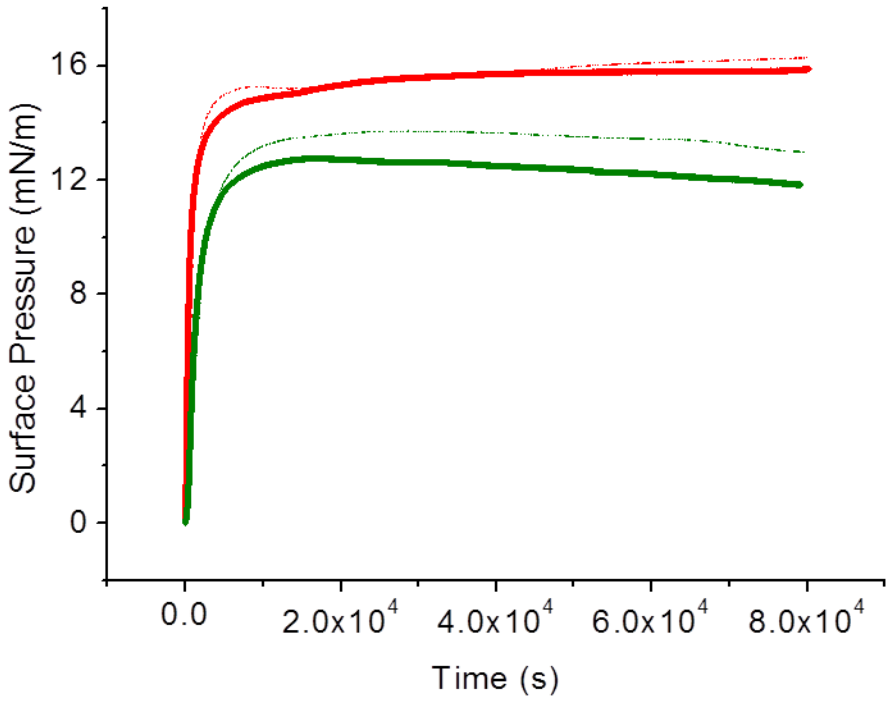

Figure 3.10 Surface pressures of proteins vs. dye-labeled proteins at 0.01 mg/mL.

Solid line: dye-labeled protein, dashed line: protein, red: BSA and BSA-TR, green: HFib and HFib-OG.

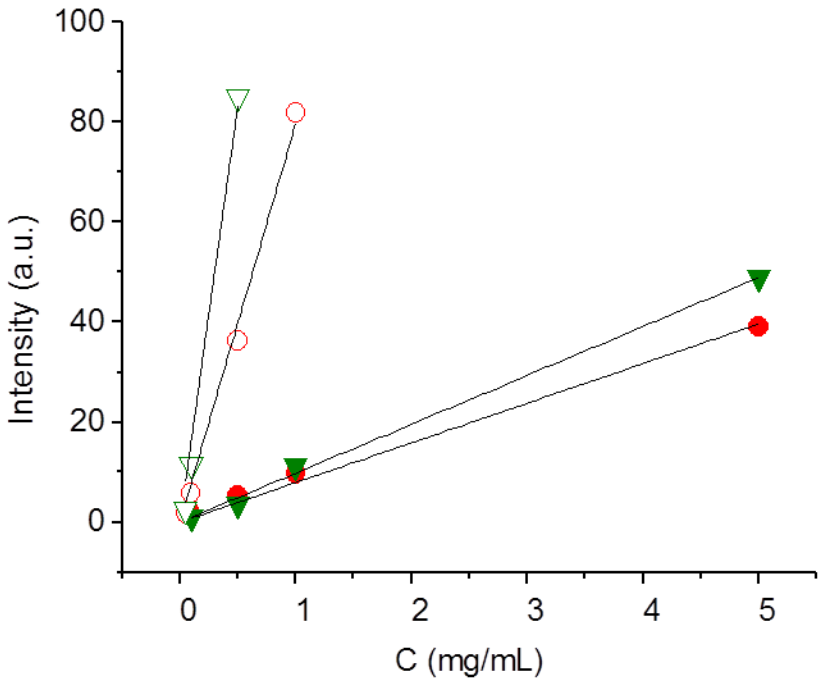

Figure 3.11 Correlation between fluorescence intensity and dye-labeled protein concentration.

Red circles: BSA-TR, green triangles: HFib-OG. Open symbols: data measured under high power settings, closed symbols: low power settings.

Table 3.2 CLSM settings used to investigate fluorescence intensity

Protein (settings)	Laser Wavelength	Laser power	PMT voltage	PMT offset	PMT gain
BSA-TR (low)	543 nm	15%	499 V	3	8
BSA-TR (high)	543 nm	55%	571V	3	8
HF-OG (low)	488 nm	20%	321 V	1	7
HF-OG (high)	488 nm	40%	571V	3	8

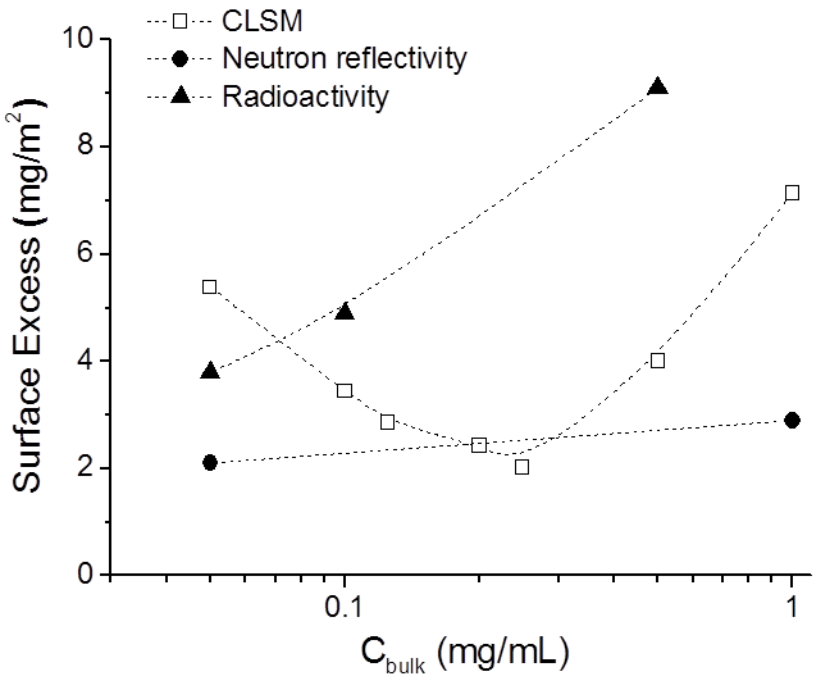

Figure 3.12 Surface excess of BSA-TR calculated from CLSM methods compared to values measured by other methods reported in the literature.

Squares: CLSM data from our measurement; dots: neutron reflectivity data; triangle: radioactivity from the literature.

Neutron reflectivity data were adapted from: Lu et al., J. Colloid Interface Sci., 1999, 213, 426–437. Radioactivity data were adapted from: Graham et al., J. Colloid Interface Sci., 1979, 79, 415-426

IV. Conclusions

In summary, we have applied CLSM to study the adsorption competition and microstructure of interfacial layers at the AWI formed by protein/F-127 mixtures. It was shown that F-127 leads to a lateral phase separation in the interfacial layer then competes protein off the interface. The semi-quantitative CLSM method described here could potentially be used to determine an effective F-127 dose in the prevention of gas embolism. Phase separation of the interfacial layer into protein-rich domains and surfactant-rich domains was observed, in which mobility of protein molecules differed substantially. Utilizing the high temporal resolution of confocal microscopy, we observed and analyzed morphological changes of the protein islands at the AWI, showing that micron-sized protein islands formed at the AWI and coalesced with each other over time. This is the first report of phase separation and dynamic morphological change of protein/surfactant interfacial layers observed in situ at sub-micrometer resolution. These findings illustrate new mechanisms of protein/surfactant interactions at the AWI in addition to the orogenic model.

V. References

(1) Almeida, H.; Amaral, M. H.; Lobao, P.; Sousa Lobo, J. M.: Pluronic F-127 and pluronic lecithin organogel (PLO): Main features and their applications in topical and transdermal administration of drugs. *Journal of Pharmacy and Pharmaceutical Sciences* **2012**, *15*, 592-605.

(2) Dumortier, G.; Grossiord, J. L.; Agnely, F.; Chaumeil, J. C.: A review of poloxamer 407 pharmaceutical and pharmacological characteristics. *Pharm. Res.* **2006**, *23*, 2709-2728.

(3) Bromberg, L. E.; Ron, E. S.: Temperature-responsive gels and thermogelling polymer matrices for protein and peptide delivery. *Adv. Drug Del. Rev.* **1998**, *31*, 197-221.

(4) Ivanova, R.; Lindman, B.; Alexandridis, P.: Evolution in structural polymorphism of pluronic F127 poly(ethylene oxide)−poly(propylene oxide) block copolymer in ternary systems with water and pharmaceutically acceptable organic solvents: from “glycols” to “oils”. *Langmuir* **2000**, *16*, 9058-9069.

(5) Suzuki, A.; Armstead, S. C.; Eckmann, D. M.: Surfactant reduction in embolism bubble adhesion and endothelial damage. *Anesthesiology* **2004**, *101*, 97-103.

(6) Eckmann, D. M.; Diamond, S. L.: Surfactants attenuate gas embolism-induced thrombin production. *Anesthesiology* **2004**, *100*, 77-84.

(7) Sobolewski, P.; Kandel, J.; Eckmann, D. M.: Air bubble contact with endothelial cells causes a calcium-independent loss in mitochondrial membrane potential. *PLoS One* **2012**, *7*.

(8) Eckmann, D. M.; Armstead, S. C.; Mardini, F.: Surfactants reduce platelet-bubble and platelet-platelet binding induced by in vitro air embolism. *Anesthesiology* **2005**, *103*, 1204-1210.

(9) Mackie, A. R.; Gunning, A. P.; Wilde, P. J.; Morris, V. J.: Orogenic displacement of protein from the air/water interface by competitive adsorption. *J. Colloid Interface Sci.* **1999**, *210*, 157-166.

(10) Gunning, P. A.; Mackie, A. R.; Gunning, A. P.; Woodward, N. C.; Wilde, P. J.; Morris, V. J.: Effect of surfactant type on surfactant-protein interactions at the air-water interface. *Biomacromolecules* **2004**, *5*, 984-991.

(11) Morris, V. J.; Gunning, A. P.: Microscopy, microstructure and displacement of proteins from interfaces: implications for food quality and digestion. *Soft Matter* **2008**, *4*, 943-951.

(12) Mackie, A. R.; Gunning, A. P.; Ridout, M. J.; Wilde, P. J.; Morris, V. J.: Orogenic displacement in mixed beta-lactoglobulin/beta-casein films at the air/water interface. *Langmuir* **2001**, *17*, 6593-6598.

(13) Mackie, A. R.; Gunning, A. P.; Ridout, M. J.; Wilde, P. J.; Patino, J. R.: In situ measurement of the displacement of protein films from the air/water interface by surfactant. *Biomacromolecules* **2001**, *2*, 1001-1006.

(14) Anderson, N. L.: The human pplasma proteome: history, character, and diagnostic prospects. *Molecular & Cellular Proteomics* **2002**, *1*, 845-867.

(15) Kotsmar, C.; Pradines, V.; Alahverdjieva, V. S.; Aksenenko, E. V.; Fainerman, V. B.; Kovalchuk, V. I.; Kr ägel, J.; Leser, M. E.; Noskov, B. A.; Miller, R.: Thermodynamics, adsorption kinetics and rheology of mixed protein-surfactant interfacial layers. *Adv. Colloid Interface Sci.* **2009**, *150*, 41-54.

(16) Rasband, W. S.: ImageJ. ImageJ; U. S. National Institutes of Health, Bethesda, Maryland, USA, http://imagej.nih.gov/ij/, , 1997-2011.

(17) Stenger, P. C.; Zasadzinski, J. A.: Enhanced surfactant adsorption via polymer depletion forces: a simple model for reversing surfactant inhibition in acute respiratory distress syndrome. *Biophys. J.* **2007**, *92*, 3-9.

(18) Kotsmar, C.; Pradines, V.; Alahverdjieva, V. S.; Aksenenko, E. V.; Fainerman, V. B.; Kovalchuk, V. I.; Krägel, J.; Leser, M. E.; Noskov, B. A.; Miller, R.: Thermodynamics, adsorption kinetics and rheology of mixed protein-surfactant interfacial layers. *Advances in Colloid and Interface Science* **2009**, *150*, 41-54.

(19) Lakowicz, J.: *Principles of Fluorescence Spectroscopy*; Kluwer Academic/Plenum Publishers: New York, Boston, Dordrecht, London, Moscow, 1999.

(20) De Feijter, J. A.; Benjamins, J.; Veer, F. A.: Ellipsometry as a tool to study the adsorption behavior of synthetic and biopolymers at the air-water interface. *Biopolymers* **1978**, *17*, 1759-1772.

(21) Yuan, T.; Weljie, A. M.; Vogel, H. J.: Tryptophan fluorescence quenching by methionine and selenomethionine residues of calmodulin: Orientation of peptide and protein binding. *Biochemistry* **1998**, *37*, 3187-3195.

(22) Bindhu, C. V.; Harilal, S. S.; Nampoori, V. P. N.; Vallabhan, C. P. G.: Solvent effect on absolute fluorescence quantum yield of rhodamine 6G determined using transient thermal lens technique. *Mod. Phys. Lett. B* **1999**, *13*, 563-576.

(23) Wang, J.; Buck, S. M.; Chen, Z.: The effect of surface coverage on conformation changes of bovine serum albumin molecules at the air-solution interface detected by sum frequency generation vibrational spectroscopy. *Analyst* **2003**, *128*, 773-778.

Chapter 4 Measuring interactions between polydimethylsiloxane and serum proteins at the air-water interface

I. Introduction

The study of polymer-protein interactions at interfaces informs the ever-increasing application of synthetic polymers in biotechnical environments. Polydimethylsiloxane (PDMS) is widely used in lubricants due to its distinctive viscoelasticity, optical clarity, and low water-solubility. These properties also favor PDMS in creating microfluidic devices for demanding biotechnological and industrial applications.[1] PDMS elastomer has been widely applied in fabricating microfluidics for cell culture systems in drug discovery. Related silicone materials find increasing use in medical applications as bioengineered fluids, implant materials and drug delivery vehicles. Silicone oil (SO), which is often composed of linear PDMS, has been employed as a temporary vitreous substitute in retinal detachment.[2] However, it was discovered recently that contact with silicone materials inhibited human corneal endothelial cell and mouse mammary fibroblast proliferation,[3,4] thus raising concerns about biocompatibility. Moreover, SO was found to induce aggregation of proteins in aqueous solution.[11] This focuses attention on SO used in pharmaceutical devices such as preloaded syringes for insulin or antibody drugs.[5-7]

Despite the prevalence of PDMS in biomedical applications, there are few studies that explore the interaction between PDMS and biopolymers from a physical-chemical perspective. The interaction between PDMS and proteins in deposited films consisting of the two components has been studied, but limited structural information could be extracted.[8,9] Besides deposited thin films on solid substrates, another approach is to use Langmuir monolayers to investigate thin-film structures at the air-water interface (AWI). Bernardini et al. applied this approach coupled with Brewster Angle Microscopy (BAM) to investigate the mixed film of PDMS and polymethylmethacrylate (PMMA) at the AWI and found that at low percentage, PMMA served as a contrast enhancer and highlighted the layering transition of PDMS.[10] How these synthetic polymers interact with protein, however, has not been studied. Here, we investigated the interaction of serum proteins with PDMS at the AWI.

Thin film structures of PDMS and IgG were formed at the AWI in order to elucidate the interaction between these two components. Using the Langmuir monolayer approach, we could control the amount of PDMS spread at the AWI and the amount of protein injected into the subphase. IgG was chosen as the model protein for the reason that it is the most abundant antibody isotype in human serum, while human serum albumin (HSA) was also used to confirm that the effect of PDMS was not specific to IgG.[11] To track the distribution of proteins in the interfacial film with optical microscopy, IgG was labeled with Texas Red. Combining surface pressure measurements, in situ fluorescence imaging and topographical studies of Pt-C replica of the films transferred onto a glass surface by scanning electron microscopy (SEM) and atomic force microscopy (AFM), the structures

of PDMS and mixed PDMS + protein films were investigated. Based on our findings, we propose a mechanistic interaction model.

II. Material and experimental methods

a. Reagents

PDMS was purchased from Fisher Chemical (Cat# S159-500). The number average molecular weight (Mn) of PDMS sample was determined by gel permeation chromatography (GPC) to be 6800 g/mol, with polydispersity index (PDI) of 1.6, using PMMA as standard, and tetrahydrofuran as solvent. Stock solution of SO was prepared by adding 5.0 μL of SO into 5.0 mL chloroform (Fisher Chemical Cat# C606-1). For fluorescence imaging, 0.2 mg/mL stock solution of BODIPY 493/503 (Life Technologies, Cat# D-3922) was added into PDMS solution to make a final concentration of 3.8 μM BODIPY in PDMS chloroform solution. In the case where Sulforhodamine 101 (Life Technologies, Cat# S359) was used, the final concentration of Sulforhodamine 101 was 4.9 μM in SO stock solution.

IgG and HSA (Sigma-Aldrich, Cat# I4506, A3782, respectively) were labeled with an amine-reactive fluorophore, Texas Red-X® succinimidyl ester (Life Technologies, Cat# T-20175). Texas Red-X® succinimidyl ester was first dissolved in dimethylformamide at the concentration of 10 mg/mL, and then a certain volume of the dye solution was slowly added into the aqueous protein solution at 10:1 dye-to-protein molar ratio while stirring. Protein solution was made by dissolving proteins (either IgG or HSA) at 2 mg/mL in 0.1 M $NaHCO_3$ buffer at pH 8.3. The vial was covered with aluminum foil and stirred

continuously for 2 h at rt. Unreacted dye was removed by running the reaction solution through an Econo-Pac 10DG column (Bio-Rad). The labeled proteins were eluted with 10 mM phosphate buffer, pH = 7.4, and further concentrated and purified by 10 kDa cutoff molecular weight centrifugal filter units (Millipore) at 7 krpm for 30 min at 4 ℃ and dialyzed by 10 kDa dialysis cassettes (Thermo Scientific) against 1 L of 10 mM phosphate buffer for 1 week at 4 ℃ while the container was covered by aluminum foil. The final concentration of labeled protein was determined by Lowry assay[12] (Thermo Scientific) using bovine serum albumin (Thermo Scientific, Cat# 23209) as the standard. Number of dyes per protein was determined by the absorbance at 280 nm and 595 nm by UV-Vis, using ε_{280} = 203,000 $cm^{-1}M^{-1}$ for IgG absorbance (or 36,000 $cm^{-1}M^{-1}$ for HSA absorbance) and ε_{595} = 80,000 $cm^{-1}M^{-1}$ for Texas Red absorbance according to the protocol provided by Life Technologies. The value was typically 0.6-2.1 depending on the loss of reactivity during the storage time of the dye solution. The labeled protein solution was aliquoted and stored at -20 ℃ for further use.

b. MALDI-TOF Mass Spectrometry

PDMS elastomers were cut into small pieces and swelled in toluene in glass vials overnight while stirring. The solvent was evaporated under vacuum to concentrate the extract. Then 10 μL chloroform was added into the tube to re-dissolve the extract. Dithranol was dissolved in chloroform at 0.25 M as the matrix, and silver trifluoroacetate dissolved at 1.25 M as the salt. The polymer/matrix/salt mixture was in volume ratio 2/1/1, and 1 μL of sample was applied onto MALDI plate and dried. MALDI-TOF MS

measurements were performed with a Bruker Daltonics Ultraflex III MALDI-TOF/TOF mass spectrometer, in a mass range from m/z 0-4,000.

c. Langmuir-Blodgett Trough Experiment

The π-C_{surf} isotherm and titration experiment was performed with a MicroTroughXS system (Kibron Inc.). The metal trough was designed for fluorescence imaging; it has a quartz glass window in the center. Surface pressure was measured by the Du Noüy-Padday technique[13] using the DyneProbe provided by Kibron Inc., while the surface area was controlled by a pair of Teflon barriers. Before each measurement, the trough was wiped with chloroform, then washed with deionized water and ethanol sequentially. This procedure was repeated three times, and the surface pressure was calibrated with deionized water. The trough was then filled with buffer and π-C_{surf} isotherms of the buffer were measured before each measurement to ensure that the increase in π was smaller than 0.2 mN/m, which indicated that surface-active contaminants had been eliminated.

d. Fluorescence Imaging

The fluorescence images were taken using an inverted fluorescence microscope (IX71, Olympus) with a long working distance objective (60× W/IR, NA 0.90, Olympus LUMPlanFL) equipped with an EM CCD camera (Hamamastu). DualView imaging system (DV2, Photometrics, Tucson, AZ) was mounted in front of the CCD camera to enable simultaneous dual-color imaging. The excitation source was a continuous wavelength mercury lamp. For Texas Red or Sulforhodamine fluorescence, an excitation

filter (540-580 nm) and emission filter (593-668 nm) were selected. For BODIPY, the excitation filter (450-490 nm) and emission filter (500-550 nm) were chosen.

e. Fluorimetry

Steady-state fluorescence data were collected on a Varian Cary Eclipse fluorescence spectrometer. IgG-TR was dissolved in 10 mM phosphate buffer at 100 μg/mL, and diluted to concentrations ranging from 0.1-10 μg/mL in Eppendorf tubes. The solutions were frozen in liquid nitrogen and lyophilized under vacuum. 1.0 mL of silicone oil (pure linear polydimethylsiloxane in liquid state) was added to each tube to re-dissolve the protein. Solutions were sonicated to ensure protein was completely dissolved. The fluorescence intensity was measured using a 0.9 mL quartz cell (Starna Cells) at excitation wavelength 550 nm (excitation slit 5 nm) and collected at 580-700 nm range (emission slit 5 nm) at 20 ℃, PMT voltage = 1000 V.

f. π-C_{surf} Isotherm Measurement

15.0 mL of 10 mM phosphate buffer at pH = 7.4 was used for the π-C_{surf} isotherm measurement. The surface area of buffer was first compressed to 7000 mm^2, then 4.3 μL of 0.96 mg/mL PDMS dissolved in chloroform was spread carefully at the air-buffer interface. After waiting 20 min for chloroform to evaporate, the barriers were relaxed to the full trough area, and then compressed while the π-C_{surf} isotherm of the PDMS was recorded. For PDMS + IgG-TR systems, 250-1000 μL of 0.020 mg/mL IgG-TR aqueous solution was injected into the subphase behind the barriers at 20 min after the PDMS chloroform solution was spread at the interface. Then the barriers were relaxed to full

trough area and the system was allowed to sit for 1 h for the protein to adsorb to the interface. All π-C_{surf} isotherms were measured by compressing the barriers at 10 mm/min.

g. Titration Experiment

Same buffer as the isotherm measurement was used for the titration measurement. 0.5-10 μL of 0.96 mg/mL PDMS in chloroform solution was spread at the interface and solvent was allowed to evaporate for 20 min, then the surface area was compressed to 3000 mm^2. IgG-TR in phosphate solution (250 μL, 0.02 mg/mL) was injected into the subphase every hour until the final concentration of protein in the solution reached 1.3 μg/mL after 4 injections. Fluorescence images were collected every 1 h after the protein injection.

h. Film Transfer onto Cover Glass

Cleaned cover glass (Fisher Scientific, Cat# 12-545-80) was used for film transfer. Cover glasses were sonicated for 10 min in acetone and ethanol sequentially and rinsed with ample deionized water. Then the cover glass was blown dry with compressed air. The sample film was first prepared at the AWI through the methods mentioned above, and then transferred onto the cover glass through the Langmuir-Schaefer method by approaching the AWI from the air phase and touching the interface for 5 s then pulling up slowly. Excessive solution on the glass was removed by a piece of Kimwipe paper gently touching the side of the cover glass and then the sample film on the cover glass was left to dry in the air covered by a petri dish. The transferred film was imaged under the fluorescence microscope to check transfer quality before further characterization.

i. Pt-C Replication and SEM Imaging

The Pt-C replication was done following a standard procedure detailed in the literature.[14] A 2.9 nm thick Pt film was deposited and then backed by 9.0 nm thick C film at 45^{o} angle deposition with the specimen stage rotating in a vacuum evaporator. The replica was released from the cover glass by floating the cover glass on 10% HF acid, which dissolves the glass after 2-3 h. Then the replica was washed by floating on highly diluted (10^{-6} by volume) household soap solution for 5 sec, on bleach solution (also 10^{-6} by volume) for 30 min and on water sequentially and finally mounted on clean 1 by 1 cm prime grade silicon wafer (Silicone Quest International Cat# 808-007). The purpose of soap solution was to reduce the surface tension difference between HF and water to prevent the breakage of the replicas, and the bleach served to further dissolve organic materials including PDMS and protein.[15] Scanning electron microscope (SEM) images were taken with a Quanta 600 FEG Mark II system at 15 kV accelerating voltage.

j. AFM Imaging

Pt-C replicas of PDMS and PDMS + IgG-TR films were also measured by atomic force microscope (Dimension 3100, Veeco/Bruker) in tapping mode with aluminium reflex coating cantilevers (Budget Sensors, Cat# Multi75AI). The AFM cantilever had a resonant frequency at 75 kHz and a force constant of 3 N/m. Height profiles were analyzed using WSxM 5.0 software,[16] and 3D AFM images were constructed using Gwyddion software.[17]

III. Results and Discussion

a. Leaching of PDMS oligomers at acidic conditions

In Chapter 2, we used PDMS elastomer to create a chamber with a flat air-water interface for optical imaging of fluorescently labeled proteins.[18] Lateral heterogeneity was described at the AWI that occurred in aqueous protein solution ($C_{protein}$ = 10^1-10^2 μg/mL) at neutral pH and on timescales of minutes to a few hours. Later, we discovered that under acidic conditions (pH = 5.0) and reduced protein concentration ($C_{protein}$ = 10^{-1}-10^0 μg/mL), unusual circular domains formed at the AWI in 1 h with dye labeled HSA or IgG (Figure 4.1). At neutral pH, the circular domains formed more slowly, only appearing after overnight incubation. Such phenomena, not observed at 1 h in the solution free of contact with PDMS, but seen reproducibly in the PDMS chamber at pH = 5.0, led us to hypothesize that the circular domains were initiated by oligomers leaching from PDMS elastomer into aqueous solution, with potential for protein interaction at the AWI. MALDI-TOF mass spectrometric analysis of toluene-extracted residues from the PDMS chamber confirmed the presence of oligomers, as shown in Figure 4.2. PDMS was identified with △ m/z of 74 between neighboring peaks indicating the repeating $(CH_3)_2OSi$ unit. Although PDMS degradation is generally considered to be a slow process, it is known to be affected by UV irradiation, pH, and temperature.[19] Acidic conditions could catalyze hydrolysis of linear high-molecular-weight PDMS,[20] thus releasing oligomers into solution that subsequently adsorb at the AWI and compete with surface-active proteins. This effect is negligible in the chamber setup described in Chapter 2 and 3 since leaching at the neutral pH used in previous studies was very slow,

and the time frame during which we characterized these interfacial layers was kept within 1 h. However, in the applications where continuous use of PDMS is common and low concentration of proteins in the μg/mL range is desired such as in ultrasensitive immunosensing, the interaction between PDMS and proteins at the interface could have a profound effect. To investigate this phenomenon in greater detail, we explored PDMS-protein interactions at the AWI under well controlled conditions.

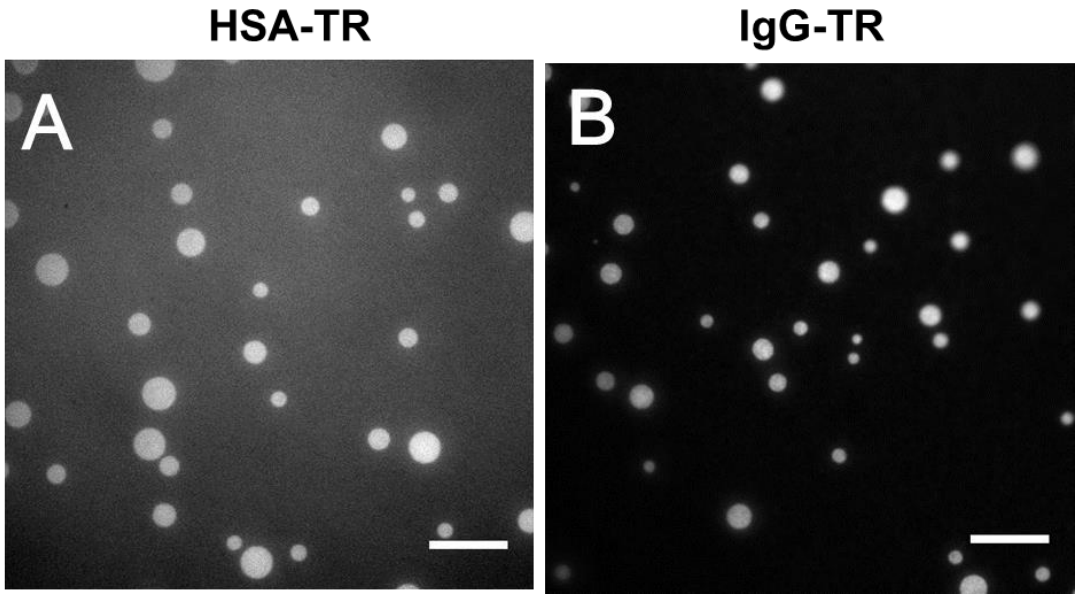

Figure 4.1 Domains observed at the air-water interface with dye-labeled serum proteins.

(A) HSA-TR at 2.0 μg/mL and (B) Immunoglobulin G labeled with Texas Red (IgG-TR) at 1.0 μg/mL in 10 mM acetic acid/sodium acetate buffer (pH = 5.0), 1h after addition of protein sample. Scale bar: 20 μm.

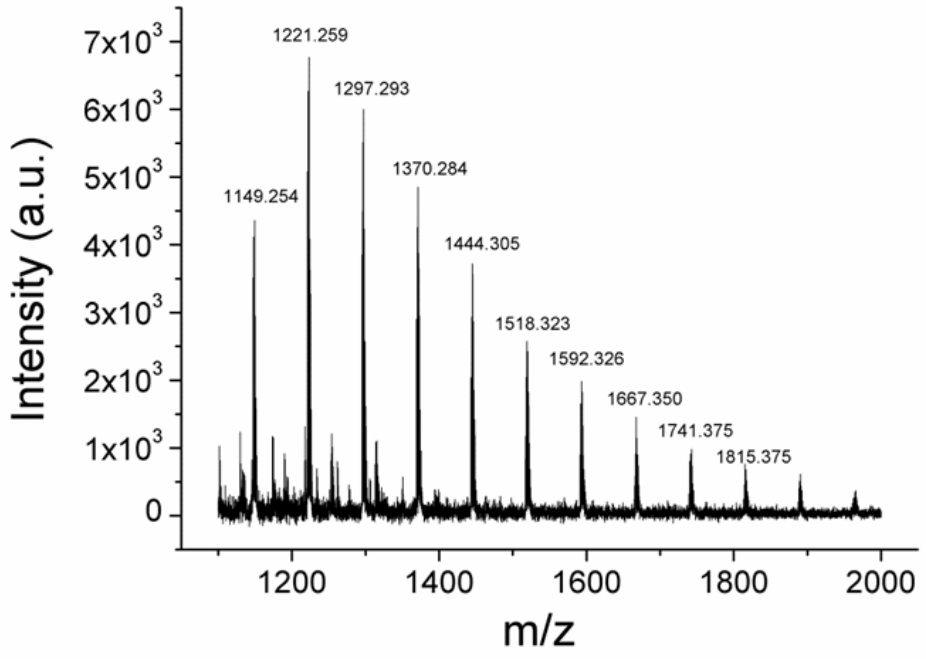

Figure 4.2 MALDI-TOF mass spectrum of extracted residues from PDMS elastomer by toluene.

△m/z of 74 between neighboring peaks indicates the repeating $(CH_3)_2OSi$ unit.

b. Surface Pressure-Surface Concentration Isotherms of PDMS and IgG-TR in Langmuir Trough.

Surface pressure (π)–surface concentration (C_{surf}) isotherm measurements were performed on PDMS and PDMS + IgG mixtures. The π-C_{surf} isotherm of PDMS is shown in Figure 4.3 A. Two marked increases in surface pressure were observed in the PDMS sample, similar to previously published results.[21-23] Two transition surface concentrations, determined from the local maximum of the first derivative of π with respect to C_{surf}, are identified as C_1 and C_2. The π-C_{surf} isotherm of PDMS was divided into four regions, and corresponding conformational models of PDMS chains have been proposed in the literature,[23,24] as summarized briefly here: In region I, C_{surf} was low and polymer chains were well spaced. In region II, as C_{surf} increased, the chains compacted and likely came in contact. The highly flexible Si-O chain allowed the polymer to adopt more ordered conformations with the more hydrophilic oxygen atoms immersed in the subphase and hydrophobic silicone-methyl groups sticking into the air. While most researchers agree on the chain conformation model of regions I and II, more controversy surrounds regions III and IV. Earlier studies using reflected infrared spectroscopy proposed the helix model: upon further compression from region III to IV, the helices slide onto each other, forming "standing helices", which leads to the second increase in surface pressure.[23,25] The helical structures of PDMS chains in regions III and IV are analogues of the structures found by X-ray diffraction and NMR of PDMS crystals.[26,27] On the other hand, Lee et al. found that the ellipticity of the PDMS film at the AWI changed abruptly from region III to region IV, not exhibiting a continuous transition as suggested by the helix model. Instead, the abrupt increase in ellipticity was proposed to indicate the formation of a multilayer

structure.[28] This alternative model of chain conformation was further strengthened by Kim et al., who found that the vibrational sum frequency intensity in region IV was not diminished as would be expected for standing helices. Thus, they identified the Si-O chain conformation in regions III and IV as a horizontal folding model on top of the monolayer.[24] Depending on whether the chain adopts helical structure or horizontal folding, C_2 resembles the transition of chain conformation from helices to standing helices or from single-folded layer to folded multilayer.

Using C_1 and C_2 as the measurement of conformational transition, we studied how the two values changed with addition of protein. Figure 4.3 B shows the π-C_{surf} isotherms of PDMS with IgG-TR added to the subphase. PDMS was first spread at the air-buffer interface at 0.4 mg/m^2, where surface pressure remained 0 mN/m. Protein was then injected into the subphase and the trough was left to equilibrate for 1 h. The small increase of π after 1 h indicated by the arrow in Figure 4.3 B showed that the proteins adsorbed to the interface and resulted in a mixture of proteins and PDMS at the interfacial layer. The interfacial layer was then compressed at 10 mm/min, while surface pressure was recorded. Three parallel experiments were averaged to give each trace shown. Comparing π vs. [IgG-TR] in four different regions in Figure 4.3 C, increasing concentration of IgG-TR in the subphase led to pronounced increase of π in regions II and IV, and moderate increase in region I. In contrast, the surface pressure in region III experienced minimal change over the range of IgG-TR concentrations studied. Furthermore, we extracted the C_{surf} of SO (C_1 and C_2), as well as the surface pressure at these transition points to evaluate the effect of IgG-TR on the phase transition of SO.

Increasing subphase concentration of IgG-TR shifted C_1 and C_2 to smaller values (Figure 4.3 D). The trend in decreasing C_1 and C_2 values indicated that IgG-TR in the interfacial layer likely reduced the available area for PDMS, and thus decreased the amount of PDMS at the interface that was necessary to undergo conformational transitions.

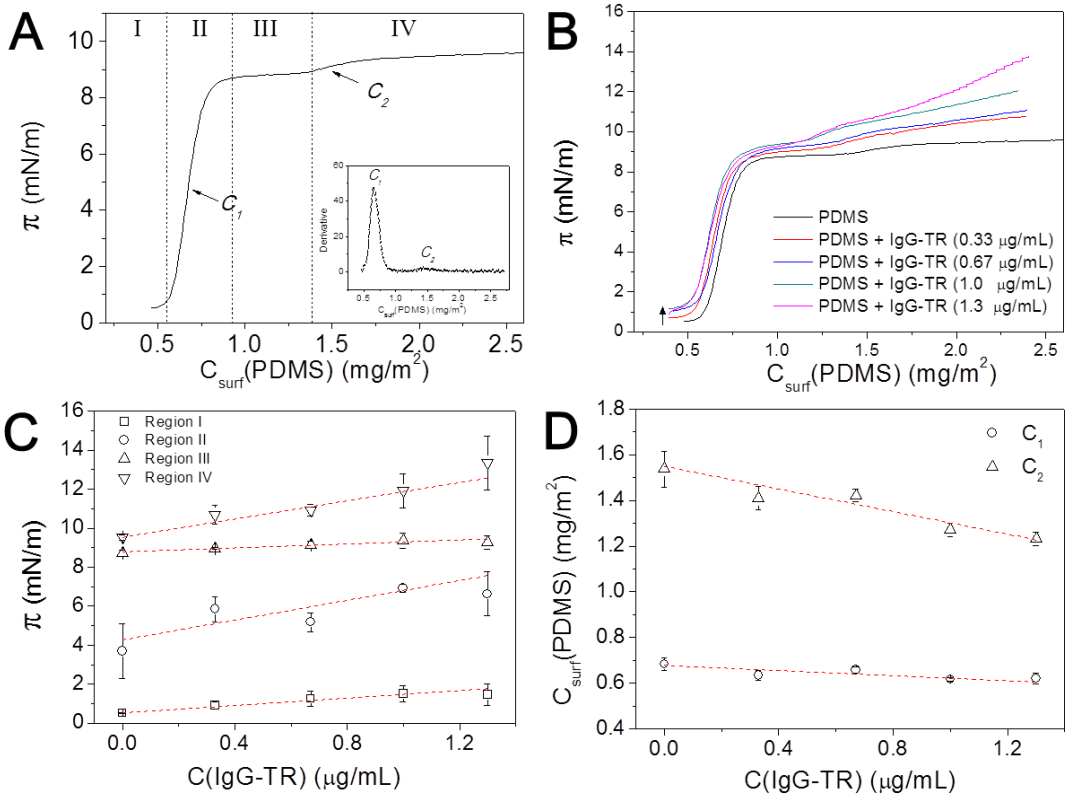

Figure 4.3 π-C_{surf} isotherms of PDMS and PDMS + IgG-TR.

(A) π-C_{surf} isotherm of SO. The isotherm shown is the average of four trials. Vertical dashed lines divide the curve into four regions, I-IV, corresponding to different proposed conformations.[24] Insert shows the first derivative of the isotherm, where C_1 and C_2 correspond to the local maxima in regions II and IV. (B) Surface pressure of PDMS (spread at the air-water interface) + IgG-TR (injected into subphase) systems. Each trace of PDMS + IgG-TR is the average of three trials. (C) Surface pressure at fixed surface concentration of SO in regions I-IV changed by subphase concentration of IgG-TR. The surface concentrations of PDMS corresponding to each line are Region I: 0.50 mg/m^2, region II: 0.67 mg/m^2, region III: 1.0 mg/m^2, region IV: 2.3 mg/m^2. (D) Transition surface concentration of PDMS changed by subphase concentration of IgG-TR.

c. Circular Domains under Fluorescence Microscopy in Langmuir Monolayer.

In parallel with the isotherm study, we applied fluorescence microscopy coupled to the Langmuir trough to study phase changes at the AWI. Circular domains with micrometer diameters were found in region IV during compression, as shown in Figure 4.4 A. The same phenomenon was also observed in the PDMS + HSA-TR system. The total interface fluorescence intensity (I_{inter}) shown in Figure 4.4 B was determined from the average intensity of each pixel (I_{avg}) times the total surface area (*Area*) of the film during the compression. Three images of randomly selected area at the AWI were analyzed to determine I_{avg}, while the total surface area was recorded by the trough system. The four regions defined by the surface pressure were indicated by dashed lines. The average intensity curve remained flat in regions I-III, and then jumped significantly in region IV, a four-fold increase. As the quantum yield of fluorophores is often solvent dependent, we measured the fluorescence intensity vs. the concentration of IgG-TR dissolved in SO to see how the change in I_{inter} would correlate to the amount of IgG-TR in the interfacial layer, which is composed mostly of SO. We found that the quantum yield decreased after the concentration of dye-labeled protein reached ~5 μg/mL (Figure 4.5). Because IgG-TR at the interface was in a layer of PDMS film, the solvent environment was comparable to the dye-labeled protein in SO. Thus, the quantity of protein at the interface in region IV exceeded that in regions I-III by at least four-fold, considering the fluorescence quenching effect at higher concentrations. The large error bars shown in Figure 4.4 B reflect significant sample heterogeneity at the AWI in region IV.

Combining the π-C_{surf} isotherm with fluorescence imaging provided information about PDMS-protein interactions at the AWI. IgG-TR partitioned into the interfacial layer in region I, occupying available surface area between loosely packed silicone chains. The moderate increase of surface pressure in region I could be explained by minimal contact between PDMS chain and protein. In region II, proteins and PDMS came into closer contact with each other, thus competing for the available surface area. Because Si-O chains are highly flexible and able to reorient themselves to occupy the surface area, they likely pushed proteins into the sub-layer and formed a PDMS monolayer at the interface in region III. This was demonstrated by the finding that surface pressures of PDMS + IgG-TR mixtures were close to that of the pure PDMS film in region III (Figure 4.3 C). The protein likely remained in the sub-layer close to the interface, as the total fluorescence intensity from IgG-TR remained essentially constant throughout regions I-III. The increase of surface pressure and fluorescence intensity in region IV indicated that upon further compression, a change in silicone chain conformation promoted the localization and interaction of proteins at the interface, especially at the circular domains.

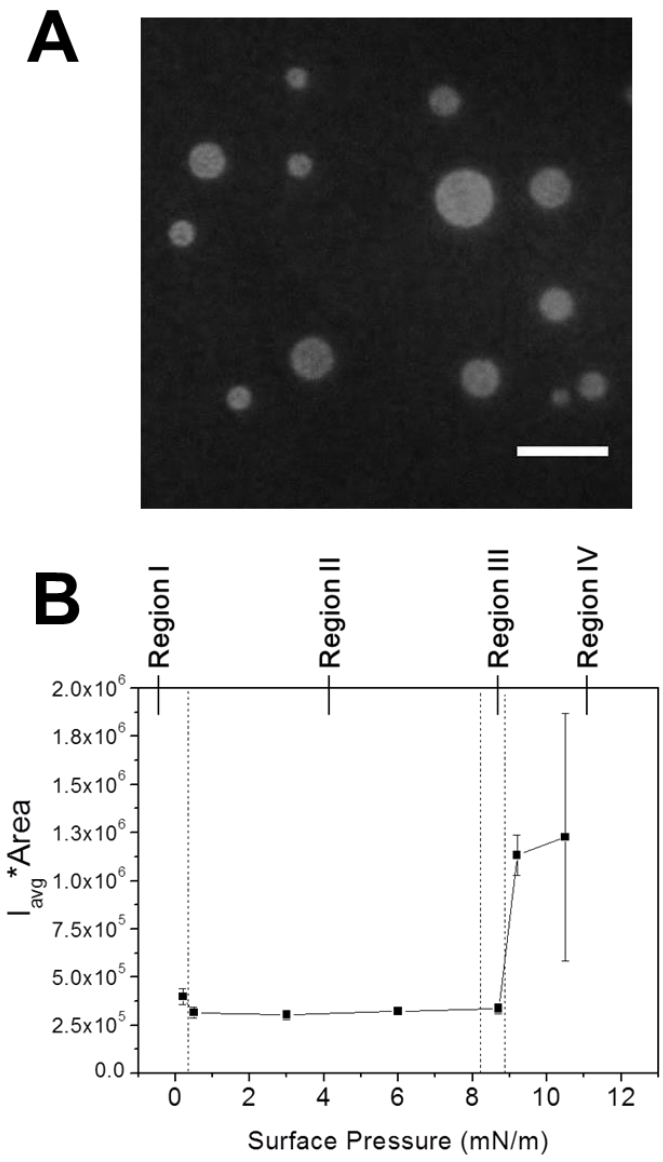

Figure 4.4 Fluorescence microscopy study of PDMS + IgG-TR film at the air-water interface during compression.

(A) Epi-fluorescence image of the film from Texas Red channel in region IV. (B) Change of fluorescence intensity of IgG-TR at the interface with compression of PDMS + IgG-TR (0.33 μg/mL) film. Scale bar: 20 μm.

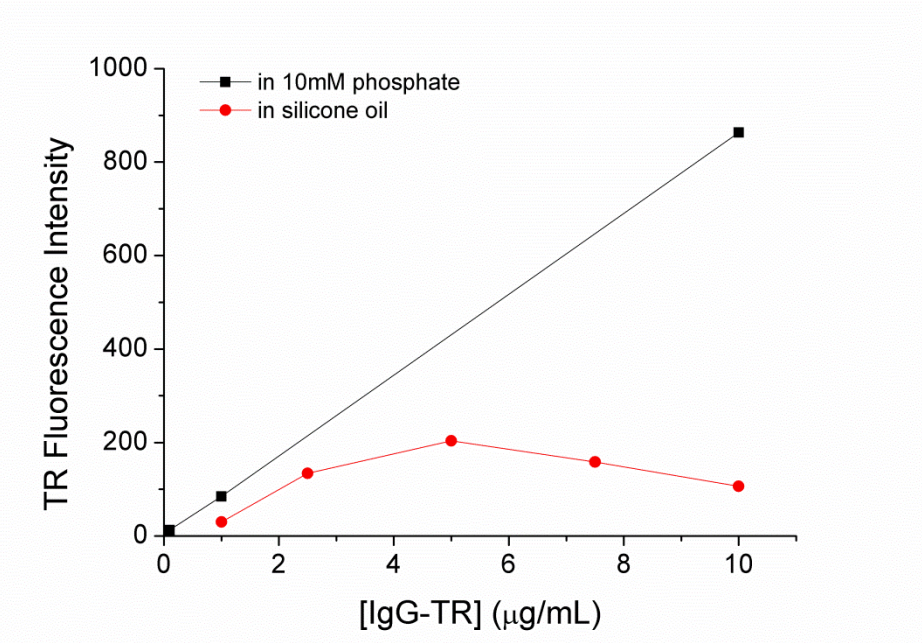

Figure 4.5 Fluorescence intensity of IgG-TR at different concentrations in phosphate buffer and in silicone oil.

Phosphate buffer: 10 mM phosphate (pH = 7.4). Stead state fluorescence was measured at excitation wavelength 550 nm (excitation slit 5 nm) and collected at 580-700 nm range (emission slit 5 nm) at 20 °C, PMT voltage = 1000 V.

d. Titration of IgG-TR into the Subphase.

To test the hypothesis that the circular domains identified by fluorescence imaging in PDMS + IgG-TR mixtures in region IV were induced by the PDMS film as a template and then labeled by preferential adsorption of protein, we carried out a titration experiment, where PDMS was first spread at the interface at C_{surf} = 3.2 mg/m^2; π increased to 9.0 mN/m. Then IgG-TR was injected into the subphase, and later adsorbed onto the PDMS film. We selected free BODIPY, which was known to preferentially stains hydrophobic moieties,[29,30] to trace the distribution of SO at the AWI. Indeed, in region IV, the circular domains were observed with BODIPY in the film (Figure 4.6 A). Similar domain structure of PDMS (Mw = 10,000 g/mol) film on water was reported by Mann et. al using Brewster Angle Microscopy.[31] The domains should correspond to locations with standing helices or multilayers. After injection of IgG-TR into the subphase to the concentration of 0.33-0.67 μg/mL, proteins preferentially localized to the circular domains at the interface (Figure 4.6 B). Zoomed-in images showed heterogeneity in IgG-TR fluorescence within some of the domains. However, the overlay of BODIPY and IgG-TR images showed that IgG-TR tends to localize at the outer edge of SO circular domains (Figure 4.6 C-E). With further increase in the amount of IgG-TR injected into the subphase, the domain features disappeared and the interface became more homogenous and dominated by TR fluorescence (Figure 4.7).

We hypothesize that preferential adsorption of IgG-TR to the circular domains was due to the greater hydrophobicity of the domains in this region. It is known that proteins preferentially adsorb to more hydrophobic surfaces.[32] On films made of polymer blends,

proteins such as concanavalin A have been observed to adsorb preferentially to the most hydrophobic regions.[33] For PDMS films in region IV, where the circular domains likely consist of highly compacted polymer chains, increased hydrophobicity in the domain should favor protein adsorption. Although BODIPY used here provided contrast between domain regions and peripheral regions, a recent study showed BODIPY could undergo photo-conversion upon irradiation and change affinity from liquid-ordered phase to liquid-disordered phase,[34] thus confusing the the interpretation of our results. A more hydrophilic dye, Sulforhodamine 101, was also used to trace the distribution of polymers at the AWI, which was similarly excluded from the circular domains in PDMS films in region IV (Figure 4.8), indicating that the domain region was more hydrophobic. This likely resulted from the high density of polymer chains in the domain.

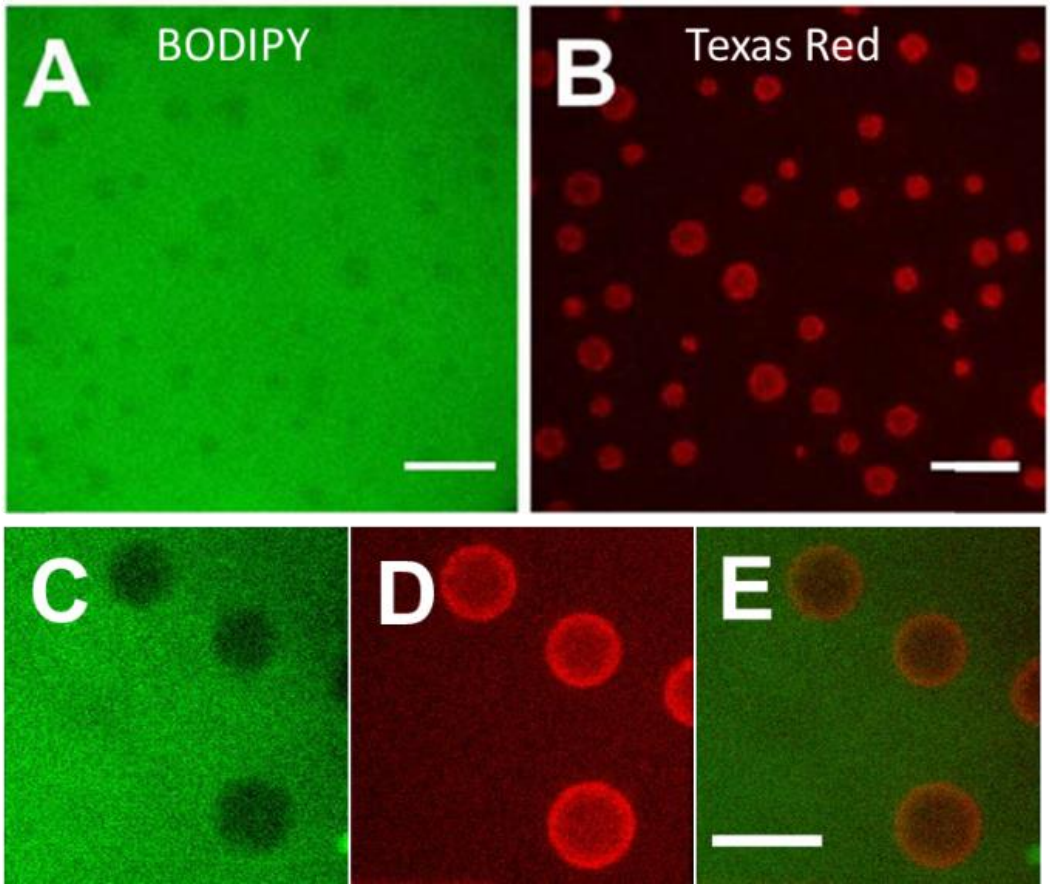

Figure 4.6 Fluorescence microscopy study of PDMS-only film and PDMS + IgG-TR film at the air-water interface.

(A) PDMS in region IV: C_{surf}(PDMS) = 3.2 mg/m^2, π = 8.9 mN/m. (B) with IgG-TR injected into subphase underneath PDMS film: C_{surf}(PDMS) = 3.2 mg/m^2, [IgG-TR] = 0.33 μg/mL, π = 9.0 mN/m. (C-E) Zoomed-in micrograph of domains with BODIPY, TR and images overlaid. Scale bar: 20 μm.

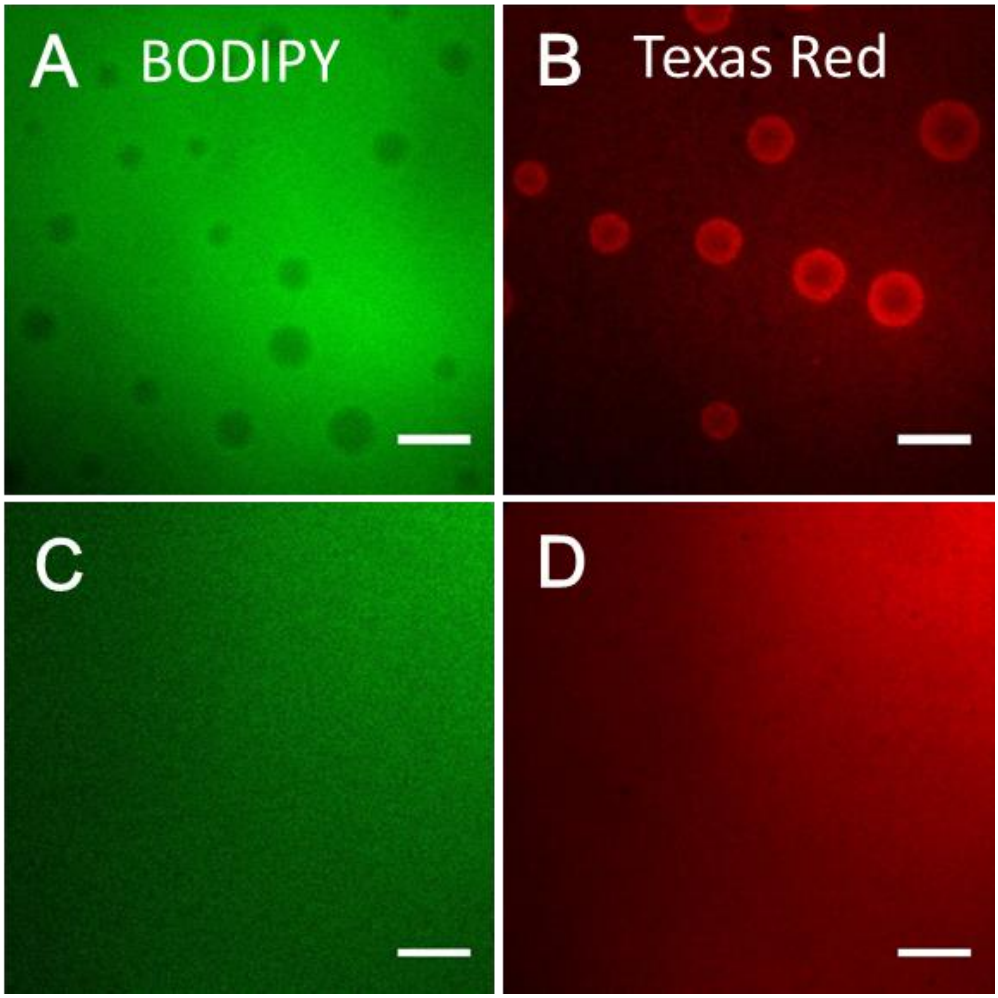

Figure 4.7 Titration of IgG-TR into the subphase underneath PDMS layer at the A/W interface.

Fluorescence microscopy images of two areas of the interfacial layer of (A-B) PDMS + 0.33 μg/mL IgG-TR in subphase, (C-D) PDMS + 1.3 μg/mL IgG-TR in subphase. C_{surf}(PDMS) = 2.6 mg/m^2. Buffer: 10 mM phosphate, pH = 7.4. Scale bar: 20 μm.

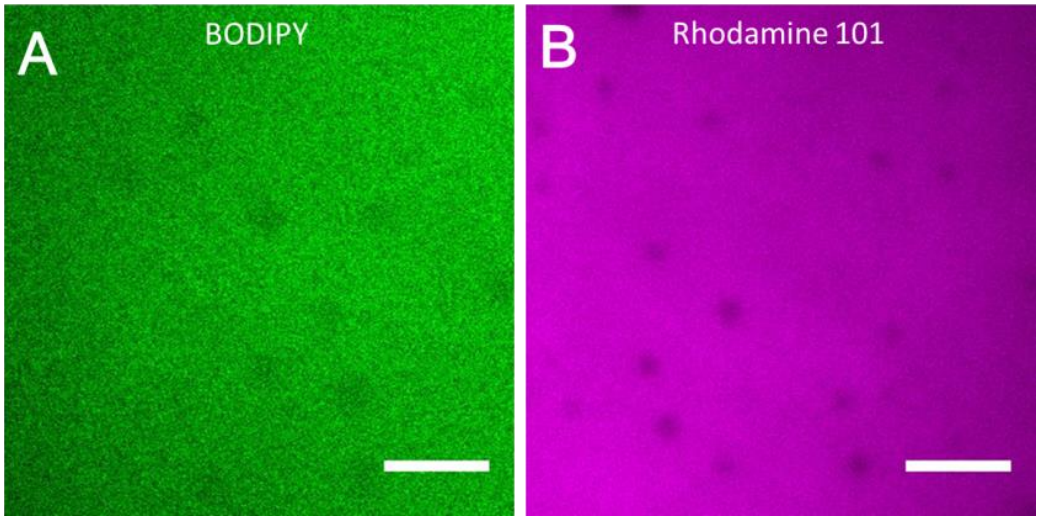

Figure 4.8 Fluorescence microscopy images of PDMS film (region IV) stained with BODIPY or Rhodamine 101.

(A) PDMS stained with BODIPY (B) PDMS stained with Rhodamine 101. Scale bar: 20 μm.

e. Characterization of the Micro-structure of Region IV Domains.

To characterize the micro-structures of domains observed in region IV, PDMS and PDMS + IgG-TR films formed at the AWI were transferred to solid substrate and replicated with a thin platinum-carbon (Pt-C) layer for SEM imaging. The PDMS or PDMS + IgG-TR films were transferred to glass coverslips through Langmuir-Schaefer approach and air-dried. The transferred samples were first imaged by fluorescence microscopy to confirm the transfer efficiency of the film for both samples (Figure 4.9 A-B). The fluorescence images showed moderate shape distortion after the transfer step, and domains were often observed at higher density close to the edges of the cover glass than in the center. Nevertheless, most features of the film were preserved on the glass substrate. Following transfer, the samples were coated with a 2.9 nm platinum film and backed with a 9.0 nm thick carbon continuous film at 45^{o} angle deposition with the specimen stage rotating. After replication, the Pt-C replica was gently separated from the cover glass and transferred to a clean silicon wafer surface for SEM imaging. The Pt-C replication for electron micrograph method has been established and applied to study polymer films, protein films and cellular components such as actin filaments in cytoskeleton.[35,36] This method is most suitable for specimens with non-periodic features, thus it served well in our system where the domains were scattered on the films. Figure 4.9 C and D show the SEM images of domains in the Pt-C replica of PDMS and PDMS + IgG-TR films, respectively.

Moreover, the Pt-C replica facilitated AFM imaging as we attempted to measure the height of the domains. Direct measurement of the domains in PDMS or PDMS + IgG-TR

film on cover glass proved challenging due to the low density of domains and the high flexibility of Si-O chains. Using low magnification SEM images of the Pt-C replica as a reference map, we were able to locate the domains more reliably under the optical channel of the AFM probe. The AFM height images of the replica of PDMS and PDMS + IgG-TR films are shown in Figure 4.10. Compared to PDMS, PDMS + IgG-TR samples showed increased roughness, presumably due to protein adsorption on the polymer film. Figure 4.10 E summarizes multiple domain heights measured by AFM in Pt-C replica in a histogram. The height measured is the height difference between the domain and the peripheral area, as the Pt-C forms a continuous conductive layer on the PDMS, with or without IgG-TR film. In Figure 4.10 E, the domain height for the case of PDMS + IgG-TR showed a much larger variance than that of the PDMS film, which is likely due to differing amounts of protein partitioning in the domains. The population of <20 nm domains in PDMS + IgG-TR was significantly larger than observed in PDMS film, likely due to one or two layers of IgG-TR. The emergence of >75 nm domains was also apparent in the PDMS + IgG-TR samples, which indicated further aggregation of IgG-TR. Nevertheless, even in the replica of PDMS-only film, the domain height difference indicated multi-layer polymer chains inside the domain comparing to the thickness of PDMS monolayer which is ~0.7 nm.[21,28] No previous reports have shown the domain height compared to the peripheral area of PDMS film in region IV to our knowledge. Using ellipsometry and neutron reflectivity, Mann et. al reported the overall film thickness of PDMS to be ~1.4 nm.[21,31] We also estimated the average thickness of PDMS film from our data, by combining the AFM height measurement and fluorescence microscopy results. The average domain height difference was 36 $\pm$ 10 nm. By

quantifying the area percentage of domains in fluorescence images of PDMS films formed at the AWI, we found the domain area accounted for 6 $\pm$ 2 % of the total surface area at $C_{surf}(PDMS)$ = 3.2 mg/m^2. This produced an overall film thickness of 2.8 nm, which is twice the thickness measured by neutron reflectivity.[28] The largest source of error could be from the area percentage of domains quantified from fluorescence imaging as well as potential exaggeration of height differences by Pt-C coating.

From the π-C_{surf} isotherm, fluorescence imaging, SEM and AFM imaging of Pt-C replica of transferred films, we propose the following mechanistic model of SO/IgG-TR interaction at the AWI: In region I, proteins adsorbed to the free surface area between randomly oriented silicone chains. The silicone chains started to adopt more ordered structure in region II, and proteins were less exposed to air, as they were squeezed out of the monolayer at the interface by ordering silicone chains. In region III, proteins stayed in the sub-layer beneath the film formed by silicone chains. In region IV, as heterogeneity in the film of standing helix structure or multilayer domains was increased by further compression, proteins preferentially adsorbed to circular PDMS domains that formed.

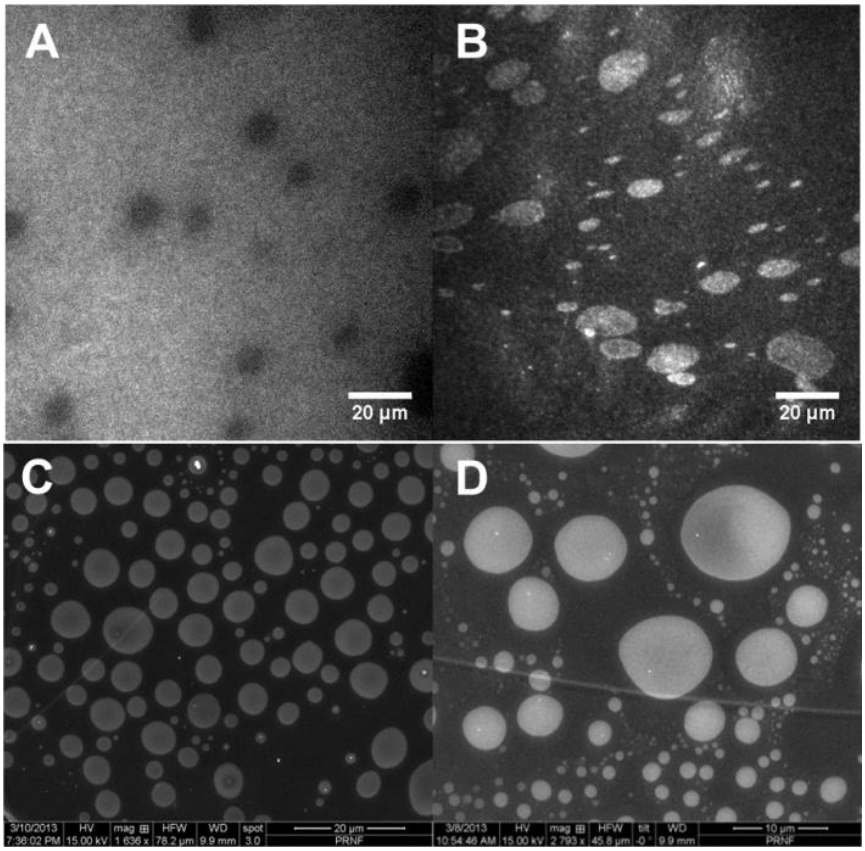

Figure 4.9 Characterization of transferred films on cover glass substrate.

(A-B) Fluorescence microscopy images of (A) PDMS and (B) PDMS + IgG-TR film transferred on glass.

(C-D) SEM images of Pt-C replica of (C) PDMS and (D) PDMS + IgG-TR transferred onto glass.

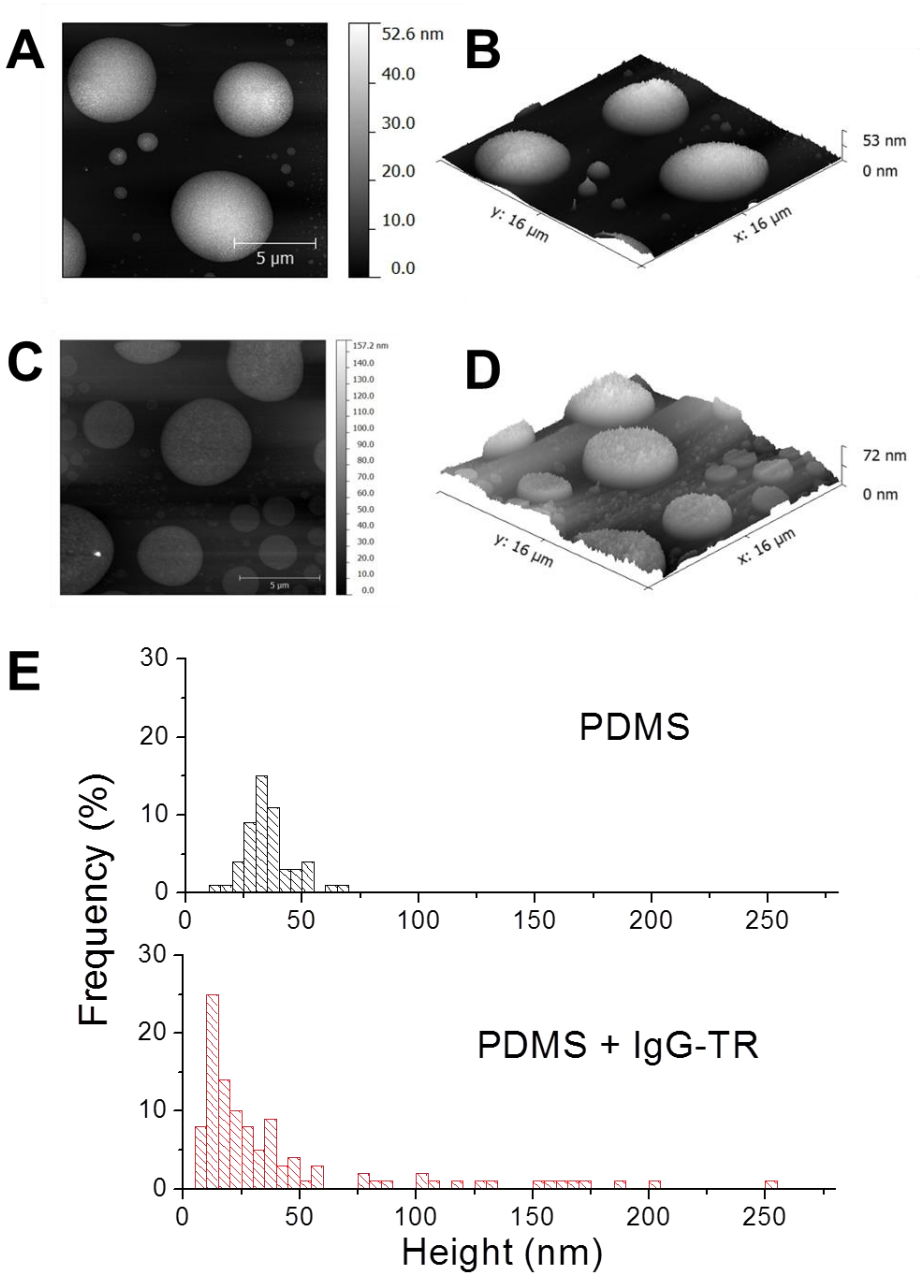

Figure 4.10 AFM height images and height analysis of Pt-C replicas.

AFM images of (A-B) PDMS and (C-D) PDMS + IgG-TR C/Pt replicas. (E) Domain height histogram of PDMS and PDMS + IgG-TR Pt-C replicas. X-axis is the height of domains, and y-axis is the % of domains analyzed.

IV. Conclusions

In summary, we have characterized synthetic polymer-protein interactions in PDMS/IgG-TR and PDMS/HSA-TR films. This study sheds light on the complex interplay between PDMS and these proteins, and should apply broadly to other proteins and PDMS interactions in general. Our study indicates that IgG adsorption favored the condensed domain region in the PDMS film. By keeping the surface concentration of PDMS below the limit required to form domain structures in region IV (~1.6 mg/m^2), it was possible to reduce significantly the amount of protein adsorbed at the interface, thereby reducing protein loss and denaturation at the interface. This work also provides a cautionary tale about the use of PDMS in biotechnology applications, particularly involving low concentrations of protein. The findings in this chapter does not contradict with the results in previous chapters, because the PDMS oligomers formed by leaching from the PDMS chamber was negligible at neutral pH and in 1h time frame. Nevertheless, PDMS can have a profound effect on protein surface behavior, and should be utilized with discretion in situations where interfacial phenomena dominate.

V. References

(1) McDonald, J. C.; Duffy, D. C.; Anderson, J. R.; Chiu, D. T.; Wu, H. K.; Schueller, O. J. A.; Whitesides, G. M.: Fabrication of microfluidic systems in poly(dimethylsiloxane). *Electrophoresis* **2000**, *21*, 27-40.

(2) Skorpik, C.; Menapace, R.; Gnad, H. D.; Paroussis, P.: Silicone oil implantation in penetrating injuries complicated by PVR-results from 1982 to 1986. *Retin.-J. Retin. Vitr. Dis.* **1989**, *9*, 8-14.

(3) Yang, C. S.; Chen, K. H.; Hsu, W. M.; Li, Y. S.: Cytotoxicity of silicone oil on cultivated human corneal endothelium. *Eye* **2008**, *22*, 282-288.

(4) Paguirigan, A. L.; Beebe, D. J.: From the cellular perspective: exploring differences in the cellular baseline in macroscale and microfluidic cultures. *Integrative biology : quantitative biosciences from nano to macro* **2009**, *1*, 182-195.

(5) Jones, L. S.; Kaufmann, A.; Middaugh, C. R.: Silicone oil induced aggregation of proteins. *J. Pharm. Sci.* **2005**, *94*, 918-927.

(6) Thirumangalathu, R.; Krishnan, S.; Ricci, M. S.; Brems, D. N.; Randolph, T. W.; Carpenter, J. F.: Silicone oil- and agitation-induced aggregation of a monoclonal antibody in aqueous solution. *J. Pharm. Sci.* **2009**, *98*, 3167-3181.

(7) Bee, J. S.; Randolph, T. W.; Carpenter, J. F.; Bishop, S. M.; Dimitrova, M. N.: Effects of surfaces and leachables on the stability of biopharmaceuticals. *J. Pharm. Sci.* **2011**, *100*, 4158-4170.

(8) Bartzoka, V.; Brook, M. A.; McDermott, M. R.: Protein-silicone interactions: How compatible are the two species? *Langmuir* **1998**, *14*, 1887-1891.

(9) Anderson, A. B.; Robertson, C. R.: Absorption spectra indicate conformational alteration of myoglobin adsorbed on polydimethylsiloxane *Biophys. J.* **1995**, *68*, 2091-2097.

(10) Bernardini, C.; Stoyanov, S. D.; Cohen Stuart, M. A.; Arnaudov, L. N.; Leermakers, F. A. M.: PMMA highlights the layering transition of PDMS in langmuir films. *Langmuir* **2011**, *27*, 2501-2508.

(11) *Antibodies: A Laboratory Manual*; Harlow, E.; Lane, D., Eds.; Cold Spring Harbor Laboratory: Cold Spring Harbor, NY., 1988.

(12) Lowry, O. H.; Rosebrough, N. J.; Farr, A. L.; Randall, R. J.: Protein measurement with the folin phenol reagent. *J. Biol. Chem.* **1951**, *193*, 265-275.

(13) Padday, J. F.; Pitt, A. R.; Pashley, R. M.: Menisci at a free liquid surface: surface tension from the maximum pull on a rod. *J. Chem. Soc., Faraday Trans. I* **1975**, *71*, 1919-1931.

(14) Svitkina, T.: Imaging cytoskeleton components by electron microscopy. *Methods Mol. Biol.* **2009**, *586*, 187-206.

(15) Svitkina, T.: Electron microscopic analysis of the leading edge in migrating cells. In *Cellular Electron Microscopy*; McIntosh, J. R., Ed.; Elsevier Academic Press Inc: San Diego, 2007; Vol. 79; pp 295-319.

(16) Horcas, I.; Fernandez, R.; Gomez-Rodriguez, J. M.; Colchero, J.; Gomez-Herrero, J.; Baro, A. M.: WSXM: A software for scanning probe microscopy and a tool for nanotechnology. *Rev. Sci. Instrum.* **2007**, *78*, 013705.

(17) Necas, D.; Klapetek, P.: Gwyddion: an open-source software for SPM data analysis. *Cent. Eur. J. Phys.* **2012**, *10*, 181-188.

(18) Liao, Z. Z.; Lampe, J. W.; Ayyaswamy, P. S.; Eckmann, D. M.; Dmochowski, I. J.: Protein assembly at the air-water interface studied by fluorescence microscopy. *Langmuir* **2011**, *27*, 12775-12781.

(19) Hillborg, H.; Gedde, U. W.: Hydrophobicity changes in silicone rubbers. *IEEE Trns. Dielectr. Electr. Insul.* **1999**, *6*, 703-717.

(20) Kaali, P.; Momcilovic, D.; Markström, A.; Aune, R.; Czel, G.; Karlsson, S.: Degradation of biomedical polydimethylsiloxanes during exposure toin vivobiofilm environment monitored by FE-SEM, ATR-FTIR, and MALDI-TOF MS. *J. Appl. Polym. Sci.* **2010**, *115*, 802-810.

(21) Mann, E. K.; Langevin, D.: Poly(dimethylsiloxane) molecular layers at the surface of water and of aqueous surfactant solutions. *Langmuir* **1991**, *7*, 1112-1117.

(22) Lenk, T. J.; Lee, D. H. T.; Koberstein, J. T.: End group effects on monolayers of functionally-terminated poly(dimethylsiloxane) at the air-water interface. *Langmuir* **1994**, *10*, 1857-1864.

(23) Mehta, S. C.; Somasundaran, P.; Maldarelli, C.; Kulkarni, R.: Effects of functional groups on surface pressure-area isotherms of hydrophilic silicone polymers. *Langmuir* **2006**, *22*, 9566-9571.

(24) Kim, C.; Gurau, M. C.; Cremer, P. S.; Yu, H.: Chain conformation of poly(dimethyl siloxane) at the air/water interface by sum frequency generation. *Langmuir* **2008**, *24*, 10155-10160.

(25) Hahn, T. D.; Hsu, S. L.; Stidham, H. D.: Reflectance infrared spectroscopic analysis of polymers at the air−water interface. 4. microstructure of poly(dimethylsiloxane). *Macromolecules* **1997**, *30*, 87-92.

(26) Damaschun, G.: X-ray investigation of the structure of silicone rubber. *Kolloid. Z. Z. Polym.* **1962**, *180*, 65-67.

(27) Schilling, F. C.; Gomez, M. A.; Tonelli, A. E.: Solid state NMR observations of the crystalline conformation of poly(dimethylsiloxane). *Macromolecules* **1991**, *24*, 6552-6553.

(28) Lee, L. T.; Mann, E. K.; Langevin, D.; Farnoux, B.: Neutron reflectivity and ellipsometry studies of a polymer molecular layer spread on the water surface. *Langmuir* **1991**, *7*, 3076-3080.

(29) Karolin, J.; Johansson, L. B. A.; Strandberg, L.; Ny, T.: Fluorescence and absorption spectroscopic properties of dipyrrometheneboron difluoride (BODIPY) derivatives in liquids, liquid membranes, and proteins. *J. Am. Chem. Soc.* **1994**, *116*, 7801-7806.

(30) Ludwig, D. B.; Trotter, J. T.; Gabrielson, J. P.; Carpenter, J. F.; Randolph, T. W.: Flow cytometry: a promising technique for the study of silicone oil-induced particulate formation in protein formulations. *Anal. Biochem.* **2011**, *410*, 191-199.

(31) Mann, E. K.; Lee, L. T.; Henon, S.; Langevin, D.; Meunier, J.: Polymer surfactant films at the air-water-interface. 1. Surface pressure, ellipsometry, and microscopic studies. *Macromolecules* **1993**, *26*, 7037-7045.

(32) Patel, A. J.; Varilly, P.; Jamadagni, S. N.; Acharya, H.; Garde, S.; Chandler, D.: Extended surfaces modulate hydrophobic interactions of neighboring solutes. *Proc. Natl. Acad. Sci. U. S. A.* **2011**, *108*, 17678-17683.

(33) Zema, J.; Rysz, J.; Budkowski, A.; Awsiuk, K.: Proteins grouped into a variety of regular micro-patterns by substrate-guided domains of self-assembling poly(ethylene oxide)/polystyrene blends. *Soft Matter* **2012**, *8*, 5550-5560.

(34) Sezgin, E.; Chwastek, G.; Aydogan, G.; Levental, I.; Simons, K.; Schwille, P.: Photoconversion of bodipy-labeled lipid analogues. *ChemBioChem* **2013**, *14*, 695-698.

(35) Ruben, G. C.: Vertical Pt-C replication for TEM, a revolution in imaging non-periodic macromolecules, biological gels and low-density polymer networks. *Micron* **1998**, *29*, 359-396.

(36) Shutova, M.; Yang, C. S.; Vasiliev, J. M.; Svitkina, T.: Functions of nonmuscle myosin II in assembly of the cellular contractile system. *PLoS One* **2012**, *7*, e40814.

Chapter 5 Conclusions and future directions

In this thesis, I have applied fluorescence microscopy in combination with tensiometry, AFM and several other methods to study the behavior of plasma proteins at the AWI. The main conclusions are summarized as following:

- Protein films formed were laterally heterogeneous at the AWI. Heterogeneity in the micrometer scale was observed under fluorescence microscopy during adsorption or at concentrations below the critical bulk concentration required to cover the AWI.
- The morphology of protein assembly at the AWI was affected by the solution conditions including ionic strength and redox potential of solution.
- Partition coefficient measurement by CLSM was developed as a semi-quantitative method to estimate the surface concentration of proteins, and determine the concentration of surfactants, such as F-127, required to completely replace proteins at the AWI.
- Pluronic F-127 caused phase separation and reduced the viscosity of proteins in the interfacial layer. Dynamics study showed that during the competition of protein and surfactant for the interfacial area, domains in the protein-rich phase tended to coalesce.
- PDMS film spread at the AWI was shown to affect plasma protein adsorption at protein bulk concentrations in the μg/mL range. Protein adsorbed at the circular domain regions in the polymer film where PDMS chains were densely packed.

In future work, physical parameters controlling the assembled structures could be further investigated, and applications of these thin bio-films may be developed. In the course of my thesis studies, progress was made on three additional projects, which are summarized below, and similarly represent areas for further investigation.

I. Two-dimensional domains formed by multivalent interaction between two proteins at the lipid-water interface

The formation of liquid droplets in solution results from a phase transition driven by weak interactions between molecules. It has been discovered in recent years that some RNAs and proteins form liquid droplets in solution through multivalent interactions between binding partners.[1] Many biopolymers possess repetitive complementary sequences that favor intermolecular interactions.[1] These assemblies are often involved in important biological functions, such as the SRC Homology 3 (SH3) domains of protein Nck interacting with the proline rich motif (PRM) of protein N-WASP, which promotes the formation of actin filament in cells.[2] It is possible to transform the 3-D droplets into 2-D domains at the AWI to study the factors that control the assembly structure through direct measurement of the physical parameters such as line tension.[3,4] However, the high solubility and the change of conformation of these proteins at the AWI have made it challenging to realize this idea directly.

Meanwhile, a monolayer of lipid anchors such as biotinylated lipids or nickel-chelating lipids, could recruit proteins modified with streptavidin or histidines to the lipid-water interface and reduce protein denaturation.[5] This strategy has been used to obtain 2-D

crystals of proteins that were otherwise hard to crystalize, such as RNA Polymerase II.[6] By mixing lipid anchors with non-interacting lipids in the monolayer, there is the potential to enrich the protein content at the interface without losing the dynamic characteristics of a fluid sublayer beneath the lipid monolayer.

In our experiment, repeating PRM or SH3 sequences were linked in tandem to generate PRM_n or $SH3_n$ (where *n* is the number of repeat units), thereby tuning the strength of the PRM-SH3 binding interaction. Both PRM and SH3 domains were designed with a cysteine and a His_6-tag at the C-terminus. The cysteines were used for covalent labeling with fluorophores. PRM_5 and $SH3_5$ were expressed in *E. coli*, isolated and purified by Chih-Jung Hsu and Wan-Ting Hsieh in the Baumgart laboratory. $SH3_5$ was labeled with Alexa594 (A594), and PRM_5 was labeled with Alexa488 (A488). Details of these proteins can be found in Wan-Ting Hsieh's thesis.[7]

The lipids used were: 1,2-dioleoyl-sn-glycero-3-[(N-(5-amino-1-carboxypentyl) iminodiacetic acid)succinyl] (nickel salt) (DGS-NTA(Ni)); lipophilic tracer DiD and 1,2-dioleoyl-sn-glycero-3-phosphocholine (DOPC). The components of the lipid monolayer tested were 3-30% (molar percentage) DGS-NTA(Ni) + 0.2% DiD + DOPC. DGS-NTA(Ni) is the lipid anchor that chelates with the His_6-tags engineered in SH3 and PRM sequence. DiD was doped into the lipid to give fluorescence contrast to locate the interface prior to the introduction of proteins. DOPC is a charge neutral lipid that constitutes for the rest of the lipid components in the monolayer. The buffer for the subphase was 4 mM phosphate, with 138 mM NaCl, pH = 7.4.

The experimental setup was illustrated in Figure 5.1. The lipid monolayer was formed by spreading 10 nmol of lipid mixture in chloroform at the air-buffer interface. After 20 min, when the solvent was evaporated, the monolayer was compressed to increase the surface pressure to 20 mN/m. PRM_5 and $SH3_5$ were pre-mixed in solution at concentrations (< 1 μM) much lower than the bulk phase separation concentration (~10^1 μM)[2] and then injected into the subphase to a final concentration of 10-67 nM. Samples were left to equilibrate for 1 h to overnight.

Domains were observed in fluorescence images of the interfacial layer as shown in Figure 5.2 A and B, with 3% DGS-NTA(Ni) in the lipid monolayer. Both the PRM_5-A488 and $SH3_5$-A594 fluorescence showed stronger intensity in domains, indicating a concentrated phase with both proteins. Control experiments using the same lipid monolayer but only $SH3_5$-A594 showed a homogeneous sublayer (Figure 5.2 C). In contrast, with only PRM_5-A488, it showed small aggregates in the sublayer (Figure 5.2 D), which was likely due to the self-association known for polypeptides with proline periodicity.[8] Nevertheless, the domain structure in PRM_5-A488 and $SH3_5$-A594 mixture was distinctly different from the aggregates formed in PRM_5-A488-only system at the lipid-water interface. The self-association of PRM_n could be reduced by decreasing the repeating unit n. Gene truncations have been carried out for PRM_n, and the sublayer structure in trough still needs to be tested. It is also worth mentioning that at higher lipid anchor concentrations, a homogeneous layer was observed in both fluorescence channels for the $SH3_5$-A594 and PRM_5-A488 mixture.

Moreover, the domain morphology was controlled by compressing and relaxing the barriers, and surface pressure was monitored simultaneously. The structure of domains changed between near-circular domains to fractals depending on the surface pressure of the film (Figure 5.3). The change of morphology was reversible which confirmed the phase separation was caused by reversible binding between $SH3_5$ and PRM_5 through electrostatic interactions.

Nevertheless, the interaction between $SH3_5$ and PRM_5 was so strong that it greatly reduced the fluidity of the domains, thus the measurement of line tension was not feasible even at lower surface pressure (~20 mN/m). Also, challenges remained in expressing and purifying the proteins in large quantities for the trough experiment, while PRM's propensity to self-associate made it difficult to calibrate the molar concentration precisely. In future work, efforts could be directed to reducing the repeating unit *n* of both proteins to decrease the intermolecular force between $SH3_n$ and PRM_n. Besides, because the same system could be tested in a model vesicle system,[7] which requires much less proteins, it makes sense to explore the phase diagram in vesicle system using properly calibrated protein and lipid conditions, and then use a Langmuir monolayer to test the physical parameters such as line tension and film viscosity.

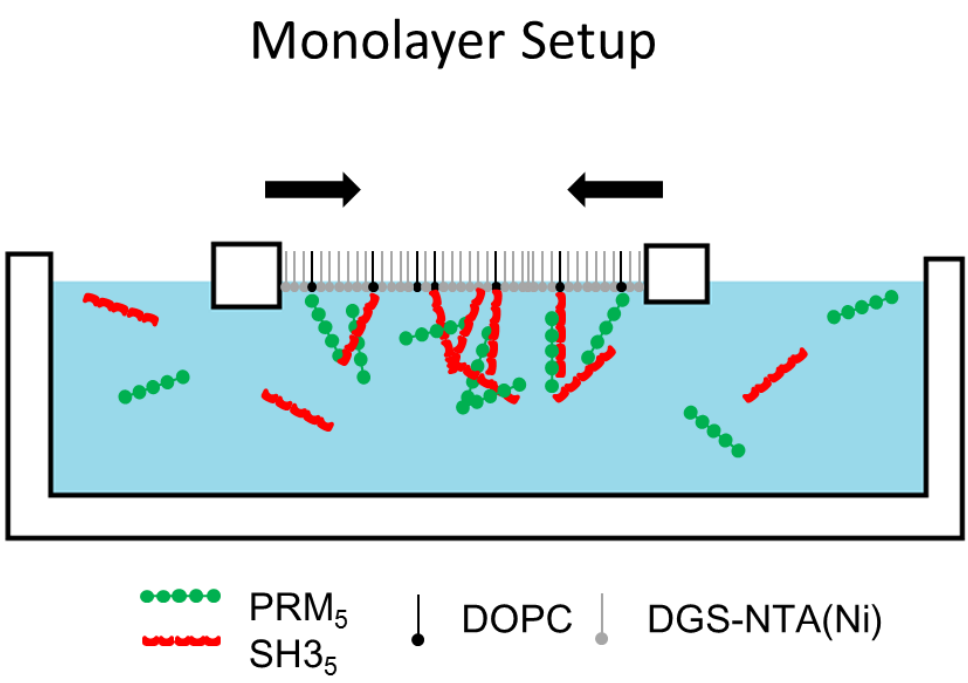

Figure 5.1 A cartoon showing the side-view of the experimental setup with lipid monolayer and protein mixtures.

The lipid mixture was spread at the AWI confined by a pair of barriers (indicated by the two squares), while the proteins (PRM_5 and $SH3_5$) were first injected under the lipid monolayer, then recruited to the sublayer due to the chelating of NTA(Ni) and His_6-tag. The surface area could be controlled by moving the barriers.

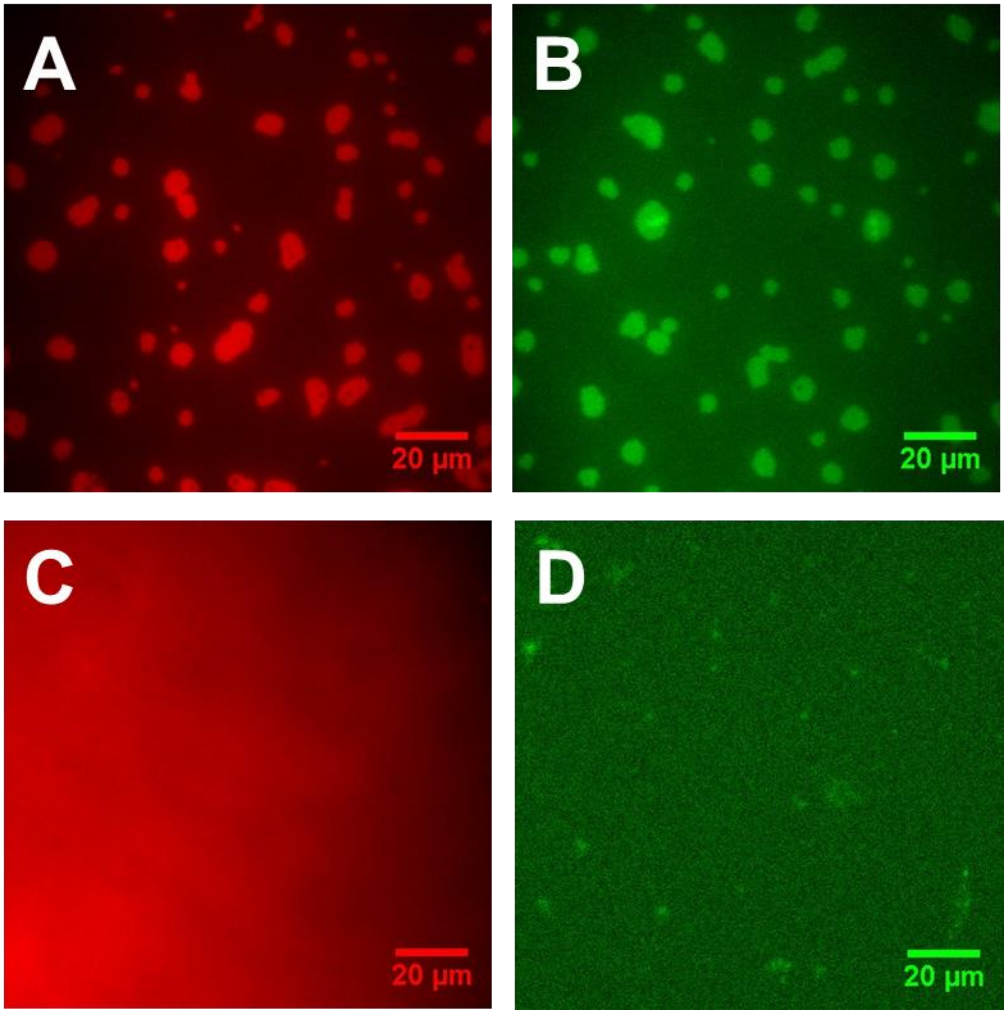

Figure 5.2 PRM_5 and $SH3_5$ protein domains observed in Langmuir monolayer.

(A) A594 fluorescence and (B) A488 fluorescence of the lipid-water interface of PRM_5-A488 (C = 67 nM) + $SH3_5$ –A594 (C = 67 nM) mixture. (C) $SH3_5$ –A594 only (C = 67 nM). (D) PRM_5-A488 only (C = 67 nM). Lipid monolayer content: 3% DGS-NTA(Ni) + 0.2% DiD + 96.8% DOPC.

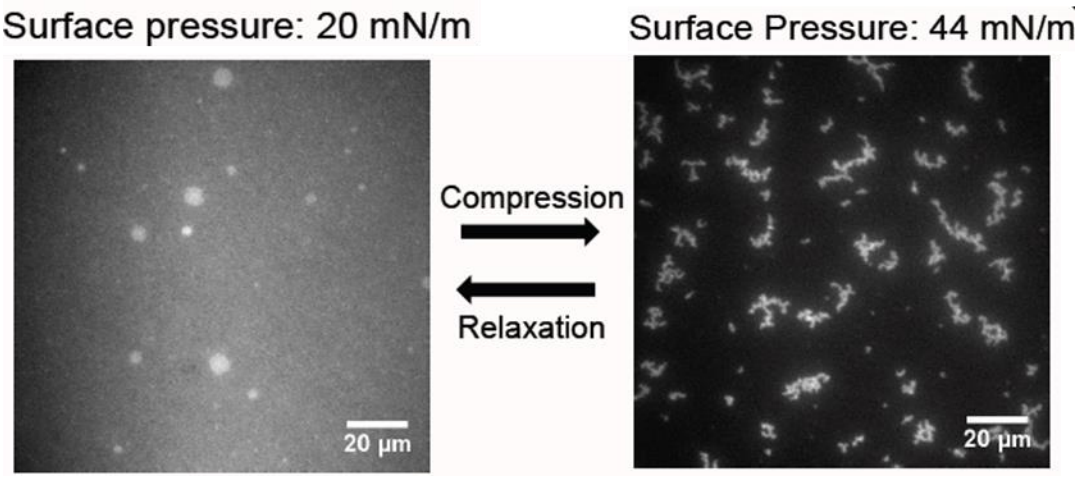

Figure 5.3 Reversible change of domain morphology.

Protein content: PRM_5-A488 (C = 33 nM) + $SH3_5$–A594 (C = 33 nM). Lipid monolayer content: 3% DGS-NTA(Ni) + 0.2% DiD + 96.8% DOPC. Fluorescence images was collected in the A594 channel.

II. Spectral imaging of molecular rotor PZn_n in vesicles and cells[‡]

Spectral imaging employed in this project is a fluorescence imaging technique that combines tunable optical filters and linear unmixing of spectral data, so that individual spectra of multiple fluorophores could be resolved. Instead of a single image slice in the XY plane, the data set of spectral imaging is a 3-D matrix with the third dimension being the wavelengths of fluorescence emission (Figure 5.4 A). Thus, comparing to the multicolor confocal images (Figure 5.4 B) where two or three emission filters were used and the intensity overlaid in one image, the unmixing of the image cube yields a stack of images that show different intensity distributions in each frame collected at different emission wavelengths over a broad range (Figure 5.4 C). Thus spectral imaging can better resolve spectral overlap and is more sensitive to spectral changes of fluorophores.

Meanwhile, in recent years, researchers have used the emission change of organic fluorophores or quantum dots to monitor the mechanical force exerted on materials with high spatial and temporal resolution.[9,10] These fluorescent reporters are very sensitive to environment, thus the local stress in the materials could be reflected in the emission change.[11] Multi(porphyrin)-based near infrared fluorophores were previously incorporated in polymersomes to make self-assembled soft materials for in vivo imaging.[12] The meso-to-meso ethyne-bridged (porphinato)zinc(II) oligomers (PZn_n), are

[‡] Part of this section was adapted from Kamat, N. P.; Liao, Z. Z.; Moses, L. E.; Rawson, J.; Therien, M. J.; Dmochowski, I. J.; Hammer, D. A. *Proceedings of the National Academy of Sciences of the United States of America* **2011**, *108*, 13984.

a group of molecular rotors with excellent sensitivity to change in environment, which is due to the change of the torsional angle between the covalently connected porphyrin rings.[13] As shown in Figure 5.5, the emission peaks of PZn_2 and PZn_3 shifted about 40 nm away from the peak in THF solution to the peak in polymersome membranes with 20% loading.

Utilizing the spectral properties of PZn_n, we applied spectral imaging to study the emission change of PZn_2 during polymersome rupture. These polymersomes were found to be photoresponsive upon irradiation.[14] The advantage of using spectral imaging is that local stress changes in the micro-scale could be detected, and monitored in realtime. Image cubes were collected with a hyperspectral CCD (CRi Nuance FX) camera coupled to an inverted fluorescence microscope (Olympus IX81). The imaging camera has an electronically tunable liquid crystal emission filter that allows collection of emission spectra in nanometer steps across a broad spectral range within seconds to minutes. The pixel resolution is 0.692 μm ⁄ pixel. Samples were excited with a mercury lamp with an excitation band-pass filter (530–550 nm). PZn_2 emission was collected by the camera from 660 to 720 nm with a 3-nm step size. Spectral unmixing was carried out using the real component analysis method included with the Nuance 2.10 software. Different spectral components in the same image cube were identified and reassigned pseudocolors to distinguish the environmental heterogeneity in the unmixed image.

As shown in Figure 5.6, localized disruption in photoactive polymersomes led to increased membrane fluidity in a region of the membrane. In Figure 5.6 A, even before the rupture of the polymersome, blue shift at the lower right of the vesicle was detected,

highlighted by the green and yellow coloration of the membrane-localized emission. Membrane rupture subsequently occurred in this region (Figure 5.6 B), and the emission spectra blue-shifted throughout the polymersome membrane, indicating a released tension after the membrane rupture. This encouraged us to explore further the correlation between membrane tension and emission shift of PZn_2 in vesicle membranes using micropipette aspiration. In Figure 5.7, increasing the tension in the polymersome mebrane caused the emission sprectra of PZn_2 to blue shift. The membrane tension could be converted from the membrane area change, and a linear correlation was established between the menbrane tension and the intensity ratio of PZn_2 at two wavelengths representing the planar and twisted conformation of PZn_2.[15]

Similar spectral properties of PZn_n should apply to nano-vesicles loaded with multi(porphyrin)-based near infrared fluorophores, which could be utilized to detect the drug releasing efficiency of these nano-vesicles. In the future, the application of PZn_n as a stress (or viscosity) sensor could be further expanded to other polymeric materials and biological systems. For example, PZn_n could be loaded into elastomers in order to detect the viscosity change and defect formation during the curing process. Also, we have done some preliminary cell studies to show that PZn_2 dissolved in DMSO and subsequently mixed with cell media could be readily taken up by macrophages without obvious toxicity (Figure 5.8). However, since the endocytosis is the dominant uptake method in macrophages, the interpretation of the spectral information was complicated as it reflected the environment of the endocytotic vesicles instead of cytosol. Other cell lines

could be tested in the future and modifications of the PZn_n chemical structure could be made to help PZn_n readily pass through the cell membrane.

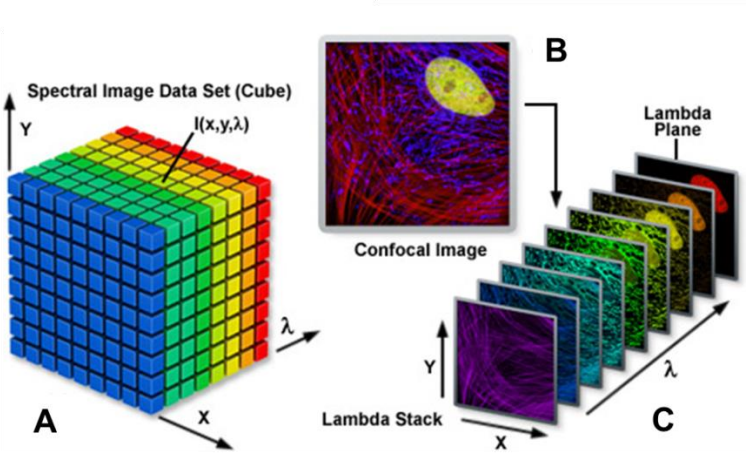

Figure 5.4 Principals of spectral imaging.

(A) Spectral image data set as an image cube. (B) A multicolor confocal image and (C) a lambda stack of unmixed images from an image cube of fixed cells stained with multiple synthetic dyes.

This figure is adapted from Carl Zeiss AG

http://zeiss-campus.magnet.fsu.edu/articles/spectralimaging/introduction.html

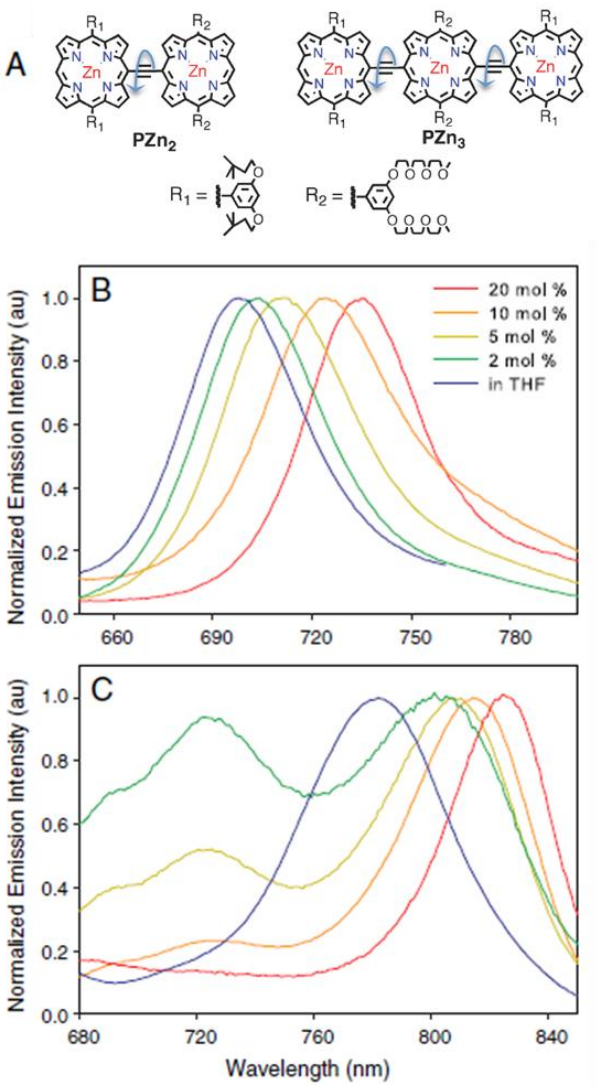

Figure 5.5 Porphyrin-based fluorophore emission showed spectral shift in different environment.

(A) Structures of PZn_2 and PZn_3. Arrows indicate the rotation of porphyrin rings. (B) PZn_2 exhibits an emission peak at 699 nm (blue) in THF; and this emission peak is dependent upon its concentration in the polymersome membrane, and ranges up to 735 nm (red) in 3800 Mr PEO-b-PBD polymer membranes at 20 mol% loading. (C) PZn_3 exhibits an emission peak at 787 nm (blue) in THF; this emission peak shifts bathochromically with increasing concentration in the polymersome membrane and ranges up to 825 nm (red) in PEO-b-PBD polymer membranes at 20 mol % loading.

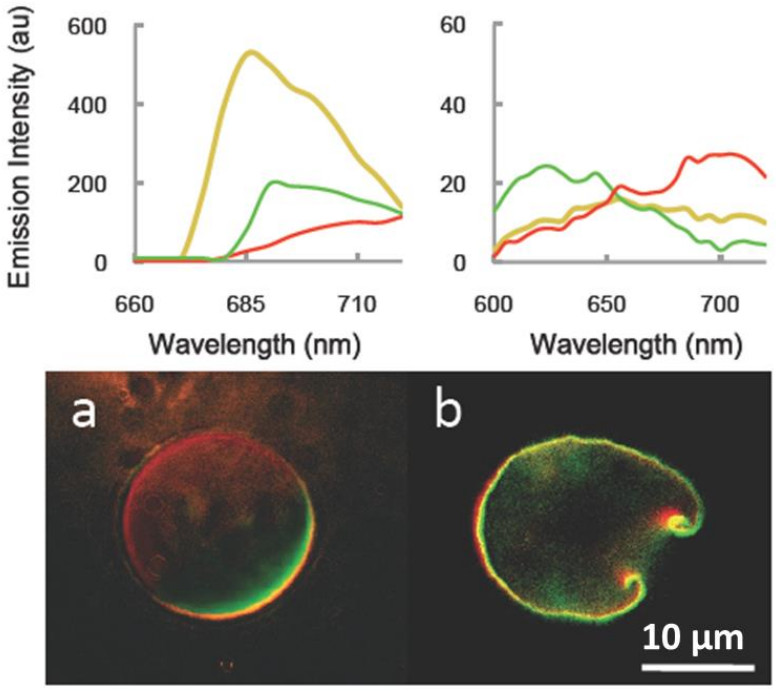

Figure 5.6 Unmixed spectra (upper row) and overlay of pseudo-color images (lower row) of a vesicle before and after photo-activated rupture.

(a) Spectral change in the vesicle upon photo-activation. (b) Ruptured vesicle after extended light exposure. Irradiation time is 5 minutes.

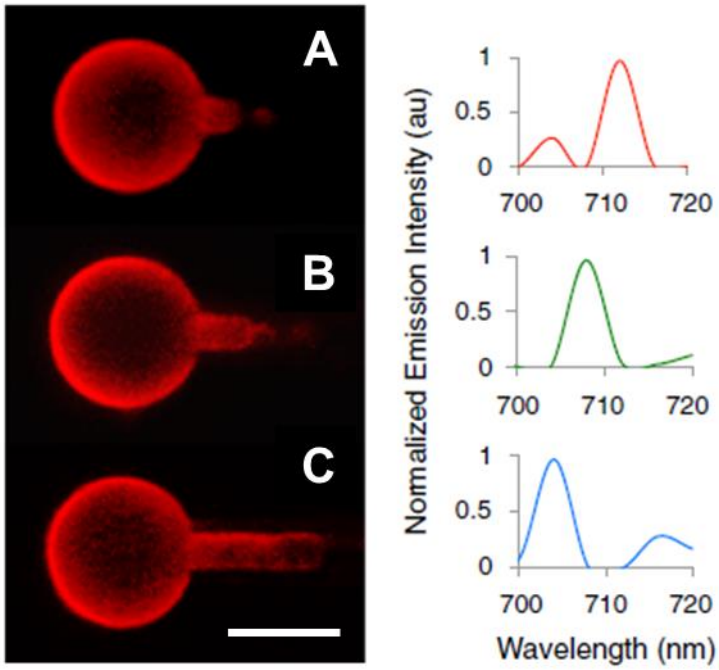

Figure 5.7 Emission spectra of PZn_2 identified by spectral imaging during micropipette aspiration.

From A to C, the tension in the polymersome membrane was (A) 0.8 dyne⁄cm (B) 1.7 dyne⁄cm (C) 4.7 dyne⁄cm. Scale bar: 30 μm.

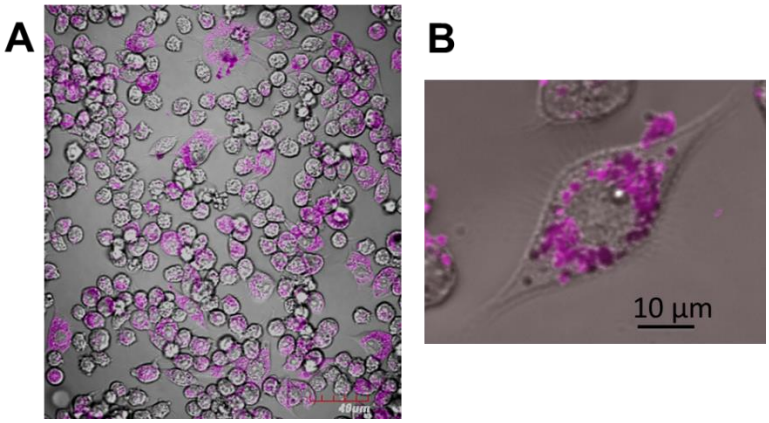

Figure 5.8 Uptake of PZn_2 by macrophage.

(A) Overlay of CLSM image of PZn_2 fluorescence and DIC image. (B) Zoom-in image of a single cell showing that PZn_2 was contained in endocytotic vesicles.

III. Imaging fluorescent anesthetics 1-aminoanthracene and photoactive analogue 1-azidoanthracene in vitro and in vivo[§]

Previously, our group identified a fluorescent molecule, 1-aminoanthracene (1-AMA) to be a general anesthetic. It was shown to immobilize reversibly tadpoles, potentiate GABAergic transmission, and localize to neuronal tissue.[16] Dr. Xinjing Tang from our group found that the emission of 1-AMA shifts to longer wavelength in more polar solvents (unpublished data). Utilizing the emission shift of 1-AMA in different environment, we applied spectral imaging to study the distribution of 1-AMA in neuronal cells as shown in Figure 5.9. Culture media of mouse neural progenitor cells was pipetted out and replaced by PBS buffer saturated with 1-AMA (~33 μm), then imaged immediately. As shown in Figure 5.9 A, 1-AMA showed stronger intensity in the cells than in the buffer. After unmixing, the emission peak of 1-AMA was at ~550 nm in cytosol compared to ~490 nm in PBS buffer (Figure 5.9 B and C). We also observed a few bright spots with emission peak at ~520 nm in the cells, which were likely from 1-AMA in the mitochondria. This distinct feature may have a strong potential in probing the biosystems involved in signal transduction and metabolism.

To identify the molecular targets and binding sites, Dr. Olena Taratula from our group synthesized the photoactive analog 1-azidoanthracene (1-AZA), which generates a reactive nitrene upon UV photolysis and crosslinks with the protein targets (Figure 5.10

[§] Part of this section was adapted from: Emerson, D. J.; Weiser, B. P.; Psonis, J.; Liao, Z.; Taratula, O.; Fiamengo, A.; Wang, X.; Sugasawa, K.; Smith, A. B., 3rd; Eckenhoff, R. G.; Dmochowski, I. J.: Direct modulation of microtubule stability contributes to anthracene general anesthesia. *J Am Chem Soc* **2013**, *135*, 5389-98.

A). We tested the photolysis of 1-AZA in vitro as shown in Figure 5.10 B. 30 μL of 1 mg/mL 1-AZA ethanol solution was mixed with 3.0 mL of 1.0 mg/mL horse spleen apo ferritin (HSAF) Tris-HCl buffer solution (20 mM, pH = 7.4). The solution was covered under aluminum foil and incubated at 4 ℃ for 1 h. Then the emission spectrum of 1-AZA was taken by before, during and after photo-activation using a near-UV transilluminator (9 mW/cm^2 at 365 nm, distance 1 cm). The emission spectra of 1-AZA are shown in Figure 5.10 B. Under these experimental conditions, 1-AZA was completely photo-converted after 15 s of irradiation, and the fluorescence intensity at 520 nm increased about 3-fold after photolysis. After purification of the photolysis product by desalting column, the protein still showed an emission peak at 480-520 nm (Figure 5.10 C), indicating that covalent cross-linking or strong binding was achieved.

Moreover, we established that 1-AZA upon photolysis could immobilize tadpoles as shown in Figure 5.11. The detailed experimental steps were included in Appendix II. 1-AZA can only immobilize tadpoles after UV irradiation. It took the tadpoles longer time to regain mobility compared to 1-AMA. This effect was consistent with the phenomenon observed with a photoactive analogue of propofol.[17] However, it was also found in the immobilization experiment that photolyzed 1-AZA was toxic to tadpoles, and ~50% of tadpoles in our test did not regain mobility. The dead tadpoles were not included in the immobilization results.

Nevertheless, 1-AZA is a photoactive anesthetic analogue that has potential use for in vivo imaging to elucidate anesthetic mechanisms. We applied 1-AZA in the in vivo imaging of two types of model animals: C. elegans nematodes and X. laevis tadpoles as

shown in Figure 5.12 and Figure 5.13. The steps of preparing *C. elegans* nematode for imaging are included in Appendix III. Photo-activation was achieved by irradiating the sample with the same near-UV illuminator mentioned above. It was observed that after photolysis, the fluorescence intensity increased significantly especially in the nerve ring of the nematode, demonstrating that 1-AZA localized in the central nervous system (CNS) in *C. elegans* (Figure 5.12). Enhanced fluorescence intensity of 1-AZA post-photolysis was also observed in tadpoles as shown in Figure 5.13. Two regions in the hindbrain and the forebrain were examined by zooming in with higher magnification. In Figure 5.13 C and D, the neuron cells with long axons could be clearly distinguished from the surrounding tissue. Lastly, the selective photo-activation of the forebrain in tadpoles was also demonstrated in our study. In Figure 5.14, the fluorescence intensity in the tadpole forebrain was quantified during the photolysis process. Intensity nearly doubled after irradiation.

Subsequent studies carried out by other researchers from our group and our collaborators found that β-tubulin was the one of the most prominent cross-linked proteins by 1-AZA after photolysis in tadpole brain, and microtubule stabilizing reagents were shown to affect the anesthetic effects of 1-AMA.[18] In the future, the connection of general anesthesia and microtubule function could be further explored by studying the dynamics of microtubule formation under the influence of general anesthetics.

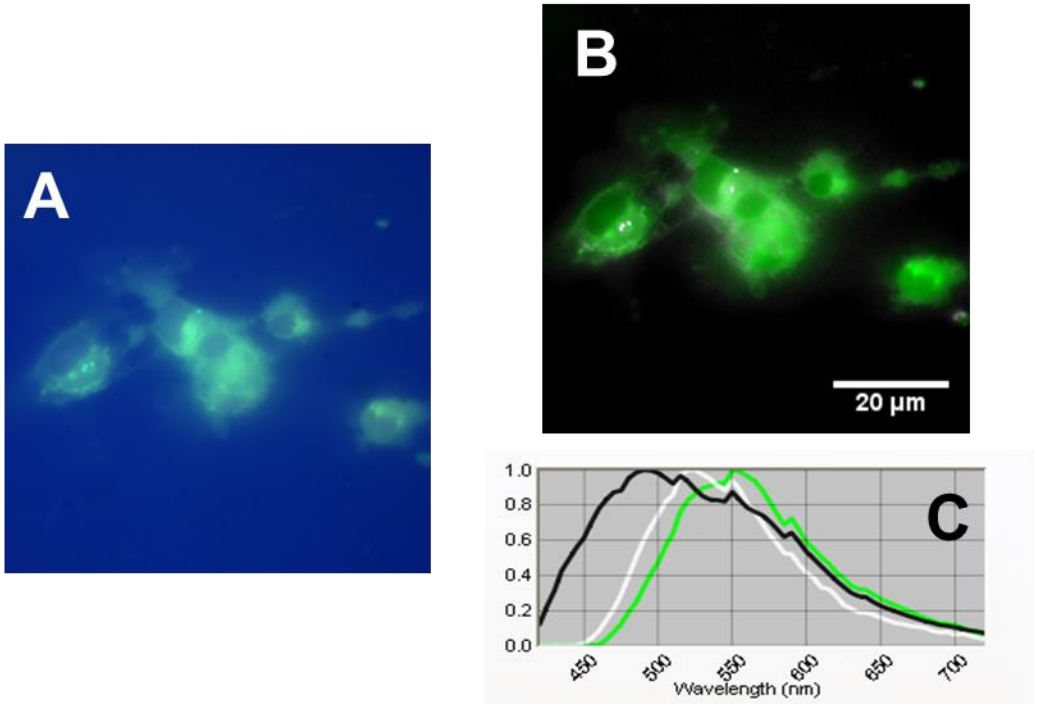

Figure 5.9 Spectral imaging of 1-AMA in mouse neural progenitor cells.

(A) Image cube of cells in PBS that contains 33 µm 1-AMA. (B) Unmixed image. Assigned pseudo-color corresponds to (C) unmixed spectra of 1-AMA, with the emission shift in cytosolic vesicles and cytosol.

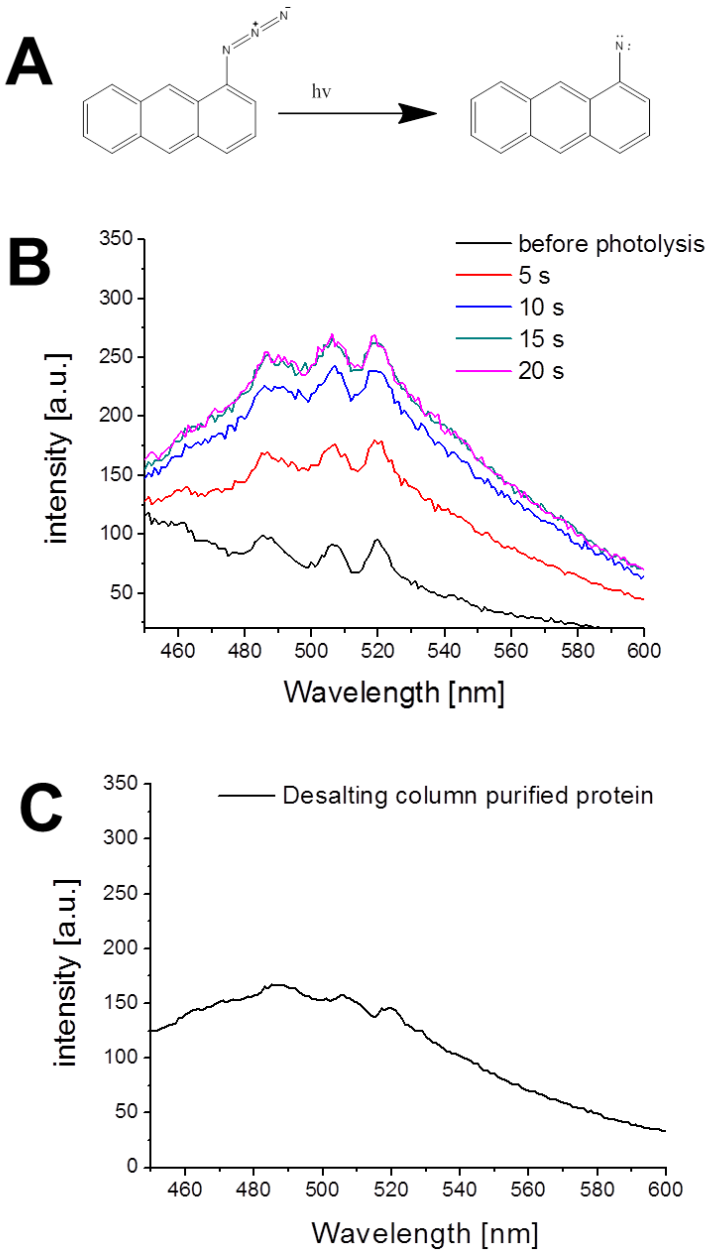

Figure 5.10 Structure and photochemical properties of 1-AZA.

(A) Photo-activation of 1-AZA. (B) Emission spectra of 1-AZA upon photolysis. (C) Emission spectra of labeled protein purified in desalting column.

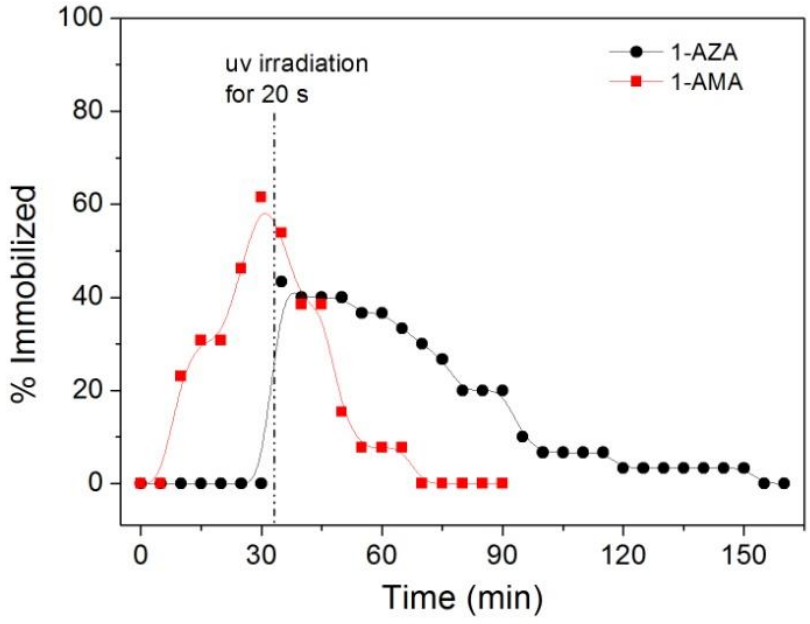

Figure 5.11 Time course comparison of immobilization effects of 1-AMA and 1-AZA on *X. laevis* tadpoles.

Dashed line indicates when the tadpole forebrains were irradiated by 351 and 364 nm laser for 20 s. $[1\text{-AZA}]_{eq}$ = 4.6μM ± 1.8μM, $[1\text{-AMA}]_{eq}$ = 7.5μM ± 2.1μM. Number of tadpoles: 30 of 1-AZA group, 13 of 1-AMA group.

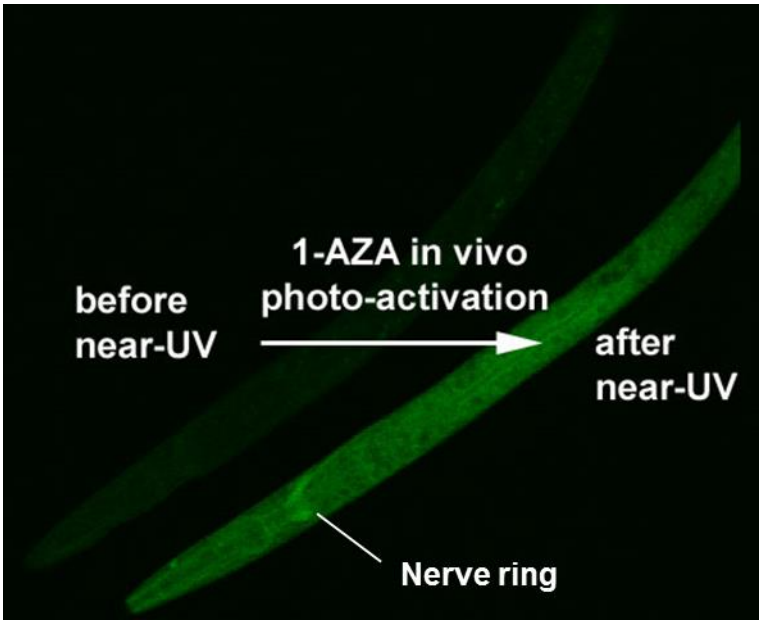

Figure 5.12 Fluorescence image of 1-AZA in *C. elegans* before and after photo-activation.

Nematode incubated 30 min in 25 μM 1-AZA M9 buffer solution in dark and imaged by CLSM with 488 nm laser. Nematode was subsequently irradiated 1 min (9 mW/cm^2 @ 365 nm) and imaged again by CLSM.

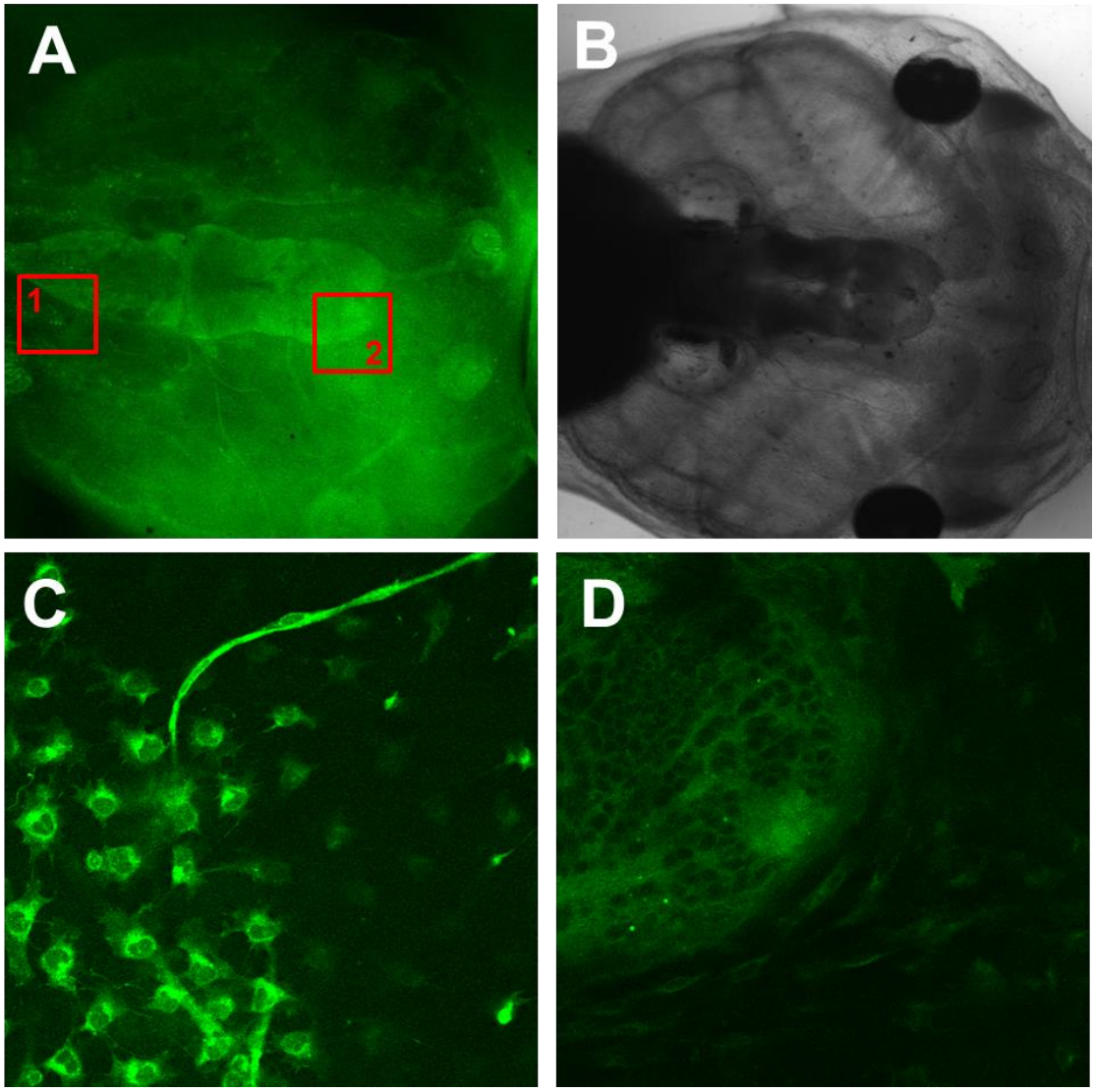

Figure 5.13 In vivo imaging of photo-activated 1-AZA in *X. laevis* tadpoles.

(A) Fluorescence image of photo-irradiated tadpole (B) DIC image of photo-irradiated tadpole. (C) Fluorescence image of ROI-1 in hind-brain showing neuronal cells were strongly fluorescent. (D) Fluorescence image of ROI-2 in forebrain. Tadpole was irradiated 30 s using the same near-UV illuminator mentioned above.

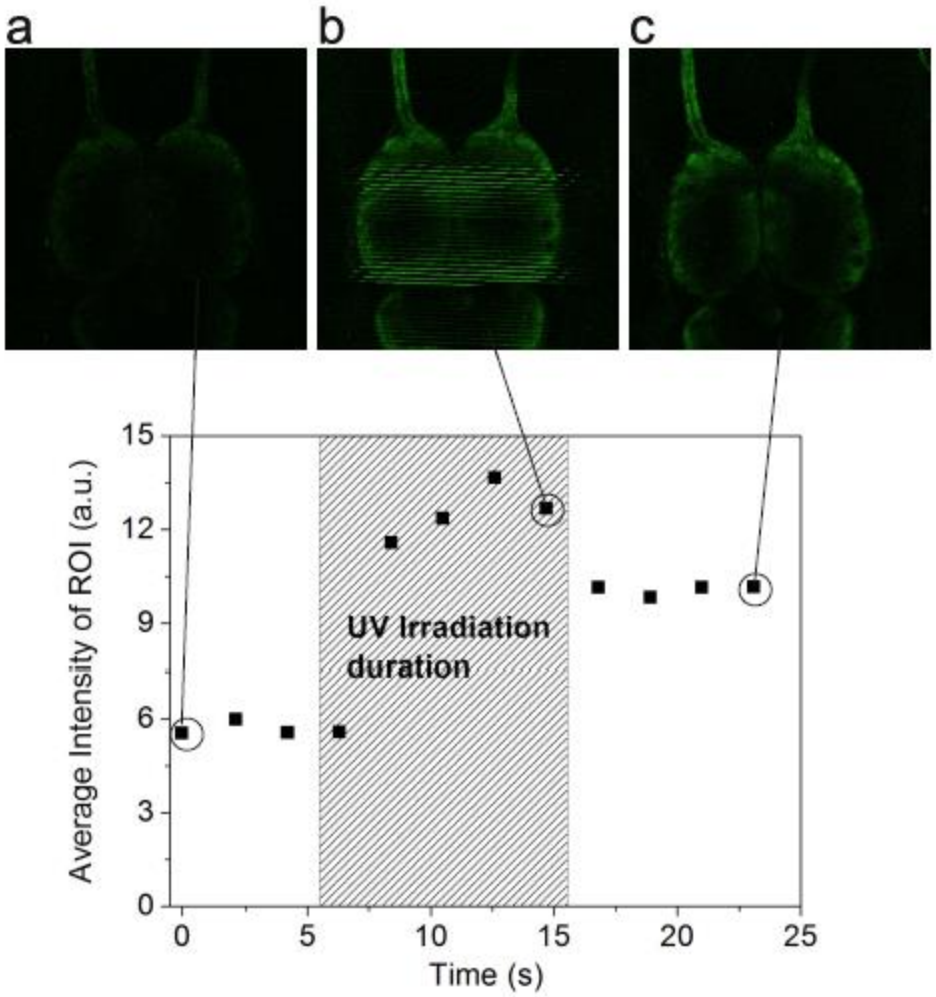

Figure 5.14 Photoactivation of 1-AZA in vivo.

Representative confocal fluorescence images of 1-AZA in a tadpole brain: before (A), during (B) and after (C) near-UV laser photolysis of a tadpole forebrain. The forebrain area was irradiated for 10 s by 351 and 364 nm lasers (100% power). Bottom plot shows the average fluorescent pixel intensity over time under 488 nm laser excitation.

IV. References

(1) Weber, S. C.; Brangwynne, C. P.: Getting RNA and Protein in Phase. *Cell* **2012**, *149*, 1188-1191.

(2) Li, P.; Banjade, S.; Cheng, H. C.; Kim, S.; Chen, B.; Guo, L.; Llaguno, M.; Hollingsworth, J. V.; King, D. S.; Banani, S. F.; Russo, P. S.; Jiang, Q. X.; Nixon, B. T.; Rosen, M. K.: Phase transitions in the assembly of multivalent signalling proteins. *Nature* **2012**, *483*, 336-340.

(3) Heinrich, M. C.; Levental, I.; Gelman, H.; Janmey, P. A.; Baumgart, T.: Critical exponents for line tension and dipole density difference from lipid monolayer domain boundary fluctuations. *J. Phys. Chem. B* **2008**, *112*, 8063-8068.

(4) Dhar, P.; Cao, Y. Y.; Fischer, T. M.; Zasadzinski, J. A.: Active interfacial shear microrheology of aging protein films. *Phys. Rev. Lett.* **2010**, *104*, 016001.

(5) Ng, K.; Pack, D. W.; Sasaki, D. Y.; Arnold, F. H.: Engineering protein-lipid interactions-Targeting of histidine-tagged proteins to metal-chelating lipid monolayers. *Langmuir* **1995**, *11*, 4048-4055.

(6) Edwards, A. M.; Darst, S. A.; Feaver, W. J.; Thompson, N. E.; Burgess, R. R.; Kornberg, R. D.: Purification and lipid-layer crystallization of yeast RNA polymerase-II. *Proc. Natl. Acad. Sci. USA.* **1990**, *87*, 2122-2126.

(7) Hsieh, W.-T.: Lipid and protein organizations in model membrane systems- membrane curvature, lipid structure, domain formation, and membrane binding kinetics. (Ph.D. thesis) Univerisity of Pennsylvania, 2013.

(8) Muiznieks, L. D.; Keeley, F. W.: Proline periodicity modulates the self-assembly properties of elastin-like polypeptides. *J. Biol. Chem.* **2010**, *285*, 39779-39789.

(9) Davis, D. A.; Hamilton, A.; Yang, J. L.; Cremar, L. D.; Van Gough, D.; Potisek, S. L.; Ong, M. T.; Braun, P. V.; Martinez, T. J.; White, S. R.; Moore, J. S.; Sottos, N. R.: Force-induced activation of covalent bonds in mechanoresponsive polymeric materials. *Nature* **2009**, *459*, 68-72.

(10) Choi, C. L.; Koski, K. J.; Olson, A. C.; Alivisatos, A. P.: Luminescent nanocrystal stress gauge. *Proc. Natl. Acad. Sci. USA.* **2010**, *107*, 21306-21310.

(11) Kuimova, M. K.; Botchway, S. W.; Parker, A. W.; Balaz, M.; Collins, H. A.; Anderson, H. L.; Suhling, K.; Ogilby, P. R.: Imaging intracellular viscosity of a single cell during photoinduced cell death. *Nature Chemistry* **2009**, *1*, 69-73.

(12) Ghoroghchian, P. P.; Frail, P. R.; Susumu, K.; Blessington, D.; Brannan, A. K.; Bates, F. S.; Chance, B.; Hammer, D. A.; Therien, M. J.: Near-infrared-emissive polymersomes: self-assembled soft matter for in vivo optical imaging. *Proc. Natl. Acad. Sci. USA.* **2005**, *102*, 2922-2927.

(13) Ghoroghchian, P. P.; Frail, P. R.; Susumu, K.; Park, T. H.; Wu, S. P.; Uyeda, H. T.; Hammer, D. A.; Therien, M. J.: Broad spectral domain fluorescence

wavelength modulation of visible and near-infrared emissive polymersomes. *J. Am. Chem. Soc.* **2005**, *127*, 15388-15390.

(14) Kamat, N. P.; Robbins, G. P.; Rawson, J.; Therien, M. J.; Dmochowski, I. J.; Hammer, D. A.: A Generalized system for photoresponsive membrane rupture in polymersomes. *Adv. Funct. Mater.* **2010**, *20*, 2588-2596.

(15) Kamat, N. P.; Liao, Z. Z.; Moses, L. E.; Rawson, J.; Therien, M. J.; Dmochowski, I. J.; Hammer, D. A.: Sensing membrane stress with near IR-emissive porphyrins. *Proc. Natl. Acad. Sci. USA.* **2011**, *108*, 13984-13989.

(16) Butts, C. A.; Xi, J.; Brannigan, G.; Saad, A. A.; Venkatachalan, S. P.; Pearce, R. A.; Klein, M. L.; Eckenhoff, R. G.; Dmochowski, I. J.: Identification of a fluorescent general anesthetic, 1-aminoanthracene. *Proc. Natl. Acad. Sci. USA.* **2009**, *106*, 6501-6506.

(17) Weiser, B. P.; Kelz, M. B.; Eckenhoff, R. G.: In Vivo Activation of Azipropofol Prolongs Anesthesia and Reveals Synaptic Targets. *J. Biol. Chem.* **2013**, *288*, 1279-1285.

(18) Emerson, D. J.; Weiser, B. P.; Psonis, J.; Liao, Z.; Taratula, O.; Fiamengo, A.; Wang, X.; Sugasawa, K.; Smith, A. B., 3rd; Eckenhoff, R. G.; Dmochowski, I. J.: Direct modulation of microtubule stability contributes to anthracene general anesthesia. *J Am Chem Soc* **2013**, *135*, 5389-5398.

Appendix

I. Matlab code for calculating partition coefficient

```
function [y1, y2, y3]=PC(tif, num)

%-------------------------------------------------------------------------
----
% This function find the partition coefficient (y1),interface intensity
(y2), and average bulk intensity (y3)
% "tif" should be the name of the image or image-stack
% "num" is the number of images in the stack

for i=1:num
    image=rgb2gray(tif(:, :, :, i)); % convert RGB color image to
grayscale image
    figure, imshow(image); % display the image to let the user find
coordinate of the ROI by moving the cursor
    rect=input('input coordinate of ROI: '); % imput value should be:
[starting_x_coordinate, starting_y_coordinate, length, height]
    disp('select background region'); % allow user to hand-select the
background area
    bg=imcrop(image); % bg is the background area
    [r c]=size(image);
    bg_int=mean(mean(bg)); % find average intensity of backgound area
    bgmatrix=ones(r, c)*bg_int;
    minus_bg_image=double(image)-bgmatrix; % subtract background from
original image
    RefROI=imcrop(image, rect);
    figure, imshow(RefROI); % display ROI for the user's reference
    ROI=imcrop(minus_bg_image, rect); % crop ROI from image after
subtracting background intensity
    [p(i), I_inter(i), I_avgbulk(i)]= partition3(ROI); % find p(i)-
partition coefficient, I_inter(i)-interface intensity, I_avgbulk(i)-
average bulk intensity
end;

figure, subplot(1, 3, 1)
plot(p, 'o');
title('Partition Coefficient');

subplot(1, 3, 2)
plot(I_inter, 'o');
title('Interface Intensity');

subplot(1, 3, 3)
plot(I_avgbulk, 'o');
title('Average Bulk Intensity');

y1 = p;
```

```
y2 = I_inter;
y3 = I_avgbulk;

%-------------------------------------------------------------------------
----
%Copyright Zhengzheng (Katie) Liao
%last edited on May 3rd, 2013.


function [y1, y2, y3]=partition3(signal)

%-------------------------------------------------------------------------
----
% this function calculate partition coefficient using a vector "signal"
% y1 is partition coefficient, y2 is interface intensity, y3 is average
bulk intensity.

avg_y=mean(signal); % average the intensity along each column
[h, w]=size(avg_y); % find the width of the averaged signal matrix

for i=1:w;
    if avg_y(:, i)<0
       avg_y(:, i)=0; % set baseline as zero
    else avg_y (:, i)=avg_y (:, i);
    end
end

figure, plot(avg_y); % plot the intensity profile for the user to find
the divding point between interface and bulk by cursor
disp('find dividing point between interface and bulk from intensity
plot');
x1=input('input x coordinate of dividing point: ');
bulksig=avg_y(x1:w);
avgbulk=mean(bulksig); % find average bulk intensity
z=find(avg_y > avgbulk, 1, 'first'); % z is the starting point where
bulk contribution counts
bulk = zeros(h,w); % initialize bulk matrix
bulk(:, z:w) = avgbulk; % set value to bulk matrix
inter = avg_y - bulk; % find interface intensity by subtracting bulk
contribution

figure, plot(avg_y), xlim([1 w]), ylim([-10 256])
hold on
plot(x1, avg_y(x1), 'x', 'Color', 'r')
plot(bulk, '--', 'Color', 'y')
hold off
% plot signal intensity, red cross marks cutting point between
interface and bulk while yellow dash line shows bulk contribution

y1 = sum(inter) / avgbulk; % find and output partition coefficient
y2 = sum(inter); % output interface intensity
y3 = avgbulk; % output average bulk intensity
```

```
%-------------------------------------------------------------------------
----
% Copyright Zhengzheng(Katie) Liao
% last edited on May 3rd, 2013.


function y=readtif(n);

%-------------------------------------------------------------------------
----
% this function reads TIFF images stored in the images folder and store
them as image-stack matrixs

files=dir('C:\Documents and Settings\Katie\My
Documents\MATLAB\images\*.tif');

for i=1:n
    str=strcat('C:\Documents and Settings\Katie\My
Documents\MATLAB\images\', files(i).name);
    tif(:, :, :, i)=imread(str);
end;

y=tif;
```

II. Experimental steps of photoactivated immobilization of tadpoles by 1-azidoanthracene

1. The 1-AZA is dissolved in ethanol (Cat. No. 459836, anhydrous, ≥99.5%, Sigma-Aldrich) as concentrated solution at around 7 mM.

2. The exact concentration is measured by UV absorbance of 100 fold diluted ethanol solution at 373 nm. Then the concentrated ethanol solution is mixed with ethanol and artificial pond water (3 mM NaCl, 30 μM $CaCl_2$, 6 μM $NaHCO_3$ in deionized water) to dilute 1-AZA to desired concentration in 0.5% ethanol. Due to the low solubility of 1-AZA in water, the concentration is later calibrated again in Step 5.

3. Each tadpole is incubated in 5.0 mL of above solution for 30 min covered under aluminum foil. The standard initial concentration of 1-AZA is 15 μM. Mobility of tadpole is checked every five minutes by poking the tadpole with a plastic spatula for a 30 min period.

4. The tadpole is transferred to a home-made imaging dish, which has a tapered channel lined by low-melt agarose (1% in deionized water, Cat. No. 161-3111, Bio-rad). The channel has the width and depth similar to the size of a tadpole, thus could reduce the movement of tadpole during laser manipulation.

5. Meanwhile, 1.0 mL of the incubation buffer was taken to measure absorbance at 383 nm immediately to determine equilibrium concentration $[1\text{-AZA}]_{eq}$.

6. A circular region of interest in the forebrain was irradiated with 351 nm and 364 nm lasers for 20 s then tadpole was transferred into 5.0 mL of fresh pond water.

7. The mobility of the tadpoles is continuously checked every 5 minutes after switching incubation buffer to fresh pond water.

8. 1-AMA is used as the control of the experiment under the same conditions (incubation of 1-AMA in 0.5% ethanol, then near-UV irradiation, and incubation of tadpoles in fresh pond water). The concentration of 1-AMA is increased to match the potency (% immobilization) of 1-AZA.

III. Preparing *C. elegans* adult worms for fluorescence imaging with 1-aminoanthracene or 1-azidoanthracene

1. Prepare M9 buffer: weigh 3 g KH_2PO_4, 6 g Na_2HPO_4, 5 g NaCl and add 1 mL of 1 M $MgSO_4$, add DI-water to 1 L and autoclave solution.

2. Prepare 1-AMA solution: add a small scoop of 1-AMA to 5mL M9 buffer, sonicate for ~30 min. Filter the solution using a 0.2 μm PTFE filter and measure absorbance at 380 nm. The saturation concentration is ~33 μM.

3. Look for densely worm-populated area on the agar plate. Pipette 50-200 μL M9 buffer to plate. Gently aspirate buffer and worms, and transfer to a clean Petri dish.

4. Remove as much remaining buffer as possible then add 200 μL 1-AMA solution to worms.

5. Repeat Step 4 twice, so that the 1-AMA concentration in buffer solution is close to the saturation concentration.

6. Incubate for 30 min at room temperature, then image the worms under fluorescence microscopy.

7. The steps for using 1-AZA are similar. 1-AZA solution is prepared by mixing M9 buffer with 1-AZA ethanol stock solution.